

WAVELET BASED MULTI-CARRIER COMMUNICATIONS
WITH BIT LOADING UNDER TIME-DOMAIN EQUALIZATION



WAVELET BASED MULTI-CARRIER COMMUNICATIONS
WITH BIT LOADING UNDER TIME-DOMAIN EQUALIZATION

A Dissertation Presented to
The Graduate School of Bangkok University

In Partial Fulfillment
of the Requirements for the Degree
Doctor of Engineering in Electrical and Computer Engineering

by
Sarbagya Buddhacharya

2019



© 2019

Sarbagya Buddhacharya

All Right Reserved

This thesis has been approved by
School of Engineering
Bangkok University

Title: Wavelet based multi-carrier communications with bit loading under time-domain equalization

Author: Sarbagya Buddhacharya

Thesis Committee:

Thesis Advisor

(Assoc. Prof. Dr. Poompat Saengudomlert)

Thesis Co-advisor

(Dr. Karel Sterckx)

Graduate Program Director

(Asst. Prof. Dr. Chakkaphong Suthaputchakun)

External Representative

(Dr. Attaphongse Taparugssanagorn)

(Asst. Prof. Dr. Wisarn Patchoo)

Dean of the School of Engineering

10 / 6 / 19

Buddhacharya, S. Doctor of Engineering in Electrical and Computer Engineering,
May 2019. Graduate School, Bangkok University

Wavelet based Multi-carrier Communications with Bit Loading under Time-domain
Equalization (104 pp.)

Advisor of Dissertation: Poompat Saengudomlert, Ph.D.

ABSTRACT

This research explores wavelet packet modulation (WPM) as a potential alternative to orthogonal frequency division multiplexing (OFDM). Unlike OFDM, equalization for WPM cannot depend on the use of cyclic prefix (CP) due to overlapped WPM symbols in the time domain. This research considers time-domain minimum-mean square error (MMSE) equalization. The imperfection of MMSE equalization induces subcarrier signal attenuation and noise amplification. These limitations are taken into account in the development of a bit loading algorithm for WPM. The investigation on the bit error rate (BER) performances is carried out assuming known channel state information (CSI) as well as unknown CSI. For known CSI, mathematical expressions for computing BERs are derived and validated using simulation. The validated mathematical expressions for BERs are used to explore the benefits of bit loading and to show that WPM performs better than OFDM. For unknown CSI, simulation studies show that WPM using MMSE equalization can provide acceptable BER performances with training sequence lengths of moderate overhead. Moreover, WPM with MMSE equalization is shown to outperform OFDM with one-tap equalization. Furthermore, bit loading is performed using the channel impulse response (CIR) estimated based on the solution of an overdetermined system of linear equations. Numerical results demonstrate that the proposed bit loading algorithm with the estimated CIR reduces the BER as compared with equalization

alone. In addition, numerical results also show that WPM with bit loading and unknown CIR performs better than OFDM with bit loading and known CIR.

Keywords: Multi-carrier modulation, Wavelet packet modulation, Bit loading, Minimum mean-square error equalization, Unknown channel state information.

Approved: _____



Signature of Advisor

ACKNOWLEDGMENT

I would like to express my sincere gratitude to my advisor Dr. Poompat Saengudomlert for his guidance and support from the start to the successful completion of my doctoral degree. His valuable suggestions always guided the research towards right directions and motivated me to proceed. I would like to thank my co-advisor Dr. Karel Sterckx for his valuable suggestions, especially during the early phase of the research. I am also grateful to external representative Dr. Attaphongse Taparugssanagorn for his constructive suggestions that motivated me to add more value to the research.

I would like to thank all of the staff members and researchers working at Bangkok University-Center of Research in Optoelectronics, Communications, and Computational Systems (BU-CROCCS) for providing a friendly environment. I would like to acknowledge the Bangkok University Teaching Assistance Scholarship, which partly supported the research.

I would like to sincerely appreciate my wife Reena Manandhar for taking care of my daughters and allowing me to focus on my research. I would like to thank my parents, sisters, and family members back in Nepal for their love and faith on me, which motivated me to work harder.

Finally, I would like to dedicate this work to my daughters Swornika (Seena) Buddhacharya and Anshika Buddhacharya.

TABLE OF CONTENTS

	Page
ABSTRACT	iv
ACKNOWLEDGMENT.....	vi
LIST OF TABLES.....	x
LIST OF FIGURES.....	xi
CHAPTER 1: INTRODUCTION.....	1
1.1 Background.....	1
1.2 Objectives.....	4
1.3 Scope and Limitations.....	5
1.4 Thesis Outlines.....	5
CHAPTER 2: LITERATURE REVIEW.....	7
2.1 Wavelets.....	7
2.2 Wavelet Transform.....	7
2.3 Filter and Filter Banks.....	12
2.4 DWT and IDWT.....	14
2.6 Wavelet Packet Modulation.....	14
2.7 Multicarrier Modulation.....	15
2.8 Peak-to-Average Power Ratio for WPM.....	18
2.9 Discussion of Related Works.....	24
CHAPTER 3: SYSTEM MODEL.....	27
3.1 WPM System Block Diagram.....	27
3.2 MMSE Equalization.....	29

TABLE OF CONTENTS (Continued)

	Page
CHAPTER 3: SYSTEM MODEL (Continued)	
3.2.1 Unknown Channel.....	29
3.2.2 Known Channel.....	32
3.3 Equalization and Bit Loading for WPM.....	36
3.3.1 Noise Power Gain Computation.....	37
3.3.2 Signal Power Gain Computation.....	39
3.3.3 Signal Power Computation.....	40
3.3.4 Bit Loading Algorithm.....	41
CHAPTER 4: WPM WITH KNOWN CSI.....	44
4.1 BER Analysis for WPM.....	44
4.2 Simulation for BER Evaluation.....	47
4.2.1 Simulation for MMSE Equalization.....	49
4.2.2 Simulation for Noise Power Gain.....	51
4.2.3 Bit Allocation.....	53
4.2.4 Simulation for BER.....	54
4.2.5 BER Comparison for WPM with and without Bit Loading.....	57
4.2.6 BER Comparison between WPM and OFDM.....	59
4.3 Findings and Discussion.....	62
CHAPTER 5: WPM WITH UNKNOWN CSI.....	63
5.1 WPM System Block Diagram with Unknown CSI.....	63
5.2 Performance Analysis for Unknown CSI.....	64

TABLE OF CONTENTS (Continued)

	Page
CHAPTER 5: WPM WITH UNKNOWN CSI (Continued)	
5.2.1 Training Length for Equalizer Filter Computation.....	66
5.2.2 BER Comparison between WPM and OFDM.....	69
5.2.3 Channel Estimation using Overdetermined Systems.....	70
5.2.4 Bit Loading with Estimated CIR.....	76
5.3 Findings and Discussion.....	78
CHAPTER 6: CONCLUSION AND SUGGESTIONS FOR FUTURE WORK.....	85
BIBLIOGRAPHY.....	88
APPENDICES.....	92
APPENDIX A: MODIFIED DWT AND IDWT FUNCTIONS.....	93
APPENDIX B: BER ANALYSIS FOR OFDM.....	98
APPENDIX C: CIR GENERATION.....	100
BIODATA.....	103
LICENSE AGREEMENT OF DISSERTATION PROJECT.....	104

LIST OF TABLES

	Page
Table 3.1 E'_b/N_0 for $M \times M$ QAM with BER = 10^{-5}	41
Table 4.1 Tapped-delay-line parameters for the indoor office test environment (ITU-R Rec. M.1225, 1997)	48
Table 4.2 Tapped-delay-line parameters for the outdoor to indoor and pedestrian test environment (ITU-R Rec. M.1225, 1997)	48
Table 4.3 Tapped-delay-line parameters for the vehicular test environment (ITU-R Rec. M.1225, 1997)	49
Table 4.4 Simulation parameters	49
Table 5.1 Simulation parameters for WPM and OFDM systems	66
Table 5.2 Training sequence lengths (in number of WPM symbols) required to achieve acceptable BER performances for channel A and channel B of each test environment for $N = 16$, $N = 32$, and $N = 64$	69
Table 5.3 Reductions of E_b/N_0 for WPM compared to OFDM to achieve the BER of 10^{-4}	74

LIST OF FIGURES

	Page
Figure 2.1 (a) Sinusoidal wave (b) Daubechies-20 wavelet (c) Haar wavelet (Fugal, 2009)	7
Figure 2.2 Time-frequency representation of signal transforms (a) time domain signal (b) Fourier transform (c) short-time Fourier transform (d) wavelet transform.....	9
Figure 2.3 Subband filtering	11
Figure 2.4 Analysis and synthesis process	14
Figure 2.5 (a) DWT with 2 stages (b) IDWT with 2 stages.....	15
Figure 2.6 Bandwidth distribution of DWT.....	15
Figure 2.7 Discrete wavelet packet transform (DWPT)	16
Figure 2.8 Inverse discrete wavelet packet transform (IDWPT)	16
Figure 2.9 Bandwidth distribution of DWPT	16
Figure 2.10 IDWPT with 8 subcarriers	17
Figure 2.11 DWPT with 8 subcarriers.....	18
Figure 2.12 Tree structure of WPM for 16 subcarriers without subcarrier combining.....	21
Figure 2.13 Time-frequency structure of WPM for 16 subcarriers without subcarrier combining	22
Figure 2.14 Tree structure of WPM for 16 subcarriers with subcarrier combining.....	22
Figure 2.15 Time-frequency structure of WPM for 16 subcarriers with subcarrier combining	23
Figure 2.16 CDF plots for PAPRs of WPM without subcarrier combining, WPM with subcarrier combining, and OFDM.....	23

LIST OF FIGURES (Continued)

	Page
Figure 3.1 System block diagram for WPM	28
Figure 3.2 Process to obtain the equalizer filter coefficients	30
Figure 3.3 Tapped delay line structure for an FIR equalizer filter.	31
Figure 3.4 Block diagram showing the noise power gain computation of each subcarrier for WPM (a) using simulation (b) using analysis (c) using analysis based on equivalent filters.	38
Figure 3.5 Block diagram showing the noise power gain computation on each subcarrier for OFDM	39
Figure 3.6 Block diagram showing the signal power gain computation on each subcarrier for WPM (a) using simulation (b) using analysis ...	40
Figure 3.7 Flow chart for the proposed bit loading algorithm.	42
Figure 4.1 Equalizer filter coefficients for channel A of the indoor office test environment from simulation with a known training sequence.	50
Figure 4.2 Equalizer filter coefficients for channel A of the indoor office test environment from analysis using the expression in (3.19).	50
Figure 4.3 Distribution of equalization error for the equalizer coefficients in Fig. 4.2	51
Figure 4.4 Noise power gains across all subcarriers for channel A of the indoor office test environment from simulation with a known training sequence.	52
Figure 4.5 Noise power gains across all subcarriers for channel A of the indoor office test environment from analysis using the expression in (3.23)	52

LIST OF FIGURES (Continued)

	Page
Figure 4.6 Noise power gains across all subcarriers rearranged from low to high frequency components for channel A of the indoor office test environment.	53
Figure 4.7 Signal power gains across all subcarriers rearranged from low to high frequency components for channel A of the indoor office test environment.	53
Figure 4.8 The ratios of noise power gains to signal power gains across all subcarriers rearranged from low to high frequency components for channel A of the indoor office test environment.	54
Figure 4.9 Bit allocation on all subcarriers for channel A of the indoor office test environment.	54
Figure 4.10 ICI across all subcarriers with bit allocation for channel A of the indoor office test environment as shown in Fig. 4.9	55
Figure 4.11 BER versus E_b/N_0 for channel A and channel B of the indoor office test environment for WPM considering MMSE equalization without bit loading.	56
Figure 4.12 BER versus E_b/N_0 for channel A and channel B of the indoor office test environment for WPM considering MMSE equalization with bit loading.	56
Figure 4.13 BER versus E_b/N_0 for channel A and channel B of the indoor office test environment for OFDM considering one-tap equalization with bit loading.	57
Figure 4.14 BER versus E_b/N_0 using MMSE equalization with and without bit loading for channel A and channel B of the indoor office test environment.	58

LIST OF FIGURES (Continued)

	Page
Figure 4.15 BER versus E_b/N_0 using MMSE equalization with and without bit loading for channel A and channel B of the outdoor to indoor pedestrian test environment.....	59
Figure 4.16 BER versus E_b/N_0 using MMSE equalization with and without bit loading for channel A and channel B of the vehicular test environment.....	60
Figure 4.17 BER versus E_b/N_0 comparison between WPM and OFDM for channel A and channel B of the indoor office test environment	60
Figure 4.18 BER versus E_b/N_0 comparison between WPM and OFDM for channel A and channel B of outdoor to the indoor pedestrian test environment.....	61
Figure 4.19 BER versus E_b/N_0 comparison between WPM and OFDM for channel A and channel B of the vehicular test environment.....	61
Figure 5.1 System block diagram for WPM with unknown CSI.	64
Figure 5.2 Transmit frame with training sequences and data symbols	65
Figure 5.3 BER-versus- E_b/N_0 considering channel A of the indoor office test environment for WPM with 16 subcarriers	67
Figure 5.4 BER-versus- E_b/N_0 considering channel A of the indoor office test environment for WPM with 32 subcarriers	68
Figure 5.5 BER-versus- E_b/N_0 considering channel A of the indoor office test environment for WPM with 64 subcarriers	69
Figure 5.6 BER-versus- E_b/N_0 comparison between WPM and OFDM for the indoor office test environment (a) channel A (b) channel B	71

LIST OF FIGURES (Continued)

	Page
Figure 5.7 BER-versus- E_b/N_0 comparison between WPM and OFDM for the outdoor-to-indoor and pedestrian test environment (a) channel A (b) channel B	72
Figure 5.8 BER-versus- E_b/N_0 comparison between WPM and OFDM for the vehicular test environment (a) channel A (b) channel B	73
Figure 5.9 CIR for channel A of the vehicular test environment (a) known (b) unknown but estimated	76
Figure 5.10 BER-versus- E_b/N_0 using MMSE equalization with and without bit loading for known and unknown CSI under the indoor office test environment (a) channel A (b) channel B	79
Figure 5.11 BER-versus- E_b/N_0 using MMSE equalization with and without bit loading for known and unknown CSI under the outdoor to indoor pedestrian test environment (a) channel A (b) channel B	80
Figure 5.12 BER-versus- E_b/N_0 using MMSE equalization with and without bit loading for known and unknown CSI under the vehicular test environment (a) channel A (b) channel B	81
Figure 5.13 BER-versus- E_b/N_0 comparison between WPM and OFDM for the indoor office test environment (a) channel A (b) channel B	82
Figure 5.14 BER-versus- E_b/N_0 comparison between WPM and OFDM for the outdoor to indoor pedestrian test environment (a) channel A (b) channel B	83
Figure 5.15 BER-versus- E_b/N_0 comparison between WPM and OFDM for the vehicular test environment (a) channel A (b) channel B	84
Figure A.1 Block diagram for the MATLAB dwt command	95
Figure A.2 Block diagram for the MATLAB idwt command	95

LIST OF FIGURES (Continued)

	Page
Figure A.3 Block diagram for the modified idwt command	97
Figure A.4 Block diagram for the modified dwt command	97



CHAPTER 1

INTRODUCTION

1.1 Background

Multi-carrier modulation (MCM) has been extensively used to satisfy the tremendously increasing demand of high data rates. Orthogonal frequency division multiplexing (OFDM) is a widely used MCM, which is adopted by many applications. However, OFDM suffers from certain limitations such as high signal peak-to-average power ratios (PAPRs), reduction in data rates due to the use of cyclic prefix (CP), and the need of complex multiplication even for applications using real signals. Due to these limitations, many alternatives to OFDM have been proposed, among which wavelet packet modulation (WPM) has been introduced as a potential candidate in several literatures (Bouwel, Potemans, Schepers, Nauwelaers, & Capelle, 2000), (Gautier, Arndt, & Lienard, 2007), (Habibi, 1995), (Lindsey, 1997), and (Negash & Nikookar, 2000).

The attributes that differ WPM from OFDM have been highlighted in (Torun, Lakshmanan, & Nikookar, 2009) and (Jamin & Mahonen, 2005). Firstly, OFDM is based on the Fourier transform, which employs the inverse fast Fourier transform (IFFT) at the transmitter and the fast Fourier transform (FFT) at the receiver. On the other hand, WPM is based on the wavelet transform, which uses the inverse discrete wavelet packet transform (IDWPT) at the transmitter and the discrete wavelet packet transform (DWPT) at the receiver. Secondly, the output length of IFFT is equal to the input length. Therefore, the length of a discrete-time signal for one OFDM symbol is equal to the input length or the number of subcarriers. However, the output length of IDWPT is larger than the input length, resulting in a discrete-time signal for one WPM symbol being longer than the input length or the number of subcarriers. Accordingly, there is overlapping between successive WPM symbols in

the time domain, while there is no such overlap in the case of OFDM. Thirdly, the output of IFFT is normally complex. Therefore, for applications where real signals are required, additional signal processing techniques, such as Hermitian symmetry or complex conjugate, are required to obtain real signals. On the contrary, the output of IDWPT is real, and does not require any additional signal processing technique to generate real signals. Hence, WPM can be more favorable for applications using real signals as compared to OFDM. Fourthly, IFFT is based on a fixed computational structure while IDWPT is based on a flexible filter-tree structure, which allows for easy reconfiguration of the subcarrier parameters, such as the number of subcarriers and the bandwidth of each subcarrier, depending on the changing channel state information (CSI) and required data rates. Lastly, OFDM symbols are shorter and non-overlapping in the time domain, whereas WPM symbols are comparatively longer and overlapping in the time domain. Therefore, OFDM symbols have higher spectral side lobes and higher interference as compared to WPM symbols.

With the MCM, signal processing techniques such as equalization and bit loading are often used to enhance the bit error rate (BER) performance. In the case of OFDM, since it has non-overlapping symbols in the time domain, equalization could be achieved by the use of cyclic prefix (CP), which facilitates equalization using a single-tap filter on each subcarrier, also known as one-tap equalization. However, due to overlapping WPM symbols in the time domain, equalization for WPM cannot depend on the use of CP. Many literatures have investigated equalization for WPM, which can be performed either in the time domain as mentioned in (Gracias & Reddy, 1998), (Bajpai, Lakshmanan, & Nikookar, 2011), (Khan, Baig, & J.Mughal, 2009), (Mohammadi, Saadane, Wahbi, & Aboutajdine, 2010), or in the frequency domain as studied by (Jamin & Mahonen, 2005), (Gupta & Tiwari, 2013). In (Jamin & Mahonen, 2005), it is highlighted that equalization in the frequency domain suffers from high computational complexity due to a combined time-frequency structure, as compared to time-domain equalization. Therefore, to reduce the computational complexity, this

research considers minimum-mean square error (MMSE) equalization in the time domain based on the fundamentals provided in (Johnson, Sethares, & Kelvin, 2011) and (Proakis & Salehi, 2008).

MMSE equalization is normally not perfect and induces noise amplification and subcarrier signal attenuation. In addition to equalization, bit loading is one of the signal processing techniques that could be used to further enhance the BER performance. There are few literatures on bit loading for WPM (Ren & Zhu, 2005) and (Chang, Lay, & Chen, 2001). However, the studies performed so far have not provided a concrete approach to perform bit loading for WPM while considering time-domain equalization. Therefore, this research investigates and provides a bit loading algorithm for WPM, considering MMSE equalization in the time domain. The proposed bit loading algorithm also takes into account noise amplification and signal attenuation induced from the imperfection of the MMSE equalization.

This research investigates the BER performance of WPM with bit loading using MMSE equalization with known CSI as well as with unknown CSI. In the case of known CSI, mathematical expressions for computing the BER performance are derived. The derived analytical expressions are first validated with the simulation results obtained from the program using MATLAB. After validation, analytical expressions are used to compare the BER performances of WPM using MMSE equalization with and without bit loading. Further, the derived BER expressions are also used to compare the BER performance of WPM with bit loading with the BER performance of OFDM with bit loading. In the case of WPM, MMSE equalization with bit loading is used while in the case of OFDM, one-tap equalization with bit loading is used.

For the case of unknown CSI, initially, investigation is performed to find the additional overhead from the training sequence lengths required to estimate the channel impulse response (CIR) such that the BER performances with unknown CSI are acceptable and comparable to the case of known CSI. The investigation considers

WPM with MMSE equalization but without bit loading. The simulation study is performed for different lengths of subcarriers, i.e., 16, 32, and 64 subcarriers. The BER performance of WPM with MMSE equalization is also compared with the BER performance of OFDM with one-tap equalization, assuming that the CSI is unknown. The proposed bit loading algorithm requires the knowledge of CIR. Therefore, to perform bit loading for WPM while CSI is unknown, a channel estimation approach using the solution of an overdetermined system of linear equations is proposed based on (Gentle, 2007). The estimated CIR is then used to perform bit loading for WPM. The BER performance of WPM with bit loading is compared with the BER performance of WPM without bit loading. Finally, the BER performance of WPM with bit loading is compared with the BER performance of OFDM with bit loading.

1.2 Objectives

The main objectives of this research are listed below.

1. This research focuses on designing and evaluating equalization and bit loading algorithms for WPM considering known CSI and unknown CSI.
2. For WPM with known CSI, this research aims to make following investigations:
 - (a) This research provides BER expressions for WPM using bit loading along with time-domain equalization.
 - (b) The analytical BER expressions are validated with simulation results obtained from the program developed using MATLAB.
 - (c) The analytical expressions are used to study the benefits of bit loading.
 - (d) The BER performance of WPM is compared with the BER performance of OFDM.
3. For WPM with unknown CSI, the following studies are performed:

- (a) This research analyzes the overhead required for training sequences to achieve acceptable BER performances.
- (b) This research provides a CIR estimation approach based on the solution of an overdetermined system of linear equations.
- (c) This research quantifies the BER performances of WPM with bit loading using the estimated CIR and compares them with the BER performances of OFDM.

1.3 Scope and Limitations

This research relies on theoretical investigations and simulation studies. This research involves the derivation of mathematical expressions, which are verified with simulation results obtained from the program developed using MATLAB. However, the research does not involve any actual experiments involving physical equipments.

The research mainly focuses on WPM as a MCM technique and provides a comparative study with OFDM, which is the well known MCM technique. However, this research does not include other MCM techniques such as the filter bank-based multi-carrier (FBMC) technique.

1.4 Thesis Outlines

This thesis starts, in chapter 1, with the general background of WPM and its features, which provides motivation for the research. In chapter 2, basic definitions, background information, and relevant related works are presented. In chapter 3, the system model is introduced. Based on this system model, simulations and theoretical analysis are carried out. This chapter also presents the MMSE equalization and the proposed bit loading algorithm. The derivations of mathematical expressions for the BER performances and simulation studies for known CSI are presented in chapter 4. In chapter 5, investigations with unknown CSI are performed. Finally, chapter 5

provides a conclusion and suggestions for future research.



CHAPTER 2

LITERATURE REVIEW

2.1 Wavelets

A sinusoidal signal is theoretically extended in the time domain from minus to plus infinity. Unlike a sinusoidal signal, a wavelet is a waveform of a limited duration with its energy concentrated in time. A sinusoidal signal is smooth and predictable. Therefore, it is more suitable for representing stationary signals with a constant frequency. However, wavelets are irregular waveforms with limited durations and are non-symmetric. Hence, they are more suitable for representing non-stationary signals (Fugal, 2009). For instance, Fig. 2.1 (a) shows a portion of an infinitely long sinusoidal signal, Fig. 2.1 (b) shows a Daubechies-20 wavelet, and Fig. 2.1 (c) shows a Haar wavelet.

2.2 Wavelet Transform

The Fourier transform is a popular method to transform a time-domain signal to the frequency domain to obtain the frequency information of the signal. However, the frequency-domain representation of a signal cannot provide the time of

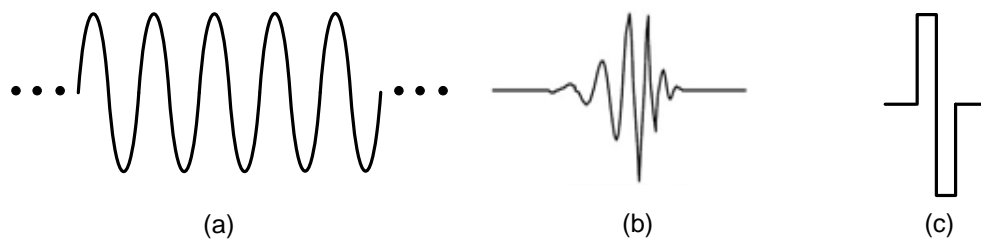


Figure 2.1: (a) Sinusoidal wave (b) Daubechies-20 wavelet (c) Haar wavelet (Fugal, 2009)

occurrence of frequencies, i.e., the Fourier transform cannot provide the time information. The time-frequency structure for the time-domain signal is shown in Fig. 2.2 (a). The equivalent frequency-domain signal can be obtained using the Fourier transform and the time-frequency structure as shown in Fig. 2.2 (b).

A time-domain continuous-time signal $x(t)$ provides the time-domain information, such as the amplitude of the signal at any time instance t . However, it does not provide the information about the frequency contents of $x(t)$. On the other hand, the frequency spectrum $X(f)$ of the signal $x(t)$, derived from the Fourier transform, contains information of the signal in the frequency domain, such as the magnitude and phase of the frequency component at each particular frequency f . However, the frequency spectrum cannot provide the temporal characteristics of the signal, such as the time instance when the frequency component appears. Therefore, $x(t)$ in time domain and $X(f)$ in frequency domain can provide either temporal information or the spectral information, but cannot provide both the time and frequency information of the signal.

One possible solution to obtain both the temporal and spectral information of the signal is short-time Fourier transform (STFT), which is also known as the windowed Fourier transform. In STFT, instead of computing the Fourier transform of the time-domain signal $x(t)$ directly, the signal $x(t)$ is first truncated by a time window $\lambda(t)$ with zero values outside specific time duration T , such as a square or Gaussian window. The truncated signal $x_\lambda(t)$ is then transformed to the frequency domain. The characteristic of the frequency spectrum thus obtained is contained within the interval T of the time window used for truncating the signal $x(t)$. The windowed signal in the time domain can be expressed as

$$x_\lambda(t) = x(t)\lambda(t) \quad (2.1)$$

The corresponding frequency-domain representation can be obtained based on the

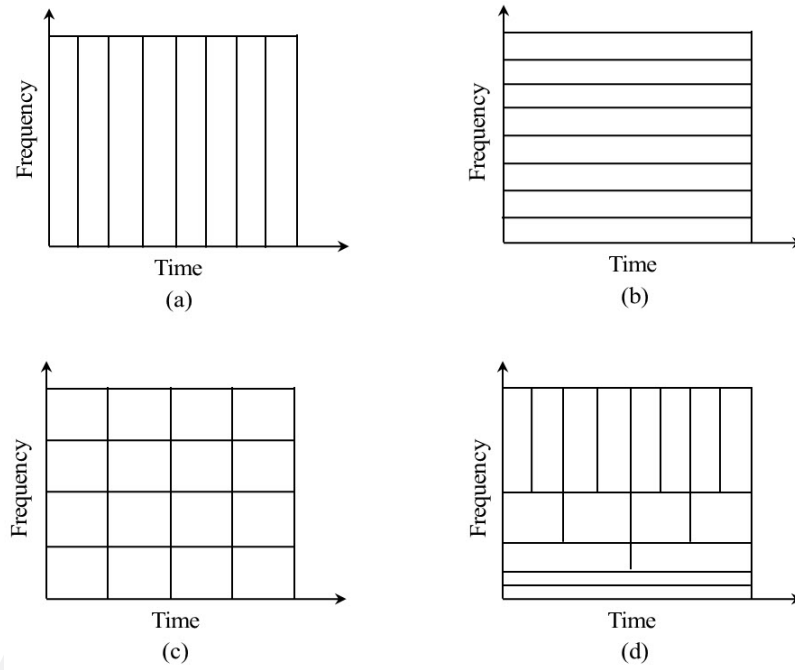


Figure 2.2: Time-frequency representation of signal transforms (a) time domain signal (b) Fourier transform (c) short-time Fourier transform (d) wavelet transform

convolution theorem of the Fourier transform as

$$X_{\lambda}(f) = X(f) * \Lambda(f) \quad (2.2)$$

where $X_{\lambda}(f)$ and $\Lambda(f)$ are the frequency spectra of $x_{\lambda}(t)$ and $\lambda(t)$ obtained through the Fourier transform. All the frequency components of the windowed signal $x_{\lambda}(t)$ are contained in the spectrum $X_{\lambda}(f)$. The temporal resolution of $x_{\lambda}(t)$ can be increased by reducing the duration T of each time window. However, with a reduction of the time window, the spectral resolution of the spectrum $X_{\lambda}(f)$ is reduced. This leads to a blurred version of the original signal spectrum $X(f)$ due to the convolution with the spectrum $\Lambda(f)$ of the time window. Moreover, it can be seen that while the temporal resolution is increased by reducing the duration of time window, the spectral resolution is reduced due to the expanded spectrum $\Lambda(f)$. Similarly, if the spectrum of

$\Lambda(f)$ is reduced for increasing the frequency resolution, the duration of the time window increases, resulting in a reduction in temporal resolution.

For a signal $x(t)$, consider that the time window $\lambda(t)$ with center τ is used to obtain the windowed signal $x(t)\lambda(t - \tau)$. The Fourier transform of this windowed signal yields the STFT (Rioul & Vetterli, 1991).

$$\text{STFT}(f, \tau) = \int x(t)\lambda(t - \tau)e^{-j2\pi ft} dt \quad (2.3)$$

The time-frequency structure of STFT is shown in Fig. 2.2 (c). In STFT, the duration of each time window is fixed, so the time-frequency resolution is also fixed across the time-frequency plane. To overcome this limitation of a fixed time-frequency resolution, the time resolution and frequency resolution can be varied in the time-frequency plane to obtain a multi-resolution analysis. This can be achieved by continuous wavelet transform (CWT). In CWT, a signal is represented in terms of a wavelet basis function known as the mother wavelet $\varphi(t)$, by continuous scaling and translation of the mother wavelet. The scale parameter u represents the broadening and narrowing factor for the duration of a time window, and the translation parameter v represents the shifting of a time window. The mother wavelet can be written as (Burrus, Gopinath, & Guo, 1998)

$$\varphi_{u,v}(t) = \frac{1}{\sqrt{|u|}} \varphi\left(\frac{t - v}{u}\right) \quad (2.4)$$

Here, the constant $\frac{1}{\sqrt{|u|}}$ is used for energy normalization. Based on this, CWT can be expressed as (Burrus et al., 1998)

$$\text{CWT}(u, v) = \frac{1}{\sqrt{|u|}} \int x(t) \varphi\left(\frac{t - v}{u}\right) dt = \int x(t) \varphi_{u,v}(t) dt \quad (2.5)$$

Unlike CWT, if the scaling and translation is performed in discrete steps, it

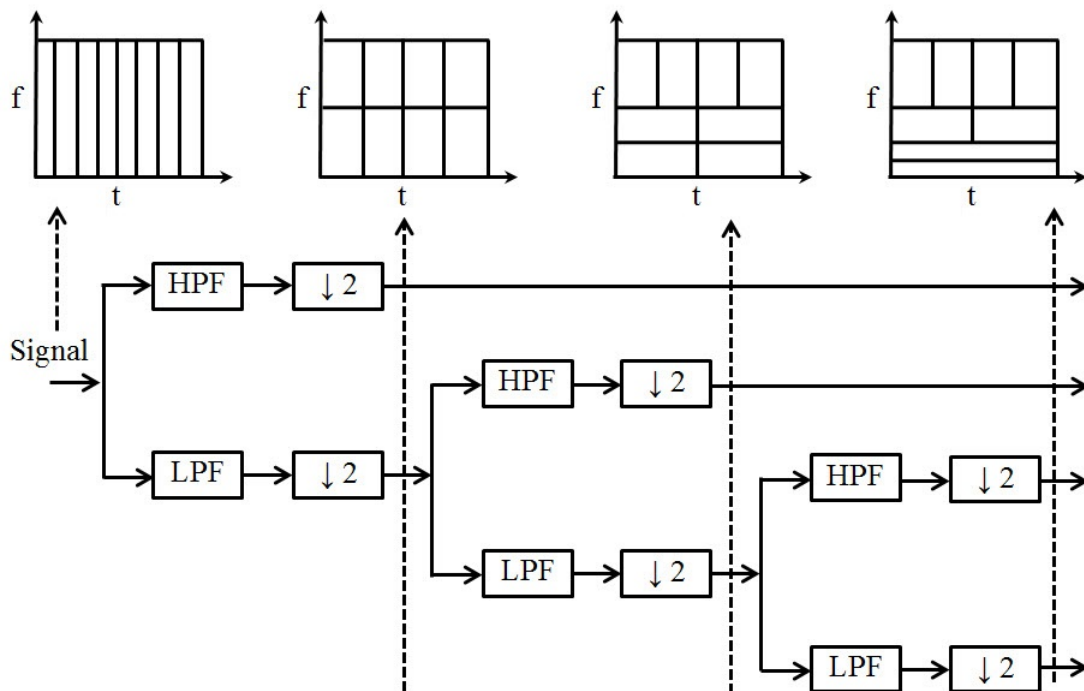


Figure 2.3: Subband filtering

is known as Discrete Wavelet Transform (DWT). DWT can be realized from banks of matched low-pass filters (LPFs) and high-pass filters (HPFs) by subband filtering.

In subband filtering, the time-domain signal is passed through a series of HPF and LPF to separate high frequency components and low frequency components. The outputs of HPF and LPF are downsampled by a factor of 2, which is indicated by $\downarrow 2$ in Fig. 2.3. The output of HPF is not further decomposed, so that it can have higher number of samples, resulting in higher time resolution. The output of LPF is further decomposed into successive high frequency components and low frequency components using HPF and LPF, which are followed by downsampling by a factor of 2. This process can continue until no samples of signals are available for further decomposition. In Fig. 2.3, 8 samples are considered. Therefore, the signal decomposition could be up to 3 levels ($2^3 = 8$). Fig. 2.3 also shows the time-frequency representation of the signal after each level of decomposition. The

result obtained at the final output is associated with time windows with variable time durations, with more samples at high frequency (high time resolution) and less samples at lower frequency (low time resolution). In Fig. 2.2 (d), the time-frequency structure for DWT with 16 samples is shown.

2.3 Filter and Filter Banks

The basic building blocks of the DWT are LPFs and HPFs. The coefficients of each LPF and each HPF are called approximate coefficients and detailed coefficients respectively (Abdullah & Hussain, 2009). These filters need to be normal and orthogonal with each other to perform the wavelet transform. This means that these filters need to form an orthonormal basis. Let vector \mathbf{g} contain the coefficients of the LPF and vector \mathbf{h} contain the coefficients of the HPF. Then, the orthonormal conditions that these filters need to satisfy can be represented as (Abdullah & Hussain, 2009)

$$\langle \mathbf{g}, \mathbf{g} \rangle = 1 \quad (2.6)$$

$$\langle \mathbf{h}, \mathbf{h} \rangle = 1 \quad (2.7)$$

$$\langle \mathbf{g}, \mathbf{h} \rangle = 0 \quad (2.8)$$

Here, $\langle \mathbf{g}, \mathbf{h} \rangle$ indicates the inner product of vectors \mathbf{g} and \mathbf{h} , where $\langle \mathbf{g}, \mathbf{h} \rangle = \sum_n g_n h_n^*$. Further, (2.6) and (2.7) refers to the normality requirement while (2.8) refers to orthogonality requirement. The filter coefficients satisfying these requirements can be used to perform the DWT.

DWT is implemented by a series of LPFs and HPFs which form the filter bank. There are mainly two types of filter banks, namely, analysis filter bank and

synthesis filter bank. An analysis filter is also known as a decomposition filter, which decomposes the signal into a number of subbands in a dyadic fashion at each level of DWT. This process is known as the analysis or decomposition process. On the contrary, the reverse operation is performed on a synthesis filter, which is also known as a reconstruction filter. The outputs of synthesis or reconstruction filters are combined at successive levels of IDWT to obtain the original signal. This process is known as the synthesis or reconstruction process. Let g_n^d and h_n^d be the analysis or decomposition LPF and HPF respectively. Similarly, let g_n^r and h_n^r be the synthesis or reconstruction LPF and HPF respectively. Let F be the filter length. These filter pairs are related to each other as (Burrus et al., 1998)

$$h_n^d = (-1)^n g_{F-1-n}^d \quad (2.9)$$

$$h_n^r = h_{F-1-n}^d \quad (2.10)$$

$$g_n^r = g_{F-1-n}^d \quad (2.11)$$

The analysis and synthesis process is shown in Fig. 2.4. The input signal is passed through the set of analysis LPFs and HPFs. It is equivalent to computing the convolution of the input signal with the coefficients of the analysis LPF and HPF. Each filter removes half of the input signal, either high frequency components by an LPF or low frequency components by an HPF. Therefore, in either case, half of the data are redundant and could be discarded. This is achieved by downsampling by a factor of 2. The reverse operation of downsampling is performed at the synthesis process, i.e., upsampling by a factor of 2. This is followed by the synthesis LPF and HPF to recover the original signal.

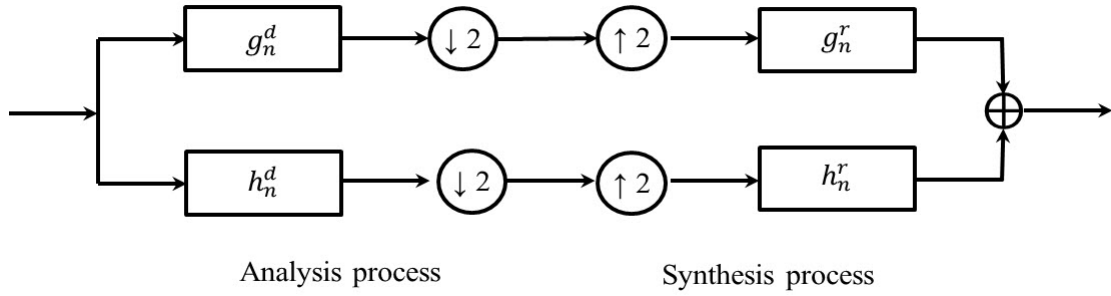


Figure 2.4: Analysis and synthesis process

2.4 DWT and IDWT

In DWT, the output of an HPF is kept intact, while the output of an LPF is decomposed at successive stages. The HPF output is passed through downsampling ($\downarrow 2$) and is not further decomposed. Therefore, it has a higher number of time samples with a higher time resolution. However, the output of an LPF after downsampling ($\downarrow 2$) is further passed through an LPF and an HPF, leading to a higher frequency resolution. The inverse operation of DWT is known as IDWT. In IDWT, the input signal is first upsampled by factor of 2 ($\uparrow 2$), and is passed through an LPF and an HPF. The output of an LPF and an HPF are combined at successive stages. At the final stage, the original signal is obtained. The DWT and IDWT with 2 stages are shown in Fig. 2.5. The bandwidth distribution of DWT with 2 stages is shown in Fig. 2.6. It can be seen that the bandwidth distribution is not uniform across the frequency, this is due to the fact that the output of an HPF is kept unchanged and only the output of an LPF is decomposed.

2.5 Wavelet Packet Modulation

In DWT, only the output of an LPF is further decomposed while the output of an HPF is left intact, so a higher subcarrier frequency corresponds to a higher bandwidth while a lower subcarrier frequency corresponds to a lower bandwidth. In

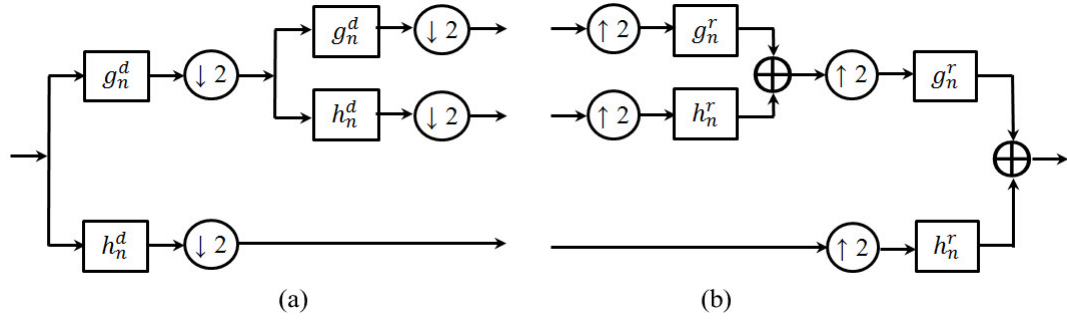


Figure 2.5: (a) DWT with 2 stages (b) IDWT with 2 stages

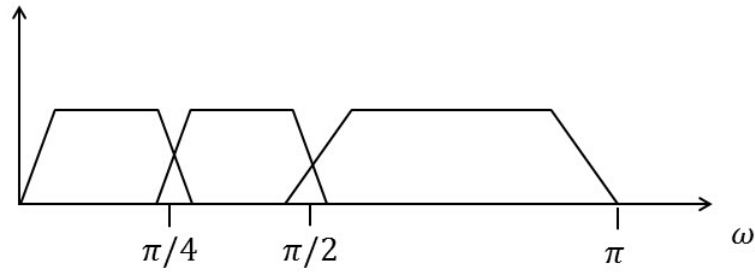


Figure 2.6: Bandwidth distribution of DWT

order to achieve the uniform bandwidth distribution across the frequency range, the output from an HPF can also be decomposed in the same fashion as the output from an LPF. This process is known as the discrete wavelet packet transform (DWPT). The inverse of DWPT is known as the inverse discrete wavelet packet transform (IDWPT). The MCM technique that uses DWPT and IDWPT is known as wavelet packet modulation (WPM). The block diagrams for 2 stages of IDWPT and DWPT are shown in Fig. 2.7 and Fig. 2.8. The frequency distribution for DWPT with 2 stages is shown in Fig. 2.9, which shows the uniform bandwidth distribution across the frequency range.

2.6 Multi-carrier Modulation

OFDM is a renowned MCM technique which is based on the Fourier transform. It uses the inverse transform, i.e., IFFT, at the transmitter and the forward

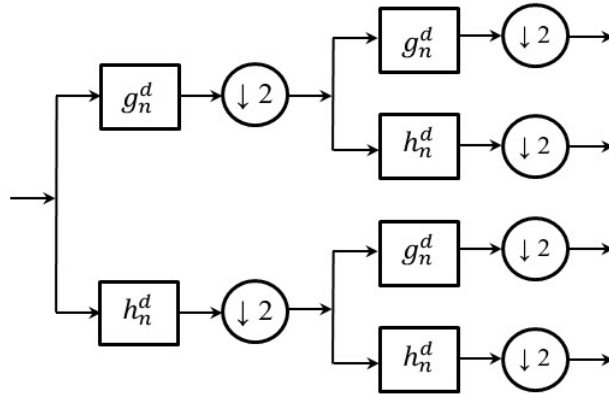


Figure 2.7: Discrete wavelet packet transform (DWPT)

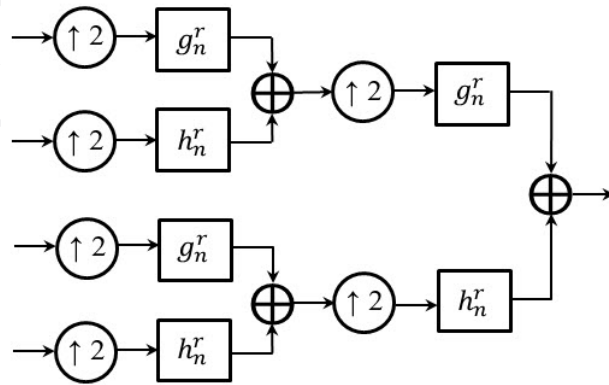


Figure 2.8: Inverse discrete wavelet packet transform (IDWPT)

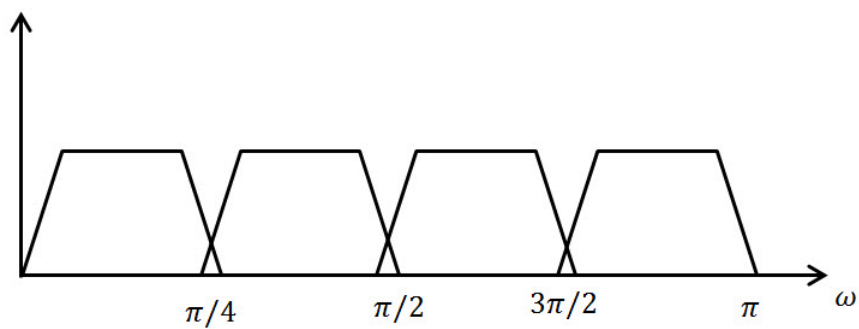


Figure 2.9: Bandwidth distribution of DWPT

transform, i.e., FFT, at the receiver. Likewise, WPM is also a MCM technique. However, it is based on the wavelet transform. WPM employs the inverse transform, i.e., IDWPT, at the transmitter and the forward transform, i.e., DWPT, at the receiver.

Like OFDM, WPM also generates orthogonal subcarriers. The key for generating orthogonal subcarriers lies on the use of a pair of quadrature mirror filters (QMFs). The QMF pair comprises of synthesis filters, which form the IDWPT used at the transmitter, and analysis filters, which forms the DWPT used at the receiver. The number of subcarriers is equal to the number of IDWPT inputs and depends on the number of synthesis or reconstruction stages of IDWPT. For n reconstruction stages, the number of IDWPT inputs or the number of subcarriers is equal to 2^n . The IDWPT with 8 subcarriers and the corresponding DWPT are shown in Fig. 2.10 and Fig. 2.11 respectively. It can be noticed that IDWPT and DWPT have 3 stages, resulting in 8 subcarriers.

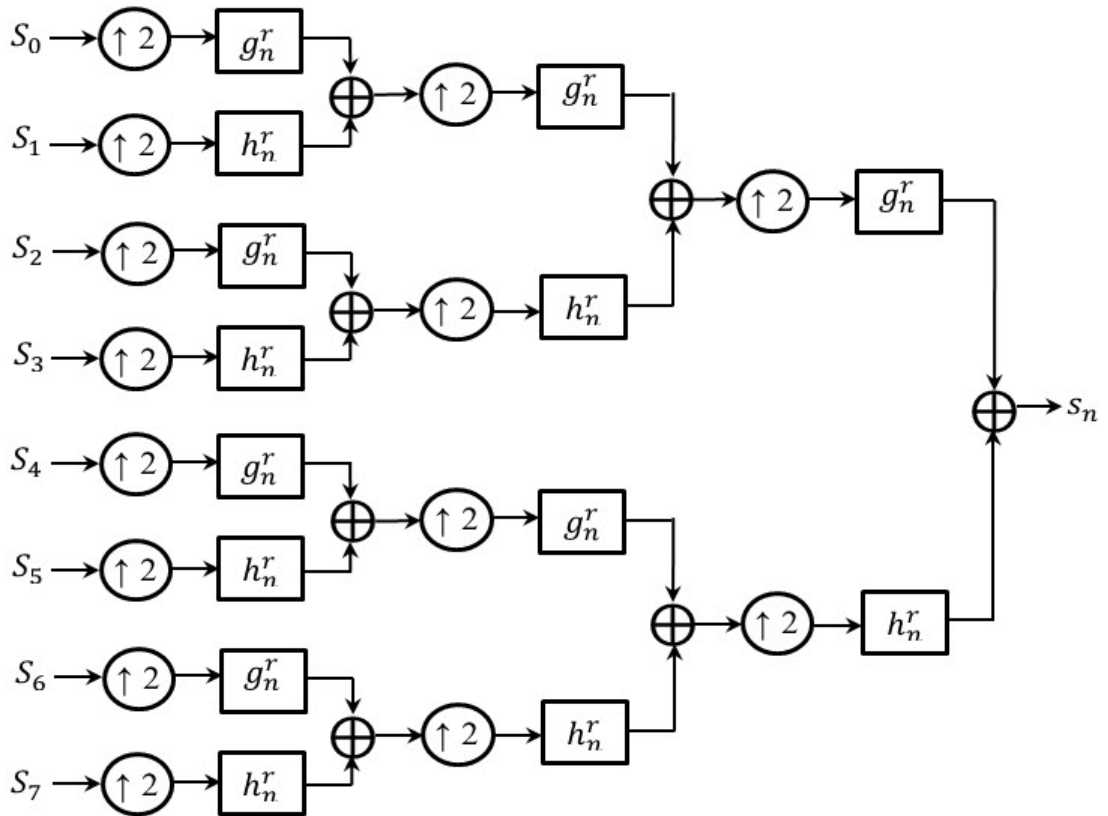


Figure 2.10: IDWPT with 8 subcarriers

Unlike OFDM, the output of the IDWPT is longer than the input. Therefore, successive WPM symbols overlap in the time domain. Because of this, WPM is also

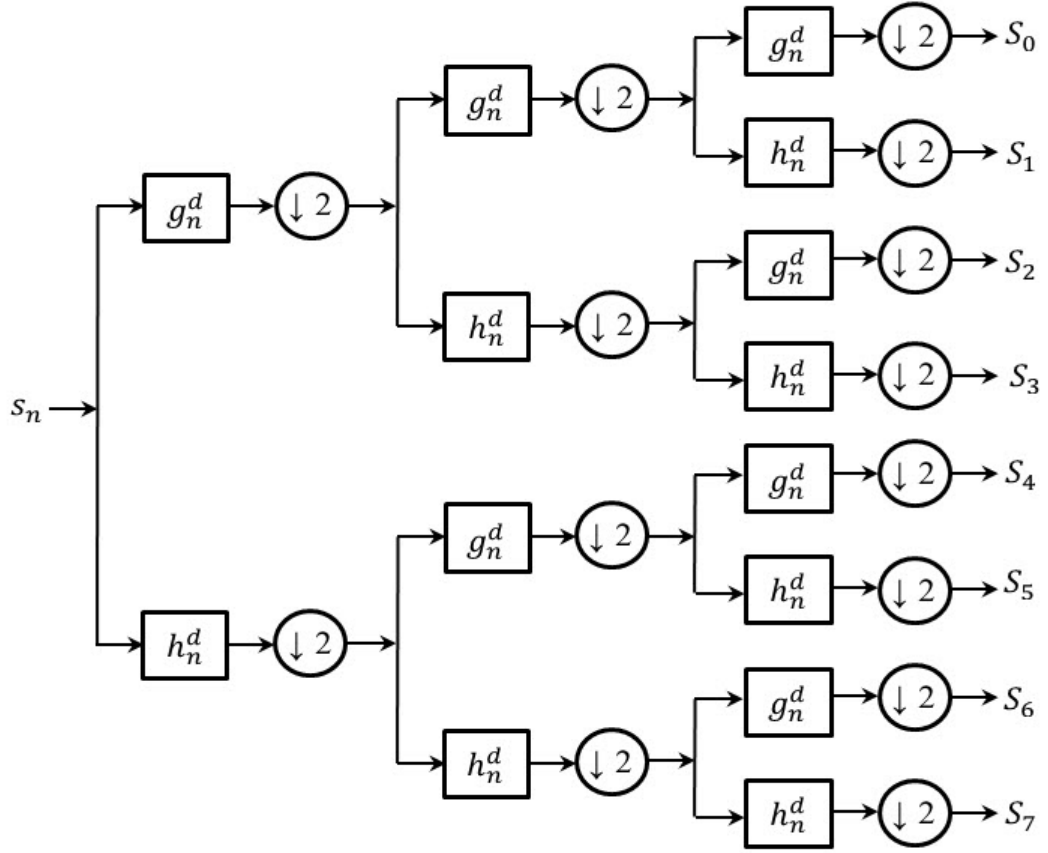


Figure 2.11: DWPT with 8 subcarriers

known as an overlapped transform. The output length of the IDWPT depends on the number of subcarriers and the length of the wavelet filter. For the wavelet filter length of F and the number of subcarriers equal to N , the length of a WPM symbol, denoted by L , can be expressed as (Burrus et al., 1998)

$$L = (N - 1)(F - 1) + 1 \quad (2.12)$$

2.7 Peak-to-Average Power Ratio for WPM

The peak-to-average power ratio (PAPR) is an important performance measure that defines the operating point of an amplifier. With a high PAPR, the operating point of an amplifier may reach beyond the normal operating region into the saturation region, resulting in signal distortion and inter-modulation interference. To

avoid such interference, a system with a high PAPR requires the use of amplifiers with wider operating ranges, which are normally more expensive. MCM normally suffers from high PAPRs. Although there are many studies performed to reduce the PAPR for OFDM, there are limited studies performed to reduce the PAPR for WPM (Torun et al., 2009), (Torun, Lakshmanan, & Nikookar, 2010), (Gautier et al., 2007), (Xian, Gewei, Ning, & Shuangxi, 2013), and (Zakaria & Salleh, 2016).

In (Torun et al., 2009), statistics of WPM signals and their power distributions are studied along with the impact on the PAPR from different wavelet families and wavelet filter lengths. The results show that orthogonal wavelets from different wavelet families have similar PAPR distributions that are also independent of the wavelet filter length. The authors have further extended this work to reduce the PAPR by generating a set of WPM frames with random phase shifts on subcarriers and selecting a set having the lowest PAPR (Torun et al., 2010). In (Gautier et al., 2007), it is shown that WPM reduces the PAPR significantly as compared to OFDM for low numbers of subcarriers, while for high numbers of subcarriers both modulations have similar PAPR performances. A tree pruning approach along with partial transmit sequences (PTSs) is implemented to reduce the PAPR for WPM in (Xian et al., 2013). This approach helps reduce the PAPR by more than 1 dB. Likewise, the PTS approach combined with the embedded side information (ESI) to the transmit frame is investigated to reduce the PAPR for WPM in (Zakaria & Salleh, 2016). This technique helps reduce the PAPR by 2.5 dB.

Similar to the tree pruning approach (Xian et al., 2013), PAPR reduction can be achieved by exploiting the flexible filter-tree structure of IDWPT used for generating time-domain WPM symbols. The approach is useful in heterogeneous communication environments, with high data-rate and low data-rate devices sharing the same transmission resources. In such scenarios, devices operating with high data rates can be assigned larger numbers of subcarriers as compared with devices operating with low data rates. For simplicity, an example case study with 16

subcarriers is illustrated, considering three devices with high data rates and four devices with low data rates. Fig. 2.12 shows the filter-tree structure of WPM without subcarrier combining and with equal bandwidth allocation to all subcarriers. The corresponding time-frequency structure of WPM is shown in Fig. 2.13. This resource utilization is similar to the case of OFDM with IFFT and FFT as the forward and inverse transforms.

In case of WPM, subcarrier combining can be realized, resulting in a modified time-frequency structure. However, this subcarrier combining is not feasible in case of OFDM. Subcarrier combining for WPM yields a higher subcarrier bandwidth with shorter symbol durations. Subcarrier combining results in reducing the number of subcarriers and ultimately reducing the PAPR. Following the example in Fig. 2.12, consider that four subcarriers are allocated to each of the three high-rate devices, and one subcarrier to each of the four low-rate devices. Each group of four subcarriers allocated to a high-rate device are combined into a single combined subcarrier. The corresponding filter-tree structure and time-frequency structure are shown in Fig. 2.14 and Fig. 2.15 respectively.

Simulation is performed to compare the cumulative distribution functions (CDFs) of the PAPRs for WPM without subcarrier combining, WPM with subcarrier combining, and OFDM. CDF plots are obtained using 64 subcarriers and shown in Fig. 2.16. Although the PAPRs for WPM without subcarrier combining and OFDM are almost the same, WPM with subcarrier combining has significantly lower PAPRs. The results reflect that the subcarrier combining feature in WPM is advantageous in reducing the PAPR for heterogeneous communication environments.

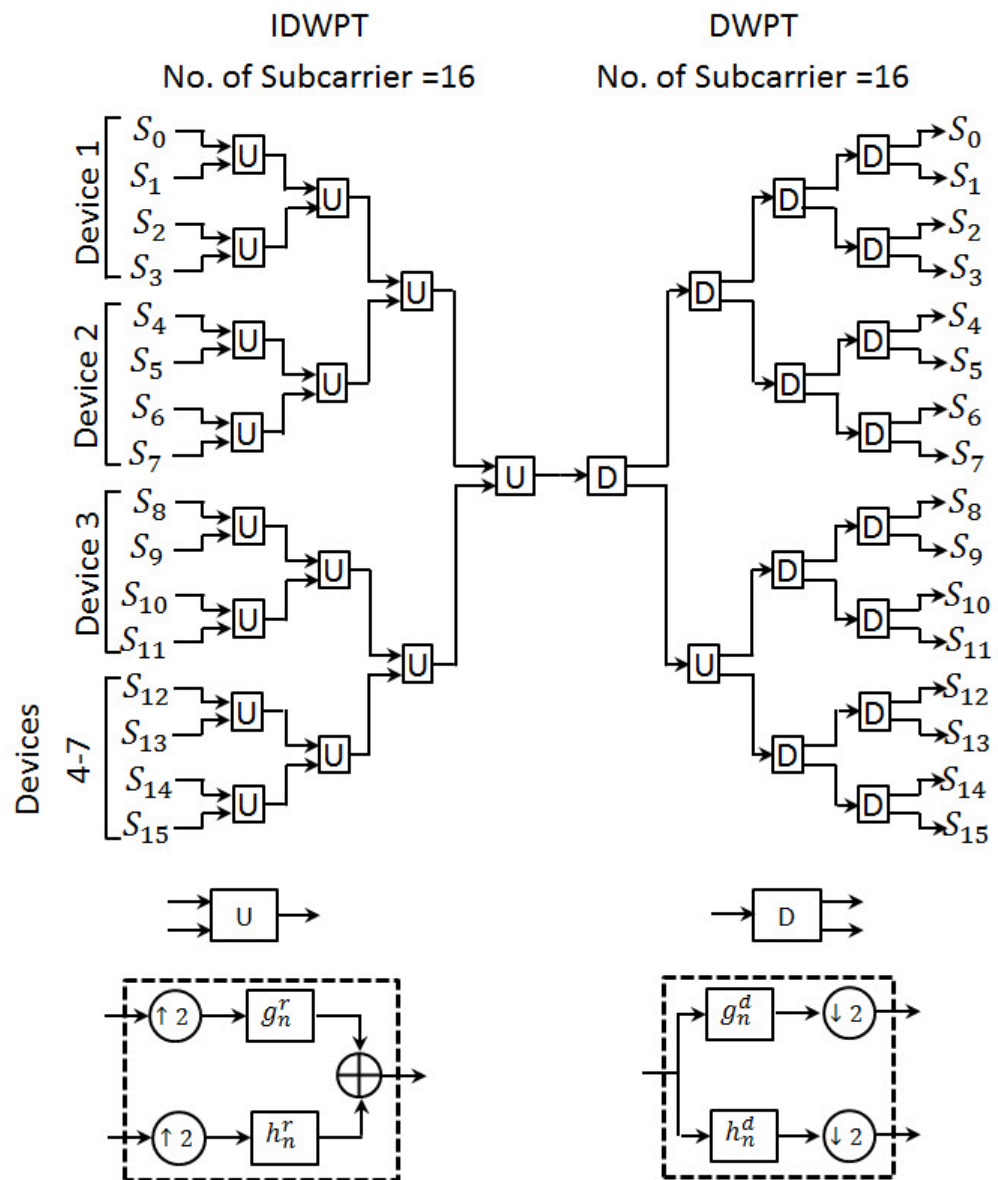


Figure 2.12: Tree structure of WPM for 16 subcarriers without subcarrier combining

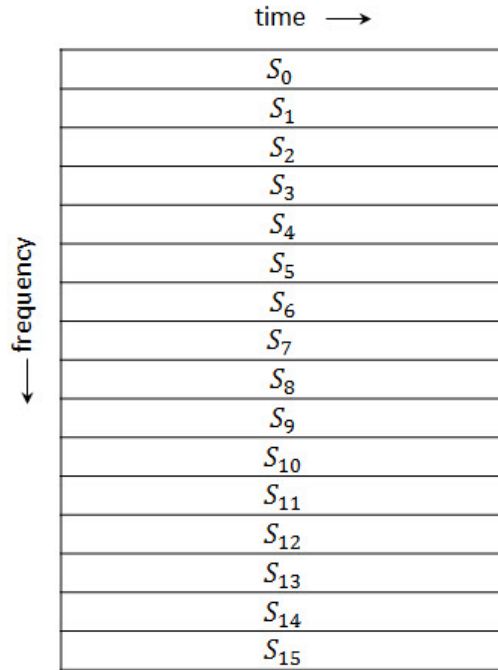


Figure 2.13: Time-frequency structure of WPM for 16 subcarriers without subcarrier combining

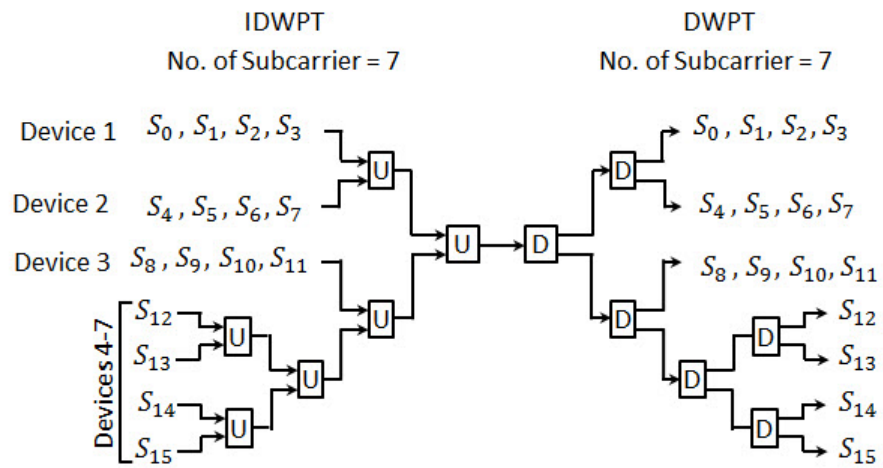


Figure 2.14: Tree structure of WPM for 16 subcarriers with subcarrier combining

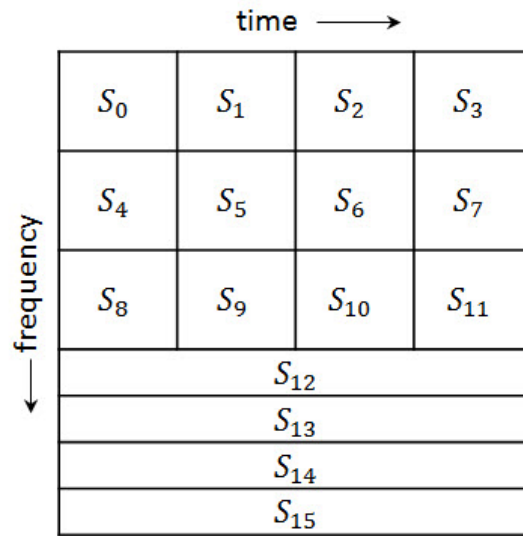


Figure 2.15: Time-frequency structure of WPM for 16 subcarriers with subcarrier combining

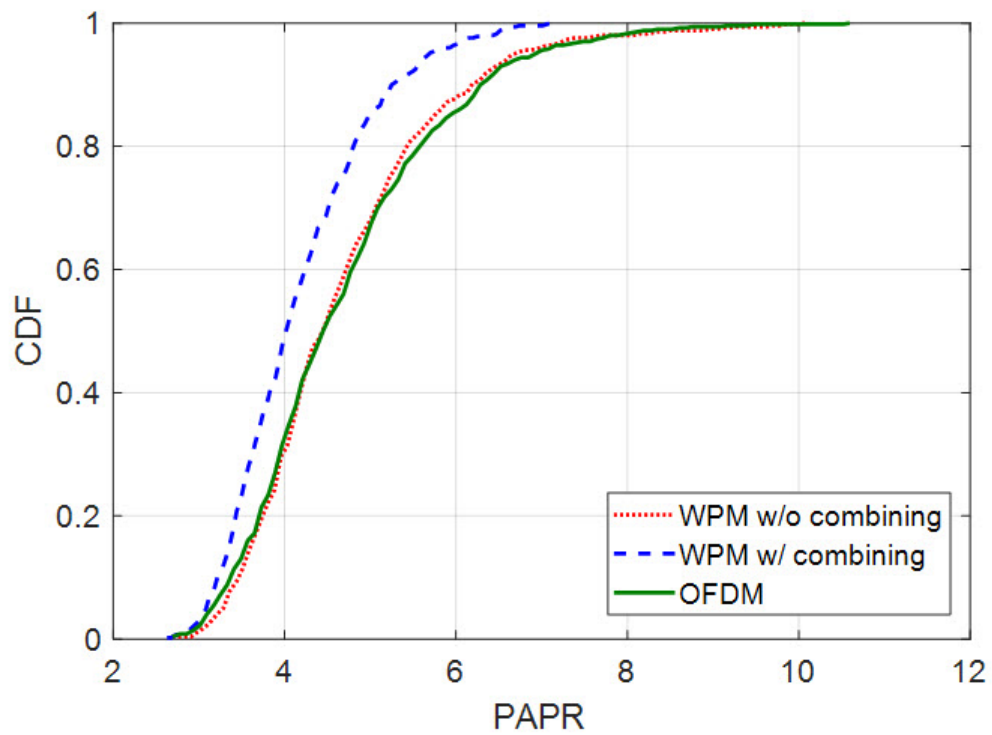


Figure 2.16: CDF plots for PAPRs of WPM without subcarrier combining, WPM with subcarrier combining, and OFDM

2.8 Discussion of Related Works

For MCM, signal processing techniques such as equalization and bit loading can be implemented to reduce the BERs. The equalization process involves the use of an equalizer filter that tries to reduce the impact of channel distortions. Equalization in OFDM can be performed through the use of CP because OFDM symbols do not overlap in the time domain. However, since WPM symbols overlap in the time domain, the use of CP is not possible for WPM. Equalization for WPM can be performed at the receiver, either in the time domain before the forward transform, i.e., DWPT, or in the frequency domain after DWPT. The literatures that explore time-domain equalization for WPM are (Gracias & Reddy, 1998), (Bajpai et al., 2011), (Khan et al., 2009), and (Mohammadi et al., 2010). Similarly, equalization for WPM in the frequency domain is studied in (Jamin & Mahonen, 2005), and (Gupta & Tiwari, 2013). These analyses consider both scenarios of known CSI and unknown CSI.

In (Gracias & Reddy, 1998), a non-ideal channel with known CSI is considered, with different subbands, i.e., subcarriers, each of which can be characterized by attenuation and delay. These subbands are represented by narrowband and orthonormal wavelets, which encounter delay and attenuation. Equalization is thus reduced to estimating delay and attenuation induced by the channel to each WPM symbol. An algorithm called minimum square variance (MSV) is applied to reduce inter-symbol interference (ISI) using the variance of the demodulated output. This approach suffers from high computational complexity when the number of subcarriers increases. Time-domain equalization for WPM using the peak distortion criterion to reduce the maximum ISI is proposed in (Bajpai et al., 2011). It also explores the impact of different wavelet families, wavelet filter lengths, and numbers of equalizer taps on the equalization performance. This method is limited to removal of ISI and not removal of inter-carrier interference (ICI). In (Khan

et al., 2009), a frequency-domain zero forcing (ZF) equalizer and a time-domain MMSE equalizer are proposed for WPM. The investigation considers known CSI. A comparative study is made among time-domain MMSE equalization, frequency-domain ZF equalization, and OFDM with CP. The results show that WPM with time-domain MMSE equalization is better than WPM with frequency-domain ZF equalization, as well as better than OFDM employing a CP with one-tap equalization. In (Jamin & Mahonen, 2005), equalization for WPM in the frequency domain is analyzed. However, the investigation points out that frequency-domain equalization needs a combined time-frequency equalization structure, making it more complicated as compared with equalization performed in the time domain.

In (Mohammadi et al., 2010) and (Gupta & Tiwari, 2013), equalization for WPM with unknown CSI is proposed based on the ZF and MMSE criteria. In (Mohammadi et al., 2010), channel estimation is accomplished using the least square (LS) method while equalization is implemented in the time domain. Numerical results demonstrate that LS channel estimation can provide the BER performance comparable to the BER performance with known CSI. However, the investigation does not include any random fading and is confined to static channels only. In addition, the proposed method requires a training sequence of 100 symbols, which increases the computational complexity tremendously. Frequency-domain equalization schemes with channel estimation accomplished by the LS and MMSE criteria are presented in (Gupta & Tiwari, 2013). Training sequences for channel estimation are transmitted through pilot carriers. Numerical results demonstrate that MMSE based channel estimation is better than LS based channel estimation. Since the proposed approach employs frequency-domain equalization, it suffers from relatively high computational complexity.

Frequency selective channels normally have non-uniform distributions of channel distortion across the subcarriers in MCM. Therefore, some subcarriers are less affected while other subcarriers are more affected by channel distortion. Hence,

transmitting more bits through subcarriers that are less affected by channel distortion can help to enhance the BER performance. This approach to allocate more bits to subcarriers that are less affected by channel distortion for a better BER performance is known as bit loading. Bit loading for WPM is explored in (Ren & Zhu, 2005) and (Chang et al., 2001). In (Ren & Zhu, 2005), bit loading is performed, following the channel variation across subcarriers, to achieve a target BER performance with the minimum total transmit power. However, the proposed scheme does not include any equalization method or any other signal processing technique to overcome ISI resulting from channel distortion. In (Chang et al., 2001), bit loading is done along with a unitary mapping filter employed to eliminate ICI. In addition, guard chips are inserted between successive WPM symbols to remove ISI. This method is similar to zero padding at the end of each WPM symbol. However, this approach suffers from large overhead due to zero padding for long WPM symbols.

CHAPTER 3

SYSTEM MODEL

3.1 WPM System Block Diagram

A WPM system block diagram with bit loading and time-domain MMSE equalization is presented in Fig. 3.1. Transmit bits are allocated to subcarriers using a bit loading algorithm, which may result in a non-uniform bit allocation on subcarriers. However, if the bit loading algorithm is not considered, all the subcarriers will have a uniform distribution of bits, which means the same symbol constellation used on all subcarriers. After bit loading, bits are fed to a serial-to-parallel converter followed by quadrature amplitude modulation (QAM) mapping, which generates WPM symbols in the time domain. These WPM symbols are transmitted through the channel. The transmitted WPM symbols are convolved with the channel impulse response (CIR) followed by the addition of additive white Gaussian noise (AWGN).

At the receiver, the received signal is passed through an equalization process to remove distortion from the channel. Since equalization is performed before the forward transform in the time domain, it is called time-domain equalization. The equalized signal is then forwarded to DWPT to obtain QAM symbols. The received QAM symbols are passed through QAM demapping and a serial-to-parallel converter to retrieve received bits. The received bits are compared with the transmitted bits and the difference between them will provide the BER.

Assume that QAM symbols S_k are input to IDWPT to generate the transmit WPM symbols s_n . Here, k represents the subcarrier index and n indicates the time index. Let N denote the number of subcarriers for each WPM symbol. Using the orthonormal expansion given in (Burrus et al., 1998), the transmitted WPM symbol can be written as

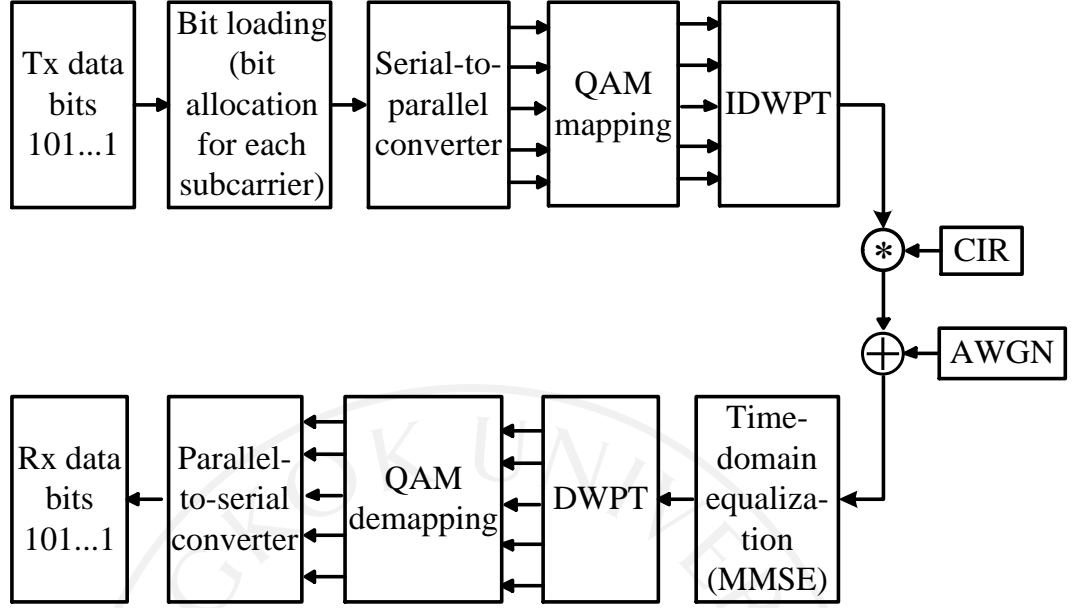


Figure 3.1: System block diagram for WPM

$$s_n = \sum_{k=0}^{N-1} S_k \phi_n^k \quad (3.1)$$

Here, the basis function of subcarrier k is denoted by ϕ_n^k . The orthonormal basis for each subcarrier k is equivalent to the IDWPT output in Fig. 3.1 obtained with $S_k = 1$ as the only nonzero input. Let us consider the CIR h_n with length C . In addition, let us consider AWGN w_n with mean zero and variance N_0 . With these assumptions, the received signal indicated by r_n can be expressed as

$$r_n = s_n * h_n + w_n \quad (3.2)$$

where the notation $*$ indicates the convolution operation. The received signal r_n is first equalized using a time-domain linear MMSE equalizer filter. The coefficients of the equalizer filter are represented by f_n . The equalization output provides the output signal y_n designated as

$$y_n = r_n * f_n \quad (3.3)$$

3.2 MMSE Equalization

Equalization is performed to remove or reduce the impact of interference, fading and distortion introduced by the channel. Equalization in OFDM is comparatively easier than WPM since OFDM can use a CP, allowing the implementation of one-tap equalization. However, since the IDWPT output is longer than its input or the number of subcarriers, successive WPM symbols overlap in the time domain. Hence, the use of a CP is not possible. This research uses linear MMSE equalizers operating in the time domain (Johnson et al., 2011) (Proakis & Salehi, 2008). Frequency-domain equalization requires a combined time-frequency structure that is substantially complex as compared to time-domain equalization (Jamin & Mahonen, 2005). Therefore, equalization is performed in the time domain instead of the frequency domain to reduce the computational complexity.

3.2.1 Unknown Channel

A method to compute the equalizer filter coefficients for an unknown channel is shown in Fig. 3.2 (Johnson et al., 2011). Here, a known training sequence is used, and can be estimated at the receiver with an appropriate delay. The training sequence is passed through the channel and AWGN is added. The received signal is fed to the equalizer. The difference between the equalizer output and the transmitted training signal defines the error, and the equalizer aims to reduce this error. Therefore, the equalizer filter coefficients can be computed in order to minimize the mean-square error (MSE) between the known training sequence and the equalized signal at the equalizer output.

The received signal after equalization can be represented as

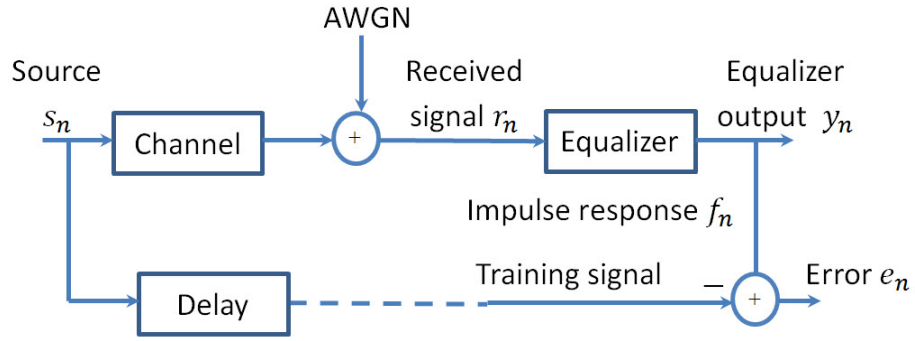


Figure 3.2: Process to obtain the equalizer filter coefficients

$$\mathbf{y} = \mathbf{R}\mathbf{f} \quad (3.4)$$

Here, \mathbf{f} represents a column vector with E equalizer coefficients and \mathbf{R} is a Toeplitz matrix written as

$$\mathbf{R} = \begin{bmatrix} r_{E-1} & r_{E-2} & \cdots & r_0 \\ r_E & r_{E-1} & \cdots & r_1 \\ r_{E+1} & r_E & \cdots & r_2 \\ \vdots & \vdots & \ddots & \vdots \\ r_{p-1} & r_{p-2} & \cdots & r_{p-E} \end{bmatrix} \quad (3.5)$$

where, p indicates the length of training sequence. The error \mathbf{e} between the equalized signal \mathbf{y} and the transmitted training sequence \mathbf{s} with some delay is computed as

$$\mathbf{e} = \mathbf{s} - \mathbf{y} \quad (3.6)$$

The MSE, denoted by J , is evaluated as

$$J = \mathbf{e}^T \mathbf{e} \quad (3.7)$$

Substituting \mathbf{e} from (3.6),

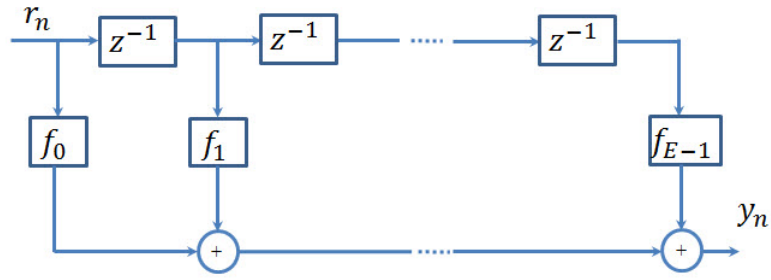


Figure 3.3: Tapped delay line structure for an FIR equalizer filter

$$\begin{aligned}
 J &= (\mathbf{s} - \mathbf{y})^T (\mathbf{s} - \mathbf{y}) \\
 &= \mathbf{s}^T \mathbf{s} - \mathbf{y}^T \mathbf{s} - \mathbf{s}^T \mathbf{y} + \mathbf{y}^T \mathbf{y} \\
 &= \mathbf{s}^T \mathbf{s} - 2\mathbf{y}^T \mathbf{s} + \mathbf{y}^T \mathbf{y}
 \end{aligned} \tag{3.8}$$

Substituting \mathbf{y} from (3.4),

$$\begin{aligned}
 J &= \mathbf{s}^T \mathbf{s} - 2(\mathbf{R}\mathbf{f})^T \mathbf{s} + (\mathbf{R}\mathbf{f})^T \mathbf{R}\mathbf{f} \\
 &= \mathbf{f}^T (\mathbf{R}^T \mathbf{R}) \mathbf{f} - 2(\mathbf{R}^T \mathbf{s})^T \mathbf{f} + \mathbf{s}^T \mathbf{s}
 \end{aligned} \tag{3.9}$$

The value of \mathbf{f} for which J is minimized can be obtained by

$$\nabla J = 2(\mathbf{R}^T \mathbf{R}) \mathbf{f} - 2(\mathbf{R}^T \mathbf{s}) = 0 \tag{3.10}$$

which yields

$$\mathbf{f} = (\mathbf{R}^T \mathbf{R})^{-1} \mathbf{R}^T \mathbf{s} \tag{3.11}$$

The equalizer thus obtained is an FIR filter with a tapped delay line structure and the filter impulse response (f_0, \dots, f_{E-1}) . The tapped delay line structure for the FIR equalizer filter is shown in Fig. 3.3.

The corresponding minimum value of J can be obtained as

$$J_{min} = \mathbf{s}^T [\mathbf{I} - \mathbf{R}(\mathbf{R}^T \mathbf{R}^{-1}) \mathbf{R}^T] \mathbf{s} \quad (3.12)$$

3.2.2 Known Channel

If the CIR is known, the equalizer coefficients can be derived using the theoretical analysis in (Proakis & Salehi, 2008). Consider the transmitted symbols s_n that are independent and identically distributed (IID) with energy per symbol E_s equal to one. Suppose that equalizer filter consists of $E = 2K + 1$ equalizer coefficients f_{-K}, \dots, f_K . Here, for convenience the number of equalizer coefficients is expressed in terms of K , which denotes the number of signal values around the symbol of interest. Suppose that the equalized signal, indicated by \hat{s}_n , is given as

$$\begin{aligned} \hat{s}_n &= f_n * r_n \\ &= f_n * (h_n * s_n + w_n) \end{aligned} \quad (3.13)$$

From the orthogonality principle, i.e., $E[(s_n - \hat{s}_n)r_{n-m}^*] = 0$ for $|m| \leq K$,

$$E[s_n r_{n-m}^*] = E[\hat{s}_n r_{n-m}^*], \quad |m| \leq K \quad (3.14)$$

Now, the left hand side of (3.14) is

$$\begin{aligned} E[s_n r_{n-m}^*] &= E \left[s_n \left(\sum_l h_l^* s_{n-m-l}^* + w_{n-m}^* \right) \right] \\ &= \sum_l h_l^* E[s_n s_{n-m-l}^*] + E[s_n w_{n-m}^*] \end{aligned}$$

Here, the second term is zero as s_n and w_{n-m}^* are independent of each other. In addition the first term is nonzero only when $n = n - m - l$, which is true for $l = -m$. Since $E[s_n^2] = 1$,

$$E[s_n r_{n-m}^*] = h_{-m}^* \quad (3.15)$$

Similarly, the right hand side of (3.14) is

$$\begin{aligned} E[\hat{s}_n r_{n-m}^*] &= E\left[\left(\sum_l f_l r_{n-l}\right) r_{n-m}^*\right] \\ &= \sum_l f_l E[r_{n-l} r_{n-m}^*] \end{aligned}$$

Evaluating $E[r_{n-l} r_{n-m}^*]$ yields

$$\begin{aligned} E[r_{n-l} r_{n-m}^*] &= E\left[\left(\sum_j h_j s_{n-l-j} + w_{n-l}\right) \left(\sum_k h_k^* s_{n-m-k}^* + w_{n-m}^*\right)\right] \\ &= \sum_j \sum_k h_j h_k^* E[s_{n-l-j} s_{n-m-k}^*] + E[w_{n-l} w_{n-m}^*] \end{aligned}$$

Here,

$$E[s_{n-l-j} s_{n-m-k}^*] = \begin{cases} 1, & \text{if } l+j = m+k \text{ or } j = k+m-l \\ 0, & \text{otherwise} \end{cases}$$

$$E[w_{n-l} w_{n-m}^*] = \begin{cases} N_0, & \text{if } l = m \\ 0, & \text{otherwise} \end{cases}$$

Therefore,

$$E[r_{n-l} r_{n-m}^*] = \sum_{k=0}^{C-1} h_{k+m-l} h_k^* + N_0 \delta_{m-l} \triangleq g_{l,m}$$

Hence,

$$E[\hat{s}_n r_{n-m}^*] = \sum_{l=-K}^K g_{l,m} f_l \quad (3.16)$$

Substituting (3.15) and (3.16) in (3.14),

$$\sum_{l=-K}^K g_{l,m} f_l = h_{-m}^*, \quad m = -K, \dots, K \quad (3.17)$$

It can be noted from (3.17), that there are $2K + 1$ simultaneous equations while $2K + 1$ equalizer filter coefficients (f_{-K}, \dots, f_K) are the unknowns. These unknown coefficients can be obtained by solving these simultaneous equations. Now, represent (3.17) in the matrix form as

$$\begin{bmatrix} g_{-K,-K} & g_{-(K-1),-K} & \cdots & g_{K,-K} \\ g_{-K,-(K-1)} & g_{-(K-1),-(K-1)} & \cdots & g_{K,-(K-1)} \\ \vdots & \vdots & \ddots & \vdots \\ g_{-K,K} & g_{-(K-1),K} & \cdots & g_{K,K} \end{bmatrix} \begin{bmatrix} f_{-K} \\ f_{-(K-1)} \\ \vdots \\ f_K \end{bmatrix} = \begin{bmatrix} h_K^* \\ h_{K-1}^* \\ \vdots \\ h_{-K}^* \end{bmatrix} \quad (3.18)$$

From (3.18), define the following notations

$$\begin{bmatrix} g_{-K,-K} & g_{-(K-1),-K} & \cdots & g_{K,-K} \\ g_{-K,-(K-1)} & g_{-(K-1),-(K-1)} & \cdots & g_{K,-(K-1)} \\ \vdots & \vdots & \ddots & \vdots \\ g_{-K,K} & g_{-(K-1),K} & \cdots & g_{K,K} \end{bmatrix} \triangleq \mathbf{\Gamma}$$

$$\begin{bmatrix} h_K^* \\ h_{K-1}^* \\ \vdots \\ h_{-K}^* \end{bmatrix} = \begin{bmatrix} 0 \\ \vdots \\ 0 \\ h_{C-1}^* \\ \vdots \\ h_0^* \\ 0 \\ \vdots \\ 0 \end{bmatrix} \triangleq \xi$$

$$\begin{bmatrix} f_{-K} \\ f_{-(K-1)} \\ \vdots \\ f_K \end{bmatrix} = \mathbf{f}$$

Here, in column vector ξ , the first $K - (C - 1)$ elements and the last K elements are equal to zero. Using these notations, the optimal filter coefficients \mathbf{f}_{opt} can be expressed in terms of $\mathbf{\Gamma}$ and ξ as

$$\mathbf{f}_{\text{opt}} = \mathbf{\Gamma}^{-1}\xi \quad (3.19)$$

Further, the MMSE can be evaluated as

$$\begin{aligned} \text{MMSE} &= E[(s_n - \hat{s}_n)(s_n^* - \hat{s}_n^*)] \\ &= E[(s_n - \hat{s}_n)s_n^*] - E[(s_n - \hat{s}_n)\hat{s}_n^*] \end{aligned}$$

Here, the second term is

$$E[(s_n - \hat{s}_n)\hat{s}_n^*] = \sum_{m=-K}^K f_m^* E[(s_n - \hat{s}_n)r_{n-m}^*] = 0$$

From the orthogonality principle, the term $E[(s_n - \hat{s}_n)r_{n-m}^*]$ is 0. This leads to

$$\begin{aligned} \text{MMSE} &= E[(s_n - \hat{s}_n)s_n^*] \\ &= E[s_n s_n^*] - E[\hat{s}_n s_n^*] \\ &= 1 - E\left[\left(\sum_m f_m r_{n-m}\right)s_n^*\right] \\ &= 1 - E\left[\sum_m f_m \left(\sum_l h_l s_{n-m-l} + w_{n-m}\right)s_n^*\right] \\ &= 1 - \sum_m f_m \left(\sum_l h_l E[s_{n-m-l}s_n^*] + E[s_n^* w_{n-m}]\right) \end{aligned}$$

Here, $h_l E[s_{n-m-l}s_n^*] \neq 0$ if $n - m - l = n$ or $l = -m$. In addition,

$E[s_n^* w_{n-m}] = 0$ since s_n^* and w_{n-m} are independent and zero-mean.

Thus,

$$\begin{aligned} \text{MMSE} &= 1 - \sum_m f_m h_{-m} \\ &= 1 - \xi^\dagger \mathbf{f} \end{aligned} \tag{3.20}$$

Finally, substituting \mathbf{f} from (3.19) yields

$$\text{MMSE} = 1 - \xi^\dagger \mathbf{\Gamma}^{-1} \xi \tag{3.21}$$

3.3 Equalization and Bit Loading for WPM

MMSE equalization is not perfect and induces noise amplification and signal attenuation. To overcome these limitations of MMSE equalization, a bit loading

algorithm that considers both noise amplification and signal attenuation is proposed. The proposed bit loading algorithm is based on the traditional water-filling method (Goldsmith, 2005). However, the conventional approach does not incorporate the equalization error. Hence, a modified bit loading algorithm is derived to take into account the equalization imperfection. In addition, the use of bit loading provides an acceptable BER performance with a moderate equalizer filter length and thus helps reduce the complexity. The proposed bit loading algorithm requires computation of the noise power gain, the signal power gain and the signal power associated with the number of bits allocated to each subcarrier. The computations of these terms are explained in the following sections.

3.3.1 Noise Power Gain Computation

The numerical computation of the noise power gain can be accomplished using the block diagram as shown in Fig. 3.4. For simulation, AWGN is generated and passed through the equalizer filter followed by DWPT as shown in Fig. 3.4 (a). The communication channel through which noise passes is considered and the signal value is made zero to ensure that the DWPT output is only due to noise. Therefore, the variance of each output signal will give the noise power gain on each subcarrier. Note that the generation of AWGN is performed only for simulation with an intention to validate the analytical approach; it is not required in the actual receiver.

The computation of the noise power gain can also be accomplished analytically using the equivalent block diagram as shown in Fig. 3.4 (b), which consists of the equalizer filter and the matched filter along with a sampler for each subcarrier. The matched filter on subcarrier k is designated as ϕ_{-n}^k , where ϕ_n^k is the basis function of subcarrier k , which is the IDWPT output due to having 1 as the only nonzero IDWPT input on subcarrier k . At the receiver, after equalization, the received WPM symbols are fed to the matched filter ϕ_{-n}^k followed by sampling to retrieve the QAM symbol on subcarrier k . This is the standard procedure employed to retrieve the

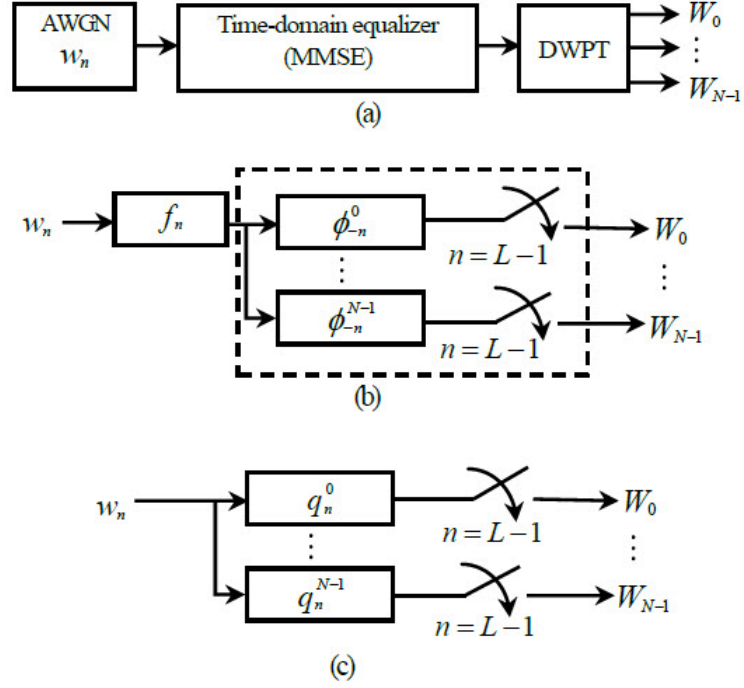


Figure 3.4: Block diagram showing the noise power gain computation of each subcarrier for WPM (a) using simulation (b) using analysis (c) using analysis based on equivalent filters.

coefficient of an orthonormal expansion in (3.1) (Proakis & Salehi, 2008). The output after sampling on subcarrier k is denoted by W_k .

The equalizer filter f_n and matched filter ϕ_{-n}^k can be combined to form an equivalent filter given by (3.22). The equivalent block diagram is shown in Fig. 3.4(c), which involves a single equivalent filter q_n^k given by

$$q_n^k = f_n * \phi_{-n}^k \quad (3.22)$$

The noise power gain on subcarrier k , indicated by γ_k , is equivalent to the variance of W_k divided by N_0 . However, when any random process is passed through a linear time invariant (LTI) filter, the power spectral density (PSD) of the output will be equal to the PSD of the input multiplied by the squared norm of the vector

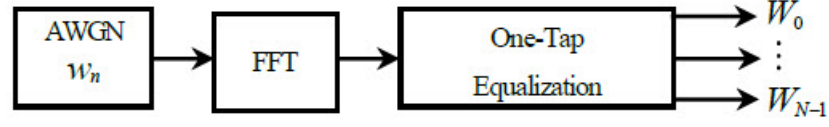


Figure 3.5: Block diagram showing the noise power gain computation on each subcarrier for OFDM

containing filter coefficients (Wong, 2011). Therefore, the noise power gain on subcarrier k can be evaluated using

$$\gamma_k = \text{var}[W_k]/N_0 = \|q_n^k\|^2 \quad (3.23)$$

For comparison, the noise power gain on subcarrier k for OFDM with the CP can be computed by passing AWGN through the fast Fourier transform (FFT) followed by one-tap equalization, as shown in Fig. 3.5. Since the considered communication channel involves only noise, the variance of each output of one-tap equalization will give the noise power gain on each subcarrier. One-tap equalization in OFDM is implemented by multiplying the received data symbol on subcarrier k by the inverse of the subcarrier gain $1/H_k$, where H_k is the FFT of CIR h_n . For this reason, the noise power amplification factor is equivalent to $1/|H_k|^2$ (Goldsmith, 2005). Therefore, the noise power gain on subcarrier k for OFDM is

$$\gamma_k = \text{var}[W_k]/N_0 = 1/|H_k|^2 \quad (3.24)$$

3.3.2 Signal Power Gain Computation

The signal power gain for WPM can be evaluated using the transmission path as shown in Fig. 3.6(a). The transmit signal is passed through the channel and the MMSE equalizer filter, which is followed by DWPT. Here, noise is assumed equal to zero so that the output is only due to signal values.

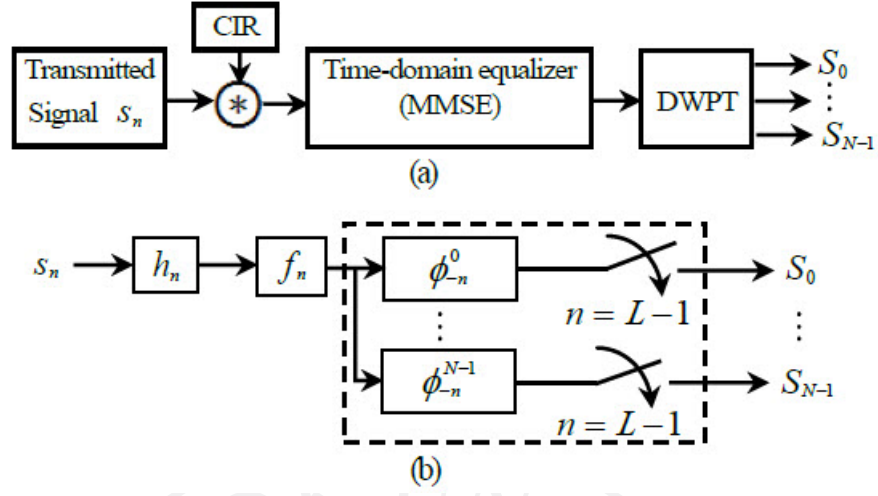


Figure 3.6: Block diagram showing the signal power gain computation on each subcarrier for WPM (a) using simulation (b) using analysis

An equivalent block diagram that is used to obtain signal power gains analytically is shown in Fig. 3.6(b). For subcarrier k , there are channel filter h_n , equalizer filter f_n , and matched filter ϕ_{-n}^k , followed by a sampler. The expression for the signal power gain on subcarrier k , denoted by η_k , is given by

$$\eta_k = \left| \langle f_n * h_n * \phi_{-n}^k, \phi_{-n}^k \rangle \right|^2 \quad (3.25)$$

where $\langle \cdot, \cdot \rangle$ denotes the inner product operation between two signals. For OFDM, one-tap equalization yields a signal power gain of 1 for all subcarriers.

3.3.3 Signal Power Computation

In the bit-loading algorithm, two bits are added to one subcarrier in each iteration because square QAM constellations are considered. Let E'_b be the received energy per bit. The values of E'_b/N_0 that are required for $M \times M$ QAM to obtain a BER of 10^{-5} are listed in Table 3.1. These E'_b/N_0 values can be obtained using (3.26), which is derived based on the union bound estimate for uncoded transmissions (Forney & Ungerboeck, 1998).

Table 3.1: E'_b/N_0 for $M \times M$ QAM with $\text{BER} = 10^{-5}$

M	No. of bits per QAM symbol	Required E'_b/N_0 (dB)
2	2	9.6
4	4	13.4
8	6	17.8
16	8	22.5

$$\text{BER} \approx \frac{2(M-1)}{M \log_2 M} Q \left(\sqrt{\left(\frac{6 \log_2 M}{M^2 - 1} \right) \times \frac{E'_b}{N_0}} \right) \quad (3.26)$$

In (3.26), $Q(x) = \frac{1}{\sqrt{2\pi}} \int_x^\infty e^{-z^2/2} dz$.

3.3.4 Bit Loading Algorithm

The proposed bit loading algorithm considers the error of MMSE equalization. In particular, the proposed bit loading algorithm considers signal attenuation and noise amplification due to imperfection of MMSE equalization. In addition to signal attenuation and noise amplification, equalization error also induces inter-carrier interference (ICI). However, the total ICI on each subcarrier from other subcarriers depends on the signal powers of those subcarriers and the signal power on each subcarrier depends on the number of bits allocated to the subcarrier. In short, the bit allocation on each subcarrier is interrelated to the ICI. In addition to this, numerical results, as will be shown in later sections, demonstrate that ICI gains are negligible as compared to the noise power gains which form the basis for bit allocation, and WPM still performs better than OFDM while ignoring ICI for bit allocation. The contribution of ICI in bit allocation is considerably less significant as compared to the complexity introduced when ICI is included in the bit loading algorithm. In light of this fact, ICI is not considered in the proposed bit loading algorithm.

The flow chart for the bit loading algorithm is shown in Fig. 3.7. It is an iterative algorithm based on signal and noise power gains across subcarriers. First, the

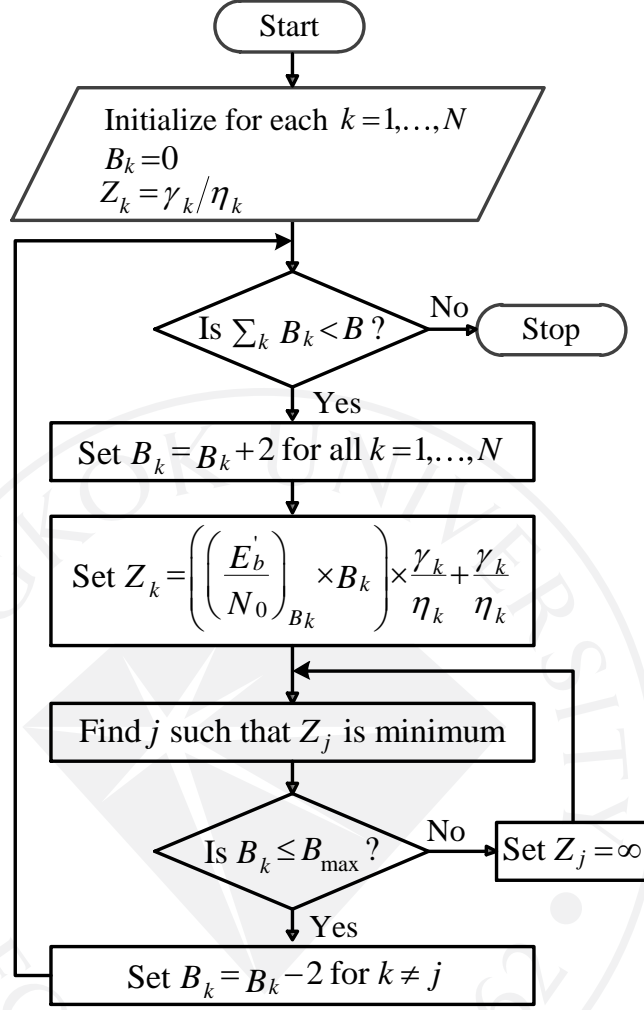


Figure 3.7: Flow chart for the proposed bit loading algorithm.

ratio γ_k/η_k is calculated for each subcarrier k , and corresponds to the normalized noise power $(\gamma_k N_0/\eta_k)$, with the constant N_0 omitted (to be explained shortly). It serves as the initial water level denoted by Z_k . At the beginning of each iteration, two bits are added to each subcarrier, and the water level Z_k is updated with respect to the additional two bits using

$$Z_k = \left(\left(\frac{E'_b}{N_0} \right)_{B_k} \times B_k \right) \times \frac{\gamma_k}{\eta_k} + \frac{\gamma_k}{\eta_k} \quad (3.27)$$

where B_k indicates the number of bits on subcarrier k , and E'_b/N_0 is the value of E'_b/N_0 that is required for subcarrier k to transmit B_k bits per symbol, as listed in Table 3.1. Because E'_b/N_0 is considered as the SNR per bit (Proakis & Salehi, 2008), the term $\left(E'_b/N_0\right)_{B_k} \times B_k$ in (3.27) corresponds to the SNR, yielding a signal power value that is equal to the first term on the right-hand side of (3.27), with the constant N_0 omitted. Therefore, Z_k in (3.27) can be viewed as the sum of signal and noise powers. Because the water-level values of Z_k are used for comparison only, it is possible to omit the common multiplicative factor N_0 from both the signal and noise powers. Then, the subcarrier j with the minimum water level and $B_j \leq B_{\max}$ is selected. At the end of each iteration, B_k is reduced by 2 for each subcarrier $k \neq j$. This is equivalent to assigning two bits to subcarrier j that minimizes the maximum water level after the assignment. The process is repeated until the total number of allocated bits is equal to the desired number of bits B , which is assumed to be twice the number of subcarriers, i.e., 2×2 QAM on each subcarrier without bit loading.

The value of B_{\max} is set to 8, resulting in possible constellations being 2×2 QAM, 4×4 QAM, 8×8 QAM, and 16×16 QAM. The process can be extended beyond 16×16 QAM, but numerical results indicate that larger constellations are not needed.

CHAPTER 4

WPM WITH KNOWN CSI

This chapter provides performance evaluation of WPM assuming that the channel state information (CSI) is known. An analytical BER expression for WPM is derived and is validated through simulation. The validated BER expression is used to explore the benefits of equalization with bit loading over equalization without bit loading. In addition, WPM is compared with OFDM in terms of the BER performance.

4.1 BER Analysis for WPM

This section provides a mathematical derivation to compute the BER for WPM. Let E_b be the energy per transmitted bit and N_0 be the power spectral density (PSD) of AWGN. The BER expression is obtained in terms of E_b/N_0 . In order to derive the analytical BER expression, the following notations are defined.

E_c = Energy per channel use.

M_k = Constellation size of $M_k \times M_k$ QAM for subcarrier k

N = Number of subcarriers

d_{\min} = Minimum distance between the signal points

Here, d_{\min} is considered to be constant for all the signal sets. For the given d_{\min} , the average symbol energy, denoted by E_s , for $M_k \times M_k$ QAM is (Forney & Ungerboeck, 1998)

$$E_s = \frac{d_{\min}^2(M_k^2 - 1)}{6} \quad (4.1)$$

Therefore, the average energy per channel use can be written as

$$E_c = \frac{1}{N} \left(\sum_{k=0}^{N-1} \left(\frac{M_k^2 - 1}{6} \right) \right) d_{\min}^2 \quad (4.2)$$

For each WPM symbol period, the energy per WPM symbol can be written as the product between the number of channel uses, which corresponds to the number of transmitted values and the energy per channel use. On the other hand, it is equivalent to the product between the number of information bits transmitted and the energy per information bit. It follows that

$$N \times E_c = \left(\sum_{k=0}^{N-1} 2 \log_2 M_K \right) \times E_b \quad (4.3)$$

yielding

$$E_b = \left(\frac{N}{\sum_{k=0}^{N-1} 2 \log_2 M_K} \right) \times E_c \quad (4.4)$$

Furthermore, the constellation size M_k for subcarrier k depends on the bit allocation obtained from bit loading. Substituting E_c from (4.2), the expression for d_{\min} can be obtained as

$$d_{\min} = \sqrt{\frac{\sum_{k=0}^{N-1} 2 \log_2 M_k}{\sum_{l=0}^{N-1} \left(\frac{M_l^2 - 1}{6} \right)} \times E_b} \quad (4.5)$$

Since the transmit signal is passed through the channel in the transmission path followed by a time-domain equalizer at the receiver, the value of E_b at the receiver should include the gain contributed from both the channel and the equalizer. Hence, E_b is scaled by the signal power gain η_k on subcarrier k at the receiver. Taking this into account, the expression for d_{\min} at the receiver becomes

$$d'_{\min} = \sqrt{\frac{\sum_{k=0}^{N-1} 2 \log_2 M_k}{\sum_{l=0}^{N-1} \left(\frac{M_l^2 - 1}{6} \right)} \times \eta_k E_b} \quad (4.6)$$

Now, considering $M_k \times M_K$ QAM, the BER for subcarrier k can be evaluated using

the union bound estimate given in (Forney & Ungerboeck, 1998) as

$$\text{BER}_k \approx \frac{2(M_k - 1)}{M_k \log_2 M_k} \mathcal{Q} \left(\frac{d'_{\min}}{\sqrt{2N_k^I}} \right) \quad (4.7)$$

where N_k^I is the corresponding interference-plus-noise power on subcarrier k , and includes ICI along with noise power. The ICI on subcarrier k from subcarrier j can be computed as

$$\beta_{k,j} = \left| \left\langle h_n * f_n * \phi_n^j, \phi_n^j \right\rangle \right|^2 \quad (4.8)$$

Likewise, the total ICI on subcarrier k contributed from all other subcarriers j such that $j \neq k$ is evaluated as

$$\beta_k^{\text{total}} = \sum_{j=0, j \neq k}^{N-1} \beta_{k,j} \quad (4.9)$$

Similar to E_b , the noise variance N_0 is also scaled by γ_k and added to β_k^{total} to obtain N_k^I as

$$N_k^I = \gamma_k N_0 + \beta_k^{\text{total}} \quad (4.10)$$

Moreover, substituting d'_{\min} from (4.6) and N_k^I from (4.10) in (4.7), BER_k can be computed as

$$\text{BER}_k \approx \frac{2(M_k - 1)}{M_k \log_2 M_k} \times \mathcal{Q} \left(\sqrt{\left(\frac{\sum_{i=0}^{N-1} 2 \log_2 M_i}{\sum_{l=0}^{N-1} \left(\frac{M_l^2 - 1}{6} \right)} \right) \times \frac{1}{2} \times \frac{\eta_k E_b}{\gamma_k N_0 + \beta_k^{\text{total}}}} \right) \quad (4.11)$$

Finally, the overall BER can be calculated using the weighted average of the BERs on all the subcarriers, as given by

$$\text{BER} \approx \sum_{k=0}^{N-1} \frac{2 \log_2 M_k}{\sum_{l=0}^{N-1} 2 \log_2 M_l} \times \text{BER}_k \quad (4.12)$$

Following the similar procedure, BER_k for OFDM with CP can be derived as shown in (4.13). The detailed computational steps are shown in appendix B.

$$\text{BER}_k \approx \frac{2(M_k - 1)}{M_k \log_2 M_k} \times Q \left(\sqrt{\frac{N}{N + N_c} \left(\frac{\sum_{i=0}^{N-1} 2 \log_2 M_i}{\sum_{l=0}^{N-1} \left(\frac{M_l^2 - 1}{6} \right)} \right) \times \frac{|H_k|^2}{2} \times \frac{E_b}{N_0}} \right) \quad (4.13)$$

In (4.13), N_c denotes the length of CP. The overall BER can be computed using (4.12), as in the case of WPM.

4.2 Simulation for BER Evaluation

The aim of simulation is to verify the analytical expressions derived in the previous section. The simulation program is developed using MATLAB following the block diagram in Fig. 3.1. Simulation is carried out for three test environments as per Rec. ITU-R M.1225 (ITU-R Rec. M.1225, 1997). The three test environments are

1. Indoor office test environment
2. Outdoor to indoor and pedestrian test environment
3. Vehicular test environment

Each test environment has two channels, namely channel A and channel B. The CIR for each test environment is modeled by a tapped-delay-line structure, with each tap defined by three parameters: the time delay relative to the first tap, the average power relative to the strongest tap, and the Doppler spectrum of each tap. The parameters of the tapped-delay-line structure for each test environment are listed in Tables 4.1-4.3. The detailed steps used to obtain the exact coefficients of the CIR

Table 4.1: Tapped-delay-line parameters for the indoor office test environment (ITU-R Rec. M.1225, 1997)

Tap	Channel A		Channel B		Doppler Spectrum
	Relative delay (ns)	Average power (dB)	Relative delay (ns)	Average power (dB)	
1	0	0	0	0	Flat
2	50	-3.0	100	-3.6	Flat
3	110	-10.0	200	-7.2	Flat
4	170	-18.0	300	-10.8	Flat
5	290	-26.0	500	-18.0	Flat
6	310	-32.0	700	-25.2	Flat

Table 4.2: Tapped-delay-line parameters for the outdoor to indoor and pedestrian test environment (ITU-R Rec. M.1225, 1997)

Tap	Channel A		Channel B		Doppler Spectrum
	Relative delay (ns)	Average power (dB)	Relative delay (ns)	Average power (dB)	
1	0	0	0	0	Classic
2	110	-9.7	200	-0.9	Classic
3	190	-19.2	800	-4.9	Classic
4	410	-22.8	1200	-8.0	Classic
5	-	-	2300	-7.8	Classic
6	-	-	3700	-23.9	Classic

using the provided parameters are shown in appendix C. In addition to the CIR, other parameters used in simulation are listed in Table 4.4.

At first, simulation is performed to validate the analytical expression for computing the coefficients of the MMSE equalizer filter and the noise power gain for each subcarrier. This is followed by validation of analytical BER expressions through simulation. Once the analytical expressions are validated, they are used for further performance analysis. The use of analytical expressions helps avoid long simulation time.

Table 4.3: Tapped-delay-line parameters for the vehicular test environment (ITU-R Rec. M.1225, 1997)

Tap	Channel A		Channel B		Doppler Spectrum
	Relative delay (ns)	Average power (dB)	Relative delay (ns)	Average power (dB)	
1	0	0	0	-2.5	Classic
2	310	-1.0	300	0	Classic
3	710	-9.0	8900	-12.8	Classic
4	1090	-10.0	12900	-10.0	Classic
5	1730	-15.0	17100	-25.2	Classic
6	2510	-20.0	20000	-16.0	Classic

Table 4.4: Simulation parameters

Parameter	Value
MCM technique	WPM, OFDM
No. of subcarriers	64
No. of MCM symbols	500
QAM signal sets	2×2 , 4×4 , 8×8
Wavelet function	db4 (Burrus et al., 1998)

4.2.1 Simulation for MMSE Equalization

The filter coefficients obtained from the analytical expression in (3.19) are compared with the filter coefficients obtained from simulation, which is performed using a known training sequence of 10 randomly generated WPM symbols. The known training sequence is applied to (3.10) to obtain the filter coefficients. Channel A of the indoor office test environment is considered and the equalizer filter coefficients of 41 taps are computed. The equalizer filter coefficients obtained from the analytical expression using (3.19) are shown in Fig. 4.2 while the equalizer filter coefficients obtained using simulation with a known training sequence are shown in Fig. 4.1. The results show that the analytical values are close to the simulation values. Therefore, the analytical expression in (3.19) can be used to obtain the filter coefficients for quasistatic channels such as slow fading channels, where training

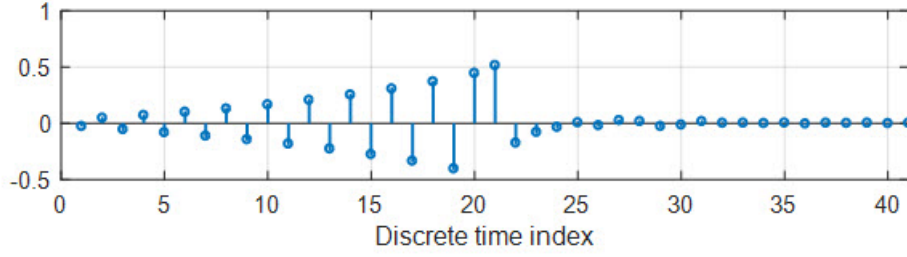


Figure 4.1: Equalizer filter coefficients for channel A of the indoor office test environment from simulation with a known training sequence.

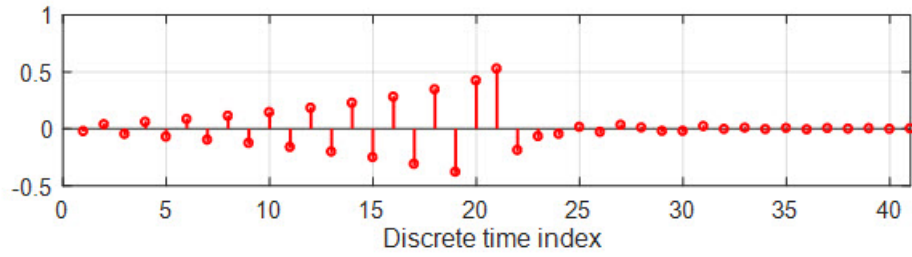


Figure 4.2: Equalizer filter coefficients for channel A of the indoor office test environment from analysis using the expression in (3.19)

sequences are transmitted occasionally to follow the changes in the channel. For further performance evaluation, equalizer filter coefficients are obtained using the analytical expression in (3.19) instead of simulation.

Furthermore, Fig. 4.3 shows the histogram of equalization errors for QAM symbols obtained from simulation results of 500 transmitted WPM symbols. The plot shows that the equalization error has a Gaussian distribution, unlike in the case of single-carrier modulation, where the equalization error is generally not Gaussian (Proakis & Salehi, 2008). This is because, in WPM, the equalization error is passed through DWPT at the receiver, resulting in a Gaussian distribution. This equalization error could not be added directly to the noise variance. However, it is incorporated as noise power amplification, signal power attenuation, and ICI.

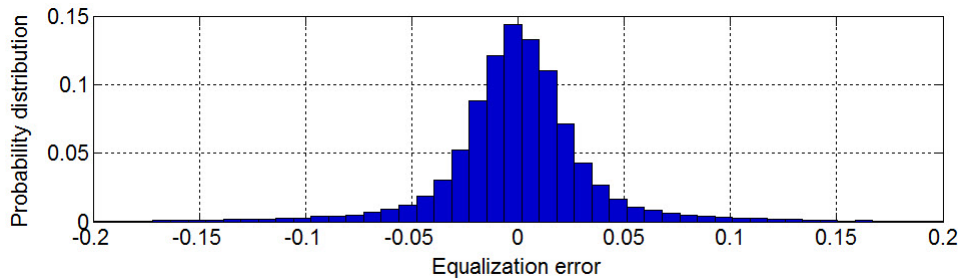


Figure 4.3: Distribution of equalization error for the equalizer coefficients in Fig. 4.2

4.2.2 Simulation for Noise Power Gain

The noise power gain on each subcarrier for WPM can be evaluated using the analytical expression in (3.23). The mathematical expression can be validated through simulation using the block diagram as given in Fig. 3.4 (a). Simulation is performed considering channel A of the indoor office test environment. Simulation results of noise power gains are plotted for all subcarriers as shown in Fig. 4.4 while the corresponding analytical values are displayed in Fig. 4.5. The plots in Figs. 4.4-4.5 demonstrate that the noise power gains obtained from the analytical expression are close to the simulation results. Therefore, for further performance analysis noise power gains are computed using the analytical expression in (3.23).

From Figs. 4.4-4.5, it can be noticed that the noise power gains are not distributed in the increasing order from low to high frequency components. The reason for this can be explained based on the DWPT structure. The structure of DWPT consists of a pair of LPF and HPF, followed by downsampling by a factor of 2. In each successive stage, the outputs of the LPF and HPF are fed to the LPF and HPF of the next stage. The decimation involved in DWPT does not effect the order of frequency components at the LPF outputs, and thus the outputs of LPFs remain in order. However, after decimation at the outputs of HPFs, high and low frequency components are swapped. This is known as band-shuffling (Lindsey, 1995). Since the

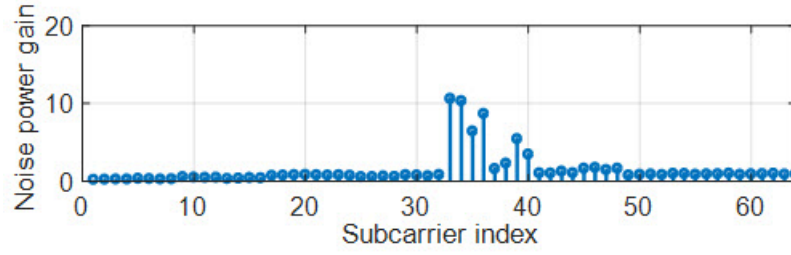


Figure 4.4: Noise power gains across all subcarriers for channel A of the indoor office test environment from simulation with a known training sequence.

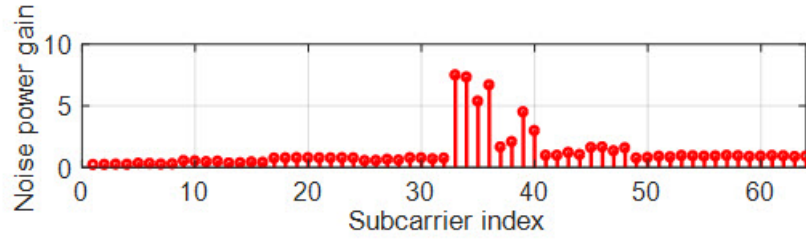


Figure 4.5: Noise power gains across all subcarriers for channel A of the indoor office test environment from analysis using the expression in (3.23)

frequency components are swapped only at the HPF outputs, and WPM has a symmetric structure, this results in the ordering of frequency components according to the gray code sequence (Bouwel et al., 2000)(Lindsey, 1995). Owing to this, the noise power gains are plotted with subcarriers reordered according to the gray code sequence, as shown in Fig. 3.4. The plot displays the noise power gains across subcarriers rearranged from low to high frequency components.

In a similar fashion, signal power gains across all subcarriers can be computed using (3.25). The signal power gains across subarriers rearranged from low to high frequency components are presented in Fig. 4.7. In the plot, subcarriers at high frequencies have signal power gains less than unity. This indicates that equalization is not perfect for high frequencies. However, the influence on the BER performance due to this imperfection of equalization is compensated by the proposed bit loading

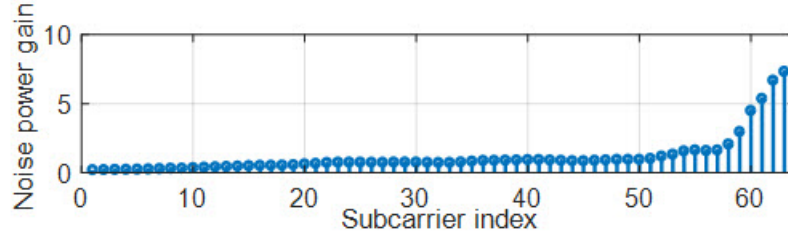


Figure 4.6: Noise power gains across all subcarriers rearranged from low to high frequency components for channel A of the indoor office test environment.

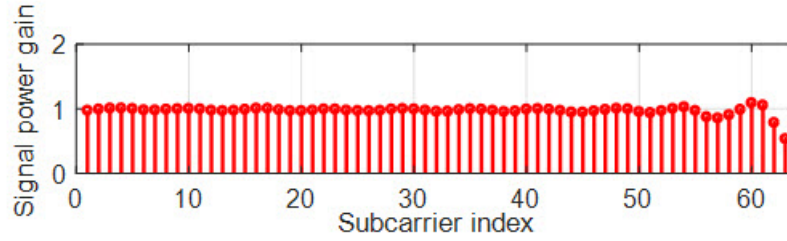


Figure 4.7: Signal power gains across all subcarriers rearranged from low to high frequency components for channel A of the indoor office test environment.

algorithm.

4.2.3 Bit Allocation

The bit loading algorithm proposed in section 3.3.4 is implemented to perform bit allocation for all subcarriers. The bit loading algorithm is based on the ratios of noise power gains to signal power gains, which act as the initial water levels. The ratio of noise to signal power gains for each subcarrier is evaluated using (3.23) and (3.25). The plot of the initial water levels is shown in Fig. 4.8. Next, considering these water levels as the basis, bit allocation for all subcarriers is obtained as displayed in Fig. 4.9. The plot demonstrates that subcarriers with lower initial water levels are allocated more bits.

In addition, based on the bit allocation shown in Fig. 4.9, ICI for each

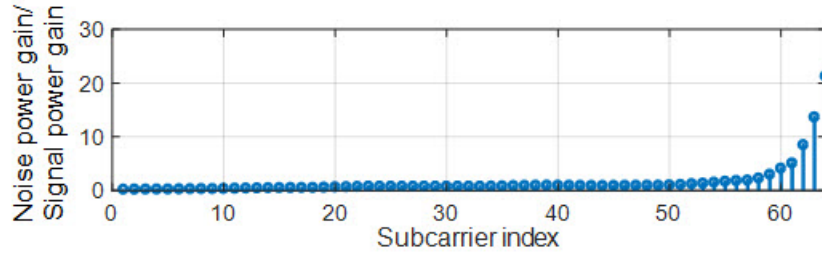


Figure 4.8: The ratios of noise power gains to signal power gains across all subcarriers rearranged from low to high frequency components for channel A of the indoor office test environment.

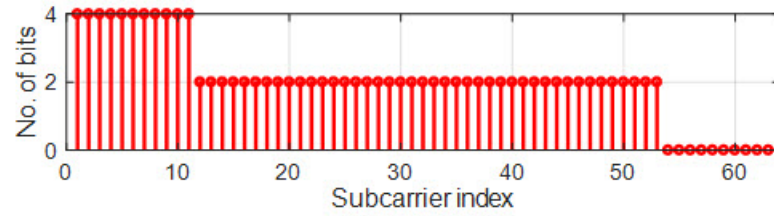


Figure 4.9: Bit allocation on all subcarriers for channel A of the indoor office test environment.

subcarrier is evaluated using (4.9). For computing ICI, $N_0 = 1$ is assumed without loss of generality. The ICI value for each subcarrier is displayed in Fig. 4.10. On the other hand, since $N_0 = 1$, noise powers are equivalent to noise power gains, which are shown in Fig. 4.6. It enlightens the fact that ICI values are significantly lower than noise powers. Therefore, it is reasonable to neglect ICI in the bit loading algorithm as the contribution from ICI is insignificant compared to noise powers.

4.2.4 Simulation for BER

In this section, numerical values obtained from the analytical expression for computing the BER are compared with simulation results. Simulation is performed based on the system in Fig. 3.1. Channel A and channel B of the indoor office test

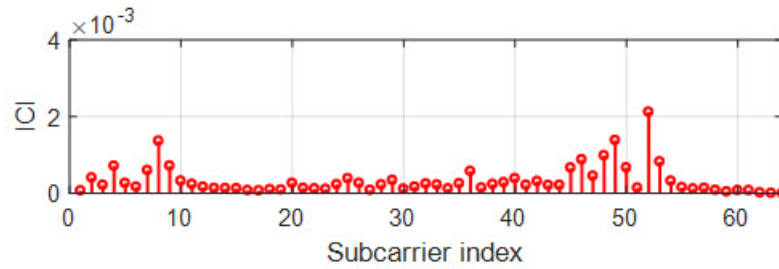


Figure 4.10: ICI across all subcarriers with bit allocation for channel A of the indoor office test environment as shown in Fig. 4.9

environment are considered. In the absence of bit loading, i.e., equalization without bit loading, all subcarriers are assigned the same QAM constellation. Here, 2×2 QAM is considered, which is equivalent to allocating 2 bits to each subcarrier. On the other hand, when equalization with bit loading is taken into account, the constellation size assigned for each subcarrier depends on the bit allocation to the subcarrier derived from the proposed bit loading algorithm. However, the number of transmitted bits per WPM symbol is kept the same for both cases, i.e., without and with bit loading.

The BER plots for WPM considering equalization without bit loading are shown in Fig. 4.11. Analytical BER values are obtained using (4.11) and (4.12). These analytical BER values are compared with the numerical results obtained from simulation. It can be seen that, for both channel A and channel B of the indoor office test environment, the BER values provided by analytical expressions are close to the simulation results. In the same way, the BER plots for WPM considering equalization with bit loading are displayed in Fig. 4.12. Like in Fig. 4.11, the BER plots demonstrate that, for both channel A and channel B of the indoor office test environment, the analytical BER values are close to the simulation results. The BER plots for WPM in Fig. 4.11- 4.12 show that the analytical BER expression can provide BER values close to simulation results.

In addition, the BER plots for OFDM are shown in Fig. 4.13. The analytical

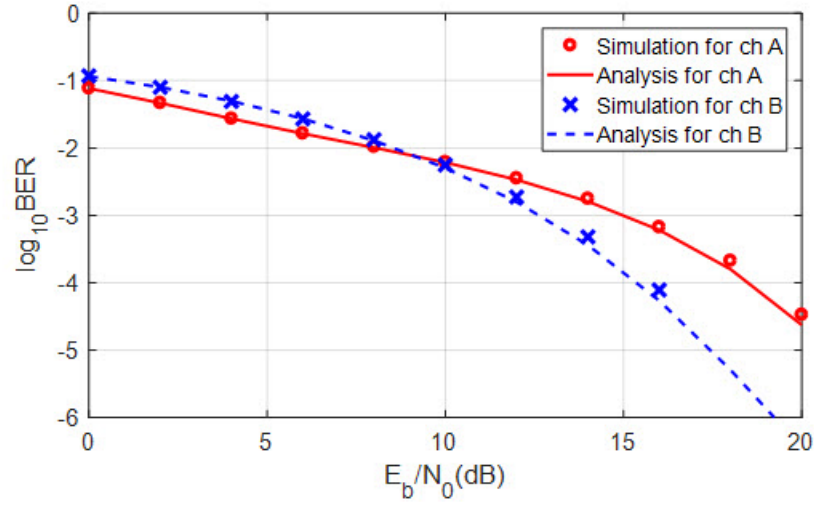


Figure 4.11: BER versus E_b/N_0 for channel A and channel B of the indoor office test environment for WPM considering MMSE equalization without bit loading.

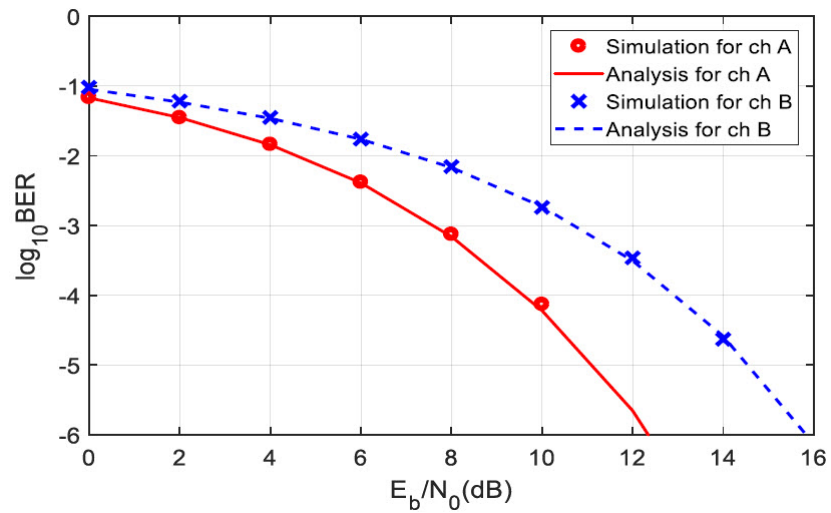


Figure 4.12: BER versus E_b/N_0 for channel A and channel B of the indoor office test environment for WPM considering MMSE equalization with bit loading.

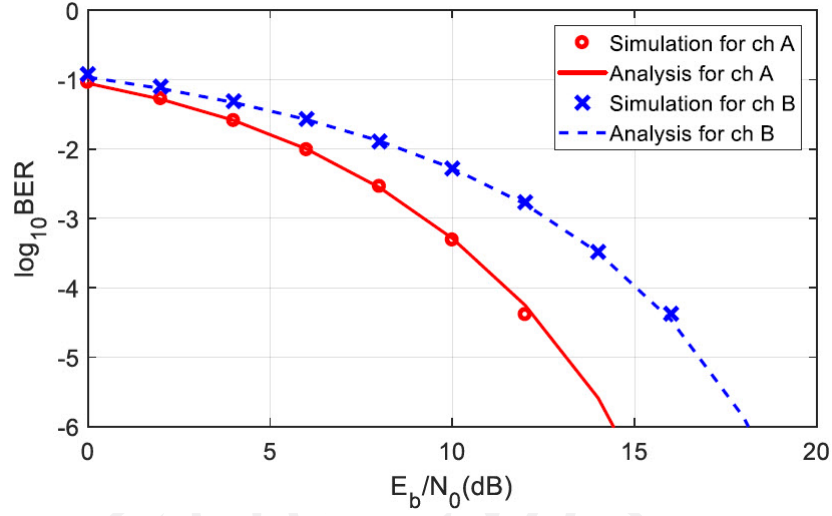


Figure 4.13: BER versus E_b/N_0 for channel A and channel B of the indoor office test environment for OFDM considering one-tap equalization with bit loading.

BER plots are based on (4.13) and (4.12). Analytical BER values are compared with simulation values for channel A and channel B of the indoor office test environment. BER values for OFDM are computed considering one-tap equalization with bit loading. The BER plots show that the analytical results are in good agreement with the simulation results. Figs. 4.11-4.13 indicate that the derived analytical expressions for computing the BER for WPM and OFDM can provide BER values that closely match with simulation results. Therefore, these analytical expressions are considered for further performance analysis.

4.2.5 BER Comparison for WPM with and without Bit Loading

After the validation of the analytical BER expression for WPM through simulation in the previous section, the BER expression is now used to explore the advantage of equalization-aware bit loading for WPM. The BER plots are obtained for both equalization with bit loading and without bit loading. The plots are drawn for

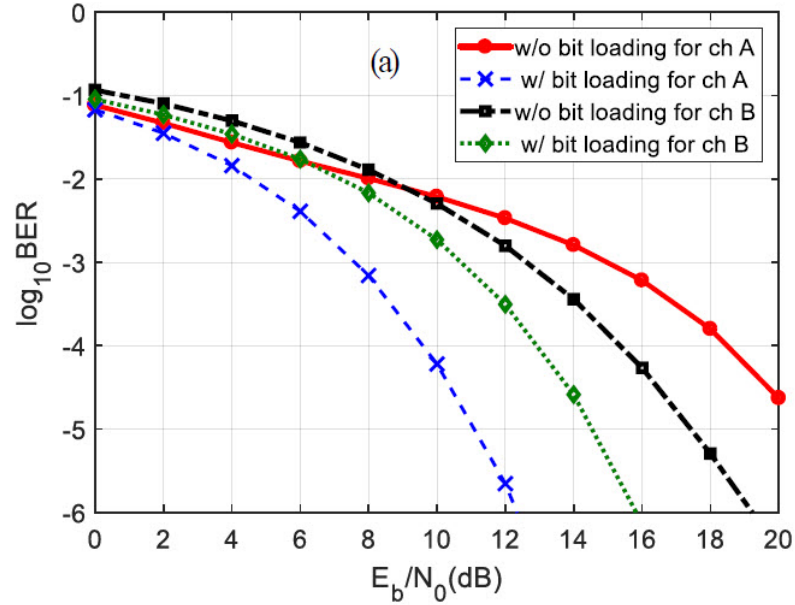


Figure 4.14: BER versus E_b/N_0 using MMSE equalization with and without bit loading for channel A and channel B of the indoor office test environment.

channel A and channel B of the indoor office test environment, the outdoor to indoor and pedestrian test environment, and the vehicular test environment, as displayed in Fig. 4.14 -4.16.

It can be noticed that the BER is further reduced when equalization with bit loading is used in comparison to when equalization without bit loading is used, for both channel A and channel B of all three test environments. Moreover, it can be seen that equalization with bit loading achieves higher BER reduction in channel A as compared to channel B for all three test environments. In particular, using equalization with bit loading, the required E_b/N_0 to achieve the target BER to 10^{-5} is reduced the most for channel A of the vehicular test environment by more than 10 dB. On the other hand, the required E_b/N_0 is reduced the least for channel B of the vehicular test environment by 1 dB. Over all, numerical results demonstrate that bit loading helps reduce the BER in cases of both channel A and channel B for all three test

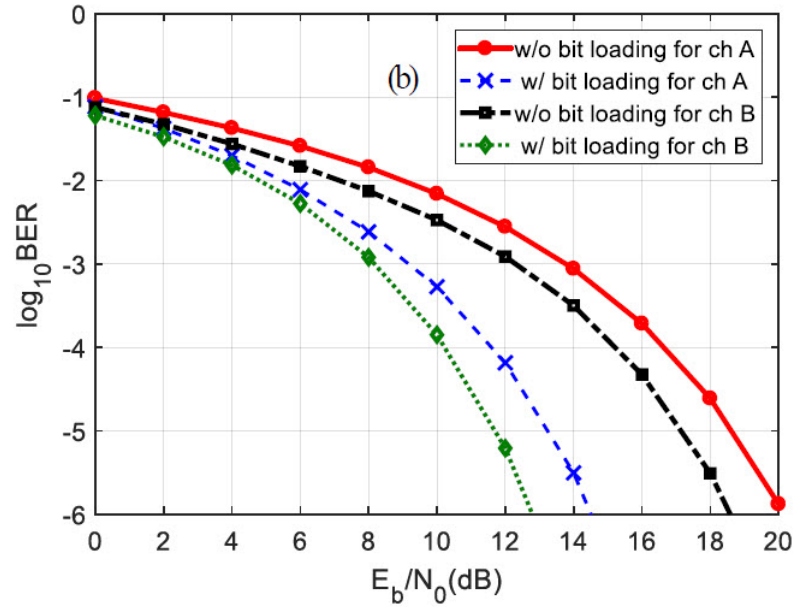


Figure 4.15: BER versus E_b/N_0 using MMSE equalization with and without bit loading for channel A and channel B of the outdoor to indoor pedestrian test environment.

environments. These results demonstrate the main advantage of bit loading.

4.2.6 BER Comparison between WPM and OFDM

In addition to comparison of equalization with and without bit loading for WPM, the BER performance of WPM is compared with that of OFDM, considering equalization with bit loading. In case of WPM, MMSE equalization with the proposed equalization-aware bit loading algorithm is considered, whereas in case of OFDM, one-tap equalization with bit loading is considered. The BERs are obtained for channel A and channel B for all three test environments, as displayed in Fig. 4.17-4.19. It can be noticed that, for most scenarios, the required E_b/N_0 to achieve the target BER of 10^{-5} is reduced by 1-2 dB in case of WPM compared to OFDM. Above all, WPM performs better than OFDM given that bit loading is implemented for each approach.

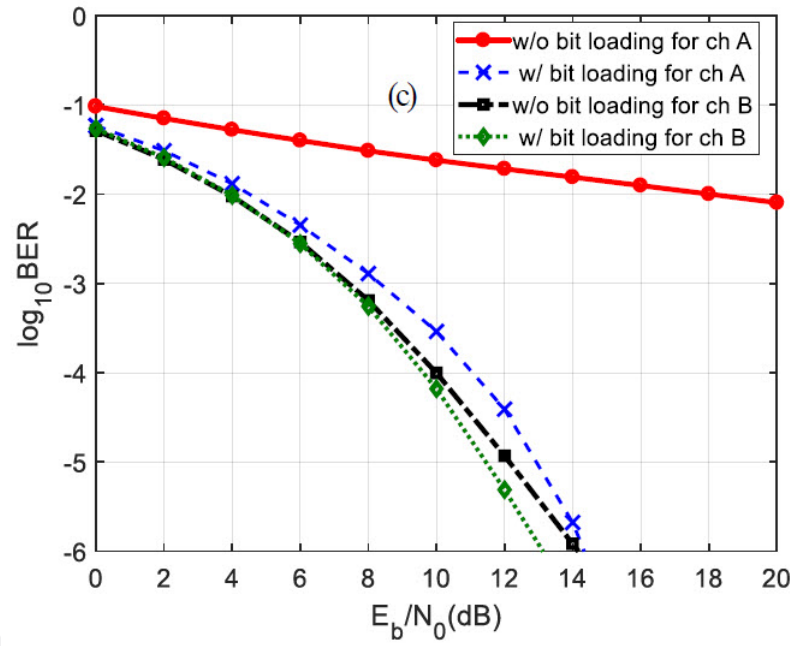


Figure 4.16: BER versus E_b/N_0 using MMSE equalization with and without bit loading for channel A and channel B of the vehicular test environment.

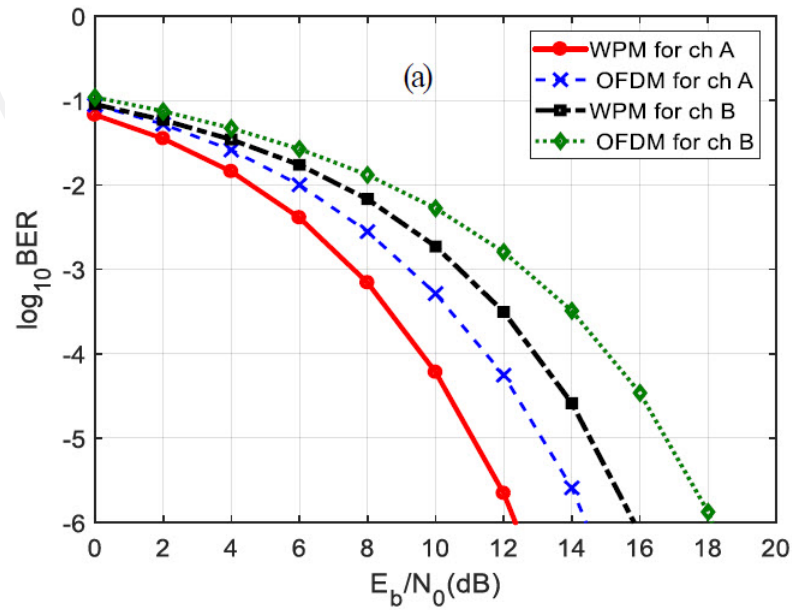


Figure 4.17: BER versus E_b/N_0 comparison between WPM and OFDM for channel A and channel B of the indoor office test environment

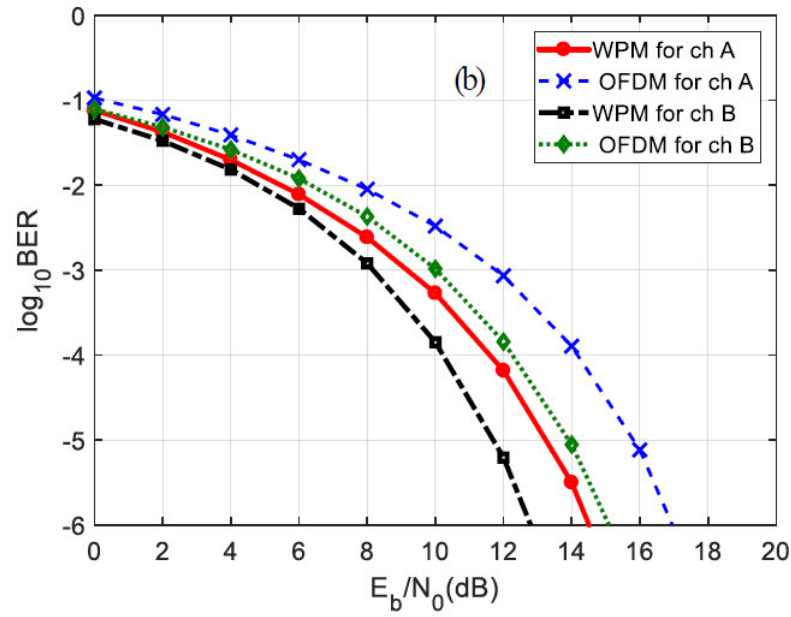


Figure 4.18: BER versus E_b/N_0 comparison between WPM and OFDM for channel A and channel B of outdoor to the indoor pedestrian test environment.

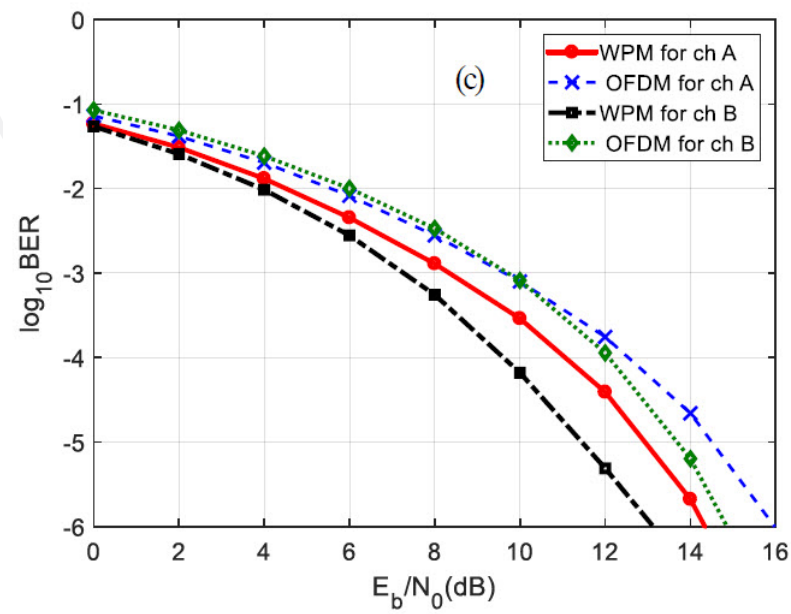


Figure 4.19: BER versus E_b/N_0 comparison between WPM and OFDM for channel A and channel B of the vehicular test environment.

4.3 Findings and Discussion

The BER performance analysis was conducted assuming that the CSI is known. A mathematical expression to compute the BER for WPM is used to investigate the benefits of bit loading for WPM. In addition, the derived BER expression is also used to compare the BER performances of WPM and OFDM. The relevant analytical expressions are first validated through simulation results obtained using MATLAB, before being used for performance analysis of WPM. Numerical results indicate that the proposed equalization-aware bit loading along with MMSE equalization helps enhance the BER performance of WPM, in contrast to equalization without bit loading. Moreover, numerical results also highlighted that, in terms of the BER performance, WPM considering MMSE equalization with the proposed equalization-aware bit loading performs better than OFDM considering one-tap equalization with bit loading.

CHAPTER 5

WPM WITH UNKNOWN CSI

This chapter investigates the BER performance of WPM considering unknown CSI. At first, impact of the training sequence length on the BER performance is investigated for WPM with time-domain MMSE equalization. The investigation quantifies the required lengths of the training sequence to achieve an acceptable BER for different numbers of subcarriers. Next, bit loading for WPM considering unknown CSI is explored. The proposed bit loading algorithm requires the knowledge of CIR. Therefore, a channel estimation method based on using the solution of an overdetermined system of linear equations is introduced. The BER performance of WPM with bit loading using the estimated CIR is computed and compared with that of WPM without bit loading. Moreover, the BER performance of WPM with bit loading is compared with that of OFDM with bit loading.

5.1 WPM System Block Diagram with Unknown CSI

The system block diagram for WPM shown earlier in Fig. 3.1 is applicable when CSI is known. However, for unknown CSI, the WPM system block diagram needs to be modified by adding a pilot carrier insertion block at the transmitter and a channel estimation block at the receiver. The modified WPM system block diagram is shown in Fig. 5.1. For WPM using equalization without bit loading, transmit data is fed to a serial-to-parallel converter, considering 2×2 QAM on each subcarrier. However, for WPM using equalization with bit loading, bits are allocated to each subcarrier based on the bit loading algorithm, except for WPM symbols which are used as a training sequence.

At specific regular intervals of QAM symbols, a randomly generated but known training sequence is inserted. QAM symbols along with the training sequence

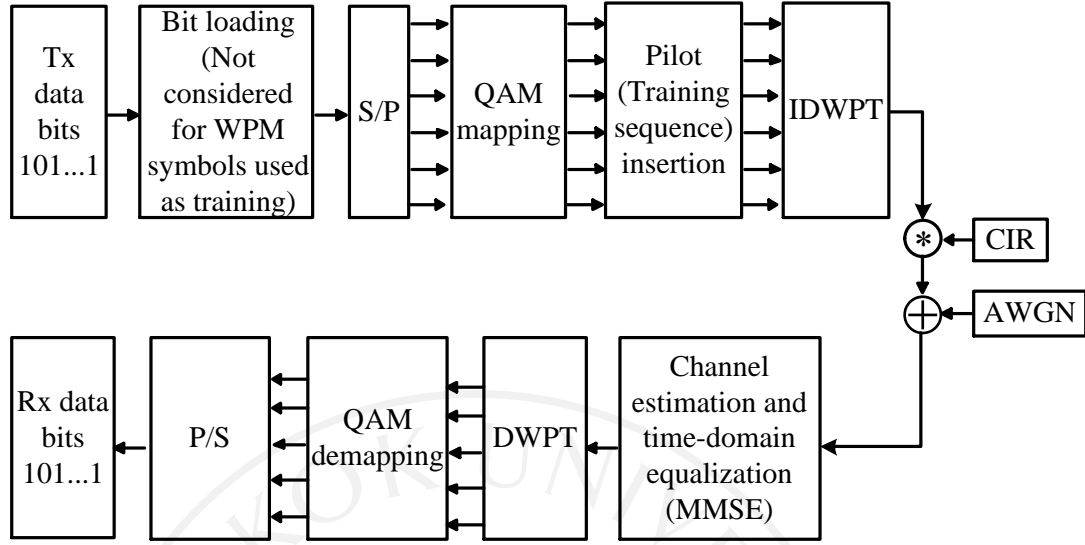


Figure 5.1: System block diagram for WPM with unknown CSI

are input to IDWPT, which generates the transmit WPM symbols in the time domain. The transmitted signal is passed through the channel with unknown channel impulse response (CIR) and additive white gaussian noise (AWGN). At the receiver, the known training sequence is used to compute the MMSE equalizer coefficients and to estimate the unknown CIR. The estimated CIR is fed back to the transmitter with a small overhead as compared with the transmitted data. The received signals are equalized using the MMSE equalizer in the time domain before it is fed to DWPT. The output of DWPT is passed through QAM demapping and a parallel-to-serial converter to obtain the received bits. The difference between the transmitted and the received bits will provide the Bit Error Rate (BER).

5.2 Performance Analysis for Unknown CSI

The BER performance of WPM with unknown CSI is studied using a simulation program developed in MATLAB. The simulation program is developed following the block diagram shown in Fig. 5.1. The overall transmit WPM symbols

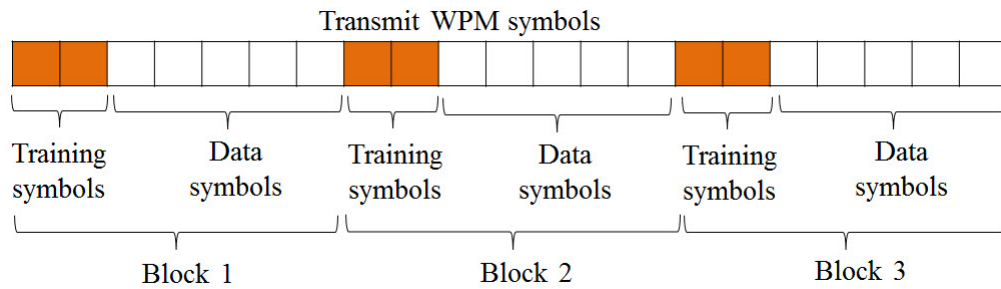


Figure 5.2: Transmit frame with training sequences and data symbols

are divided into separate blocks of equal length. Each block contains a known training sequence, which is followed by transmit data symbols. The transmit WPM frame structure is shown in Fig. 5.2. The channel is assumed to be quasistatic and remains constant for each block. A Rayleigh fading channel model is randomly generated for each block, using the power delay profiles for channel A and channel B of the three test environments as given in Tables 4.1- 4.3 (ITU-R Rec. M.1225, 1997). The three test environments are : (1) indoor office test environment, (2) outdoor to indoor and pedestrian test environment, and (3) vehicular test environment.

The BERs for each test environment are evaluated considering the data rate of 10 Mbps. The simulation parameters are listed in Table 5.1. Here, with 64 subcarriers and 2×2 QAM on each subcarrier (i.e., 2 bits on each subcarrier), the total number of bits transmitted on each block with 100 MCM symbols is $(2 \times 64) \times 100 = 12800$ bits. A block of 100 MCM symbols includes both training symbols and data symbols. Furthermore, with the data rate of 10 Mbps, the total time to transmit 12800 bits, i.e., one block duration, is equal to $12800/10,000,000 = 1.28$ ms. The block duration of 1.28 ms is shorter than a typical coherence time of at least 2 ms (Goldsmith, 2005), (Andrews, Ghosh, & Muhamed, 2007), & (Tse & Viswanath, 2005). This makes the quasistatic assumption reasonable.

At first, simulation is conducted to find the training sequence lengths required to achieve the acceptable BER performance for different wavelet filter lengths, considering WPM with MMSE equalization but without bit loading. It is

Table 5.1: Simulation parameters for WPM and OFDM systems

Parameter	Value
MCM technique	WPM, OFDM
No. of subcarriers	16, 32, 64
Equalizer filter length	41
No. of MCM symbols	1000
No. of transmitted bits	32000, 64000, 128000
QAM signal set	2×2
Wavelet function	db4 (Burrus et al., 1998)
OFDM CP	$\frac{1}{4} \times \text{No. of subcarriers}$
Data block size	100 MCM symbols
No. of blocks	10
No. of transmitted bits per block	3200, 6400, 12800

followed by the BER computation for WPM considering equalization with bit loading using the estimated CIR. The BERs of WPM with bit loading using the estimated CIR are then compared with those for WPM without bit loading. Finally, the BER performance of WPM with bit loading is compared with that of OFDM with bit loading for both known and unknown CSI.

5.2.1 Training Length for Equalizer Filter Computation

In this section, simulation is conducted to explore the required length of the training sequences while using MMSE equalization for WPM to obtain the desired BER performance. The investigation is performed for different numbers of subcarriers: 16, 32, and 64 subcarriers. Simulation results are obtained for channel A of the indoor office test environment. The BER performance of MMSE equalization with unknown CSI relies on the number of signal values employed for the training. A sufficiently long training sequence yields the BER performance comparable to the case with known CSI, as demonstrated by simulation results as follows.

The BER plot for WPM using MMSE equalization with 16 subcarriers is shown in Fig. 5.3. The plot compares the BER obtained for unknown CSI with that for known CSI, using different lengths of training sequences. It can be noticed from

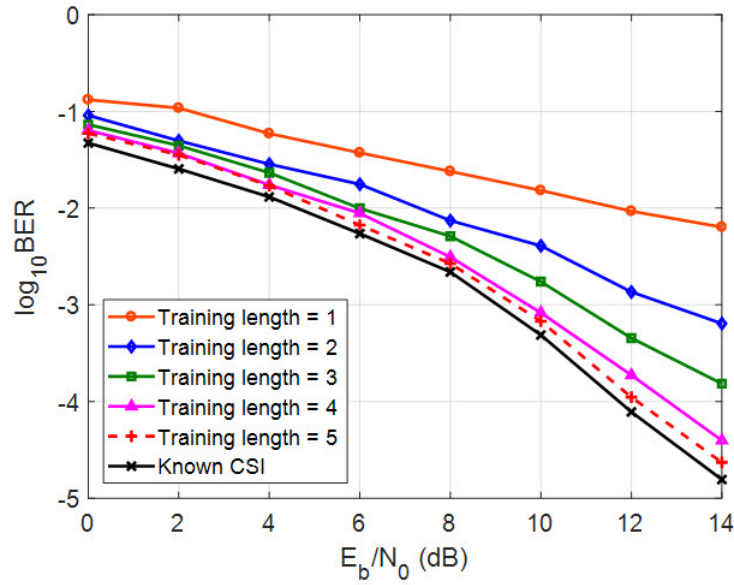


Figure 5.3: BER-versus- E_b/N_0 considering channel A of the indoor office test environment for WPM with 16 subcarriers

the plot that the BER with the training length of 1 WPM symbol is significantly higher than that for the known CSI. However, as the training sequence length is increased to 2, 3, and 4 WPM symbols, the BER decreases and approaches the BER for known CSI. Finally, with the training length of 5 WPM symbols, the BER for unknown CSI becomes comparable to that for known CSI.

The BER plots for 32 and 64 subcarriers are shown in Fig. 5.4-5.5. The plots show that, for 32 subcarriers, the training sequence length of 2 WPM symbols is required. Moreover, for 64 subcarriers, the training sequence length of 1 WPM symbol is enough to obtain the BER comparable with that for known CSI. It can be observed that, as the training sequence length increases, the BER performance for unknown CSI approaches that for known CSI. In addition, with the increasing number of subcarriers, the length of a WPM symbol increases and the number of signal values per WPM symbol also increases. Therefore, for the same number of WPM symbols invested in the training, a higher number of subcarriers implies more signal values for the

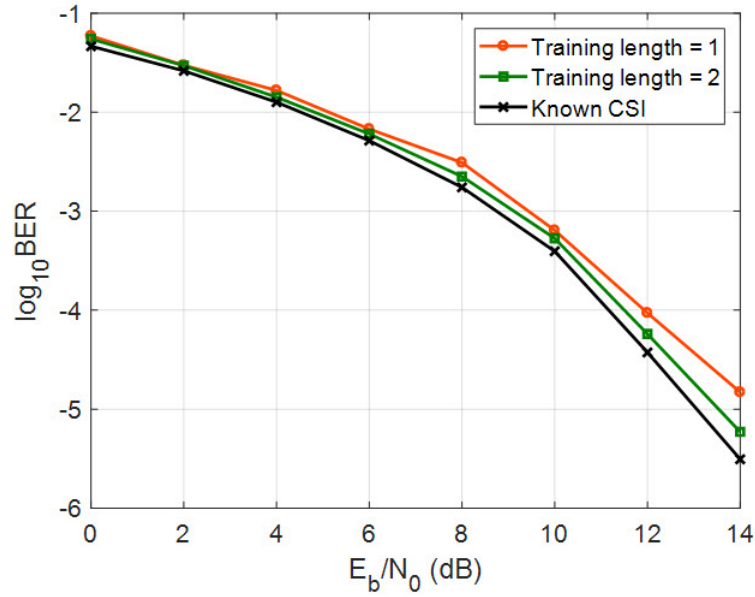


Figure 5.4: BER-versus- E_b/N_0 considering channel A of the indoor office test environment for WPM with 32 subcarriers

training, resulting in a more accurate computation of the equalizer coefficients, and thus providing a better BER performance. As an illustration, for the training sequence length of 1 WPM symbol with 16 subcarriers, the length of signal values is 16, while with 64 subcarriers the length of signal values is 64. Hence, for the same number of training WPM symbols, the number of signal values employed for training with 64 subcarriers is higher than that with 16 subcarriers.

The required training sequence lengths to achieve the acceptable BER performance for channel A and channel B of all three test environments are listed in Table. 5.2. The lengths of training sequences are obtained for 16, 32 and 64 subcarriers. In the case of 16 subcarriers, the maximum required training sequence length is 5 WPM symbols. Similarly, for 32 subcarriers, the maximum required training sequence length is 2 WPM symbols, while for 64 subcarriers 1 WPM symbol is sufficient in all the considered scenarios. The overhead due to the training sequence length for the block size of 100 WPM symbols are at most 5% for 16 subcarriers, and

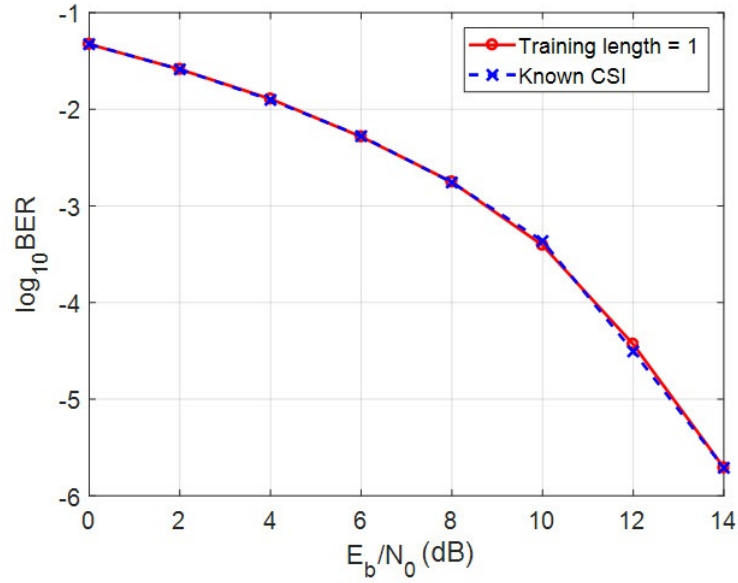


Figure 5.5: BER-versus- E_b/N_0 considering channel A of the indoor office test environment for WPM with 64 subcarriers

Table 5.2: Training sequence lengths (in number of WPM symbols) required to achieve acceptable BER performances for channel A and channel B of each test environment for $N = 16$, $N = 32$, and $N = 64$

Test environment	Channel	Training sequence length		
		$N=16$	$N=32$	$N=64$
Indoor office	A	5	2	1
	B	5	2	1
Outdoor-to-indoor & pedestrian	A	4	1	1
	B	5	1	1
Vehicular	A	4	1	1
	B	4	1	1

at most 1% for 64 subcarriers.

5.2.2 BER Comparison between WPM and OFDM

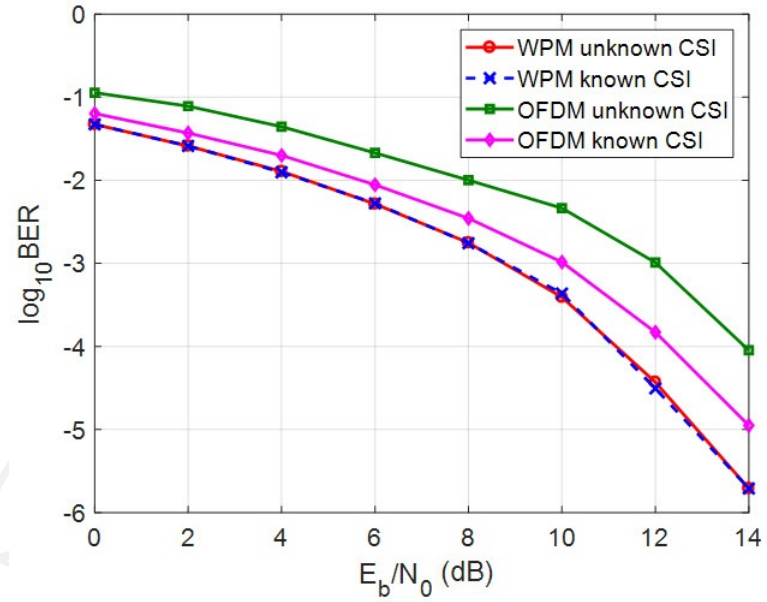
In this section, the BER performance of WPM with MMSE equalization is compared with that of OFDM with one-tap equalization considering both known and

unknown CSI. The BERs are plotted for WPM with known CSI, WPM with unknown CSI, OFDM with known CSI, and OFDM with unknown CSI. For OFDM with unknown CSI, channel estimation is done based on the LS channel estimation method given in (Kumar & Grover, 2012). BER plots are obtained for WPM and OFDM using 64 subcarriers, and the training sequence length of 1 symbol is used for both WPM and OFDM for unknown CSI. The BER plots for channel A and channel B of three test environments are given in Fig. 5.6-5.8.

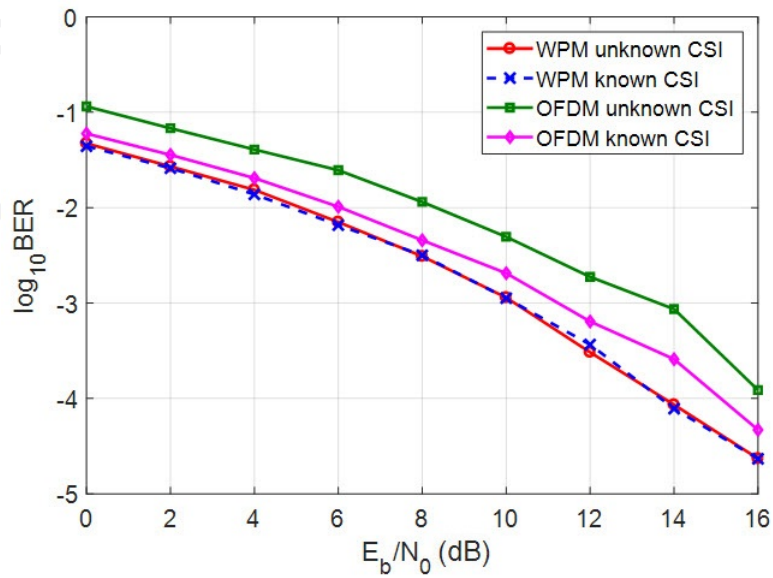
BER plots of OFDM for channel A and channel B in all the test environments, show that BERs for known CSI are lower than those for unknown CSI. Moreover, the BERs of WPM with unknown CSI are in fact lower than those for OFDM with known CSI. Note that the BERs obtained for OFDM with known CSI are minimal, and irrespective of the channel estimation method used the BERs cannot be reduced further. The reductions in E_b/N_0 to achieve the BER of 10^{-4} for WPM as compared with OFDM are listed in Table. 5.3. From the table, it can be seen that channel A of the vehicular test environment has the maximum E_b/N_0 improvement of 2 dB, while channel B of the indoor office test environment has the minimum E_b/N_0 improvement. WPM has the overhead of 1 WPM symbol for the training sequence, while OFDM suffers from the overhead due to the use of CP in addition to the 1 OFDM symbol for the training sequence. In general, WPM results in less overhead as compared to OFDM. However, even with the moderate overhead, the BER performance of WPM with MMSE equalization is better than OFDM with one-tap equalization.

5.2.3 Channel Estimation using Overdetermined Systems

The proposed bit loading algorithm depends on computation of the noise power gain, the signal power gain, and the signal power based on the number of bits allocated to each subcarrier. The computation of signal power gain η_k is given by (3.25), and requires the knowledge of CIR h_n . Therefore, when CSI is unknown, the

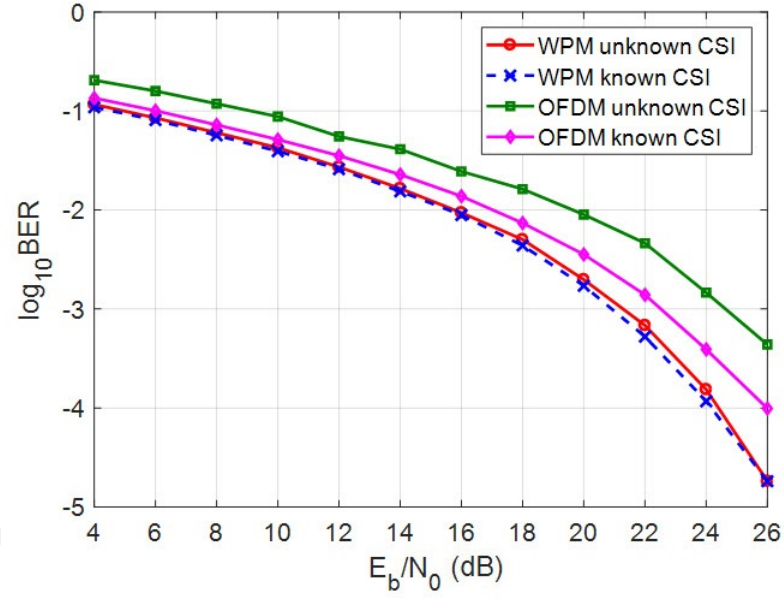


(a)

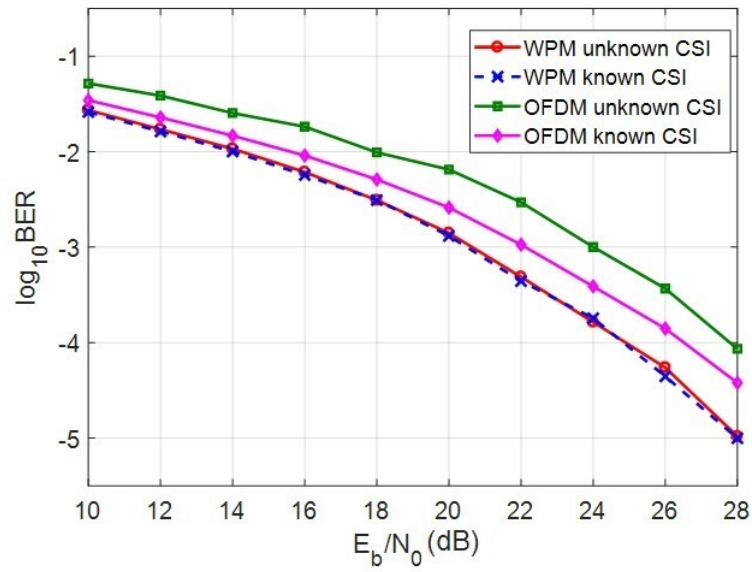


(b)

Figure 5.6: BER-versus- E_b/N_0 comparison between WPM and OFDM for the indoor office test environment (a) channel A (b) channel B

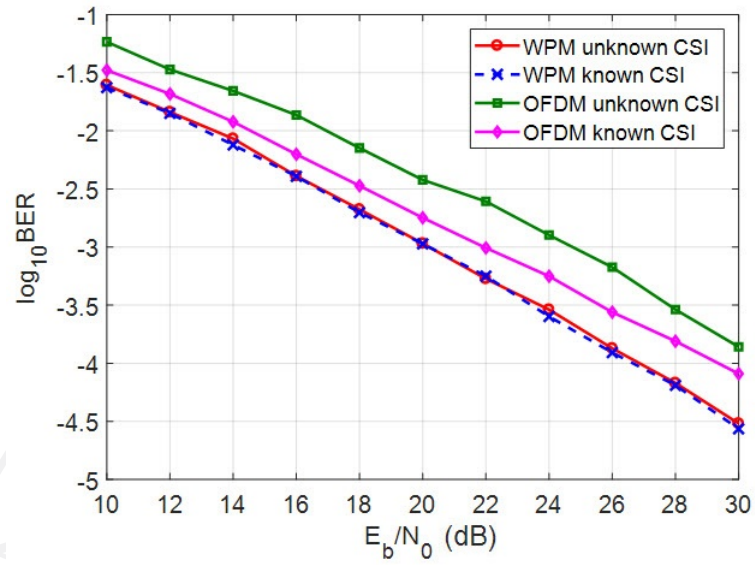


(a)

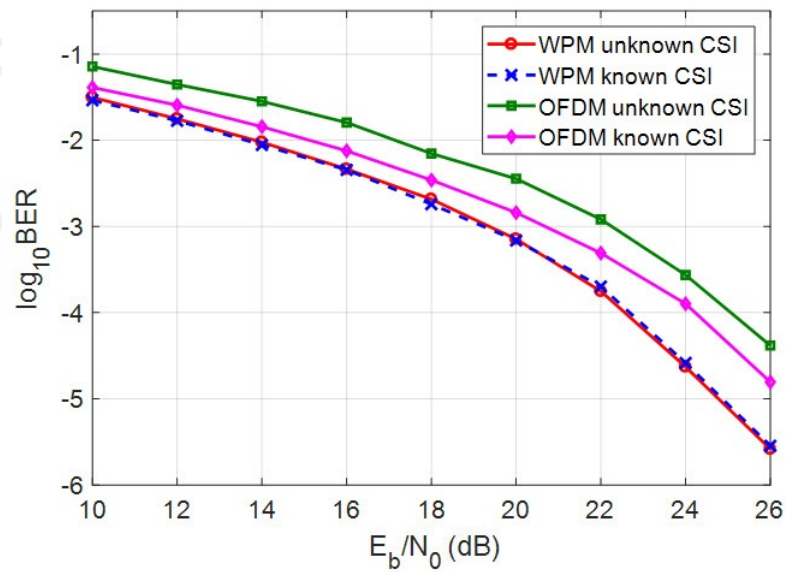


(b)

Figure 5.7: BER-versus- E_b/N_0 comparison between WPM and OFDM for the outdoor-to-indoor and pedestrian test environment (a) channel A (b) channel B



(a)



(b)

Figure 5.8: BER-versus- E_b/N_0 comparison between WPM and OFDM for the vehicular test environment (a) channel A (b) channel B

Table 5.3: Reductions of E_b/N_0 for WPM compared to OFDM to achieve the BER of 10^{-4}

Test environment	Channel	E_b/N_0 reduction
Indoor office	A	1.5 dB
	B	1 dB
Outdoor-to-indoor and pedestrian	A	2 dB
	B	1.5 dB
Vehicular	A	2.5 dB
	B	1.5 dB

CIR needs to be estimated. A channel estimation method based on using the solution of an overdetermined system of linear equations is introduced based on the theory given in (Gentle, 2007).

An overdetermined system consists of more equations than the number of unknowns. In our scenario, unknown variables are the CIR h_n , which are estimated using the known training sequence. The received signal r_n before equalization as given by (3.2) can be expressed in the matrix form as

$$\mathbf{r} = \mathbf{S}\mathbf{h} \quad (5.1)$$

where \mathbf{r} is a column vector containing r_n , \mathbf{S} is a Toeplitz matrix containing the training sequence s_n of length L , and \mathbf{h} is a column vector containing h_n . Consider the estimated CIR denoted by \hat{h}_n . In particular, \mathbf{r} , \mathbf{h} , $\hat{\mathbf{h}}$, and \mathbf{S} can be written as

$$\mathbf{r} = \begin{bmatrix} r_{C-1} & r_C & \cdots & r_{L-1} \end{bmatrix} \quad (5.2)$$

$$\mathbf{h} = \begin{bmatrix} h_0 & h_1 & \cdots & h_{C-1} \end{bmatrix} \quad (5.3)$$

$$\hat{\mathbf{h}} = \begin{bmatrix} \hat{h}_0 & \hat{h}_1 & \cdots & \hat{h}_{C-1} \end{bmatrix} \quad (5.4)$$

$$\mathbf{S} = \begin{bmatrix} s_{C-1} & s_{C-2} & \cdots & s_0 \\ s_C & s_{C-1} & \cdots & s_1 \\ s_{C+1} & s_C & \cdots & s_2 \\ \vdots & \vdots & \ddots & \vdots \\ s_{C-1+L-1} & s_{C-2+L-1} & \cdots & s_{L-1} \end{bmatrix} \quad (5.5)$$

The estimated CIR, denoted by \hat{h}_n , is computed such that the corresponding MSE is minimized. The MSE with respect to the estimated CIR $\hat{\mathbf{h}}$ is given as

$$\epsilon = \|\mathbf{S}\hat{\mathbf{h}} - \mathbf{r}\|^2 \quad (5.6)$$

Expanding (5.6) leads to

$$\begin{aligned} \epsilon &= (\mathbf{S}\hat{\mathbf{h}} - \mathbf{r})^T (\mathbf{S}\hat{\mathbf{h}} - \mathbf{r}) \\ &= (\mathbf{S}\hat{\mathbf{h}})^T (\mathbf{S}\hat{\mathbf{h}}) - \mathbf{r}^T (\mathbf{S}\hat{\mathbf{h}}) - (\mathbf{S}\hat{\mathbf{h}})^T \mathbf{r} + \mathbf{r}^T \mathbf{r} \\ &= (\mathbf{S}^T \mathbf{S})(\hat{\mathbf{h}}\hat{\mathbf{h}}^T) - 2(\mathbf{S}\hat{\mathbf{h}})^T \mathbf{r} + \mathbf{r}^T \mathbf{r} \\ &= (\mathbf{S}^T \mathbf{S})(\hat{\mathbf{h}}\hat{\mathbf{h}}^T) - 2(\mathbf{S}^T \mathbf{r})\hat{\mathbf{h}}^T + \mathbf{r}^T \mathbf{r} \end{aligned} \quad (5.7)$$

For the minimization of ϵ , setting $\nabla \epsilon = 0$ leads to

$$2(\mathbf{S}^T \mathbf{S})\hat{\mathbf{h}} - 2(\mathbf{S}^T \mathbf{r}) = 0 \quad (5.8)$$

yielding

$$\hat{\mathbf{h}} = (\mathbf{S}^T \mathbf{S})^{-1} \mathbf{S}^T \mathbf{r} \quad (5.9)$$

As a specific example, the estimated CIR $\hat{\mathbf{h}}$ is computed employing (5.9) with the training sequence length of 1 WPM symbol, and is compared with the known CIR \mathbf{h} for channel A of the indoor office test environment as shown in Fig. 5.9. From

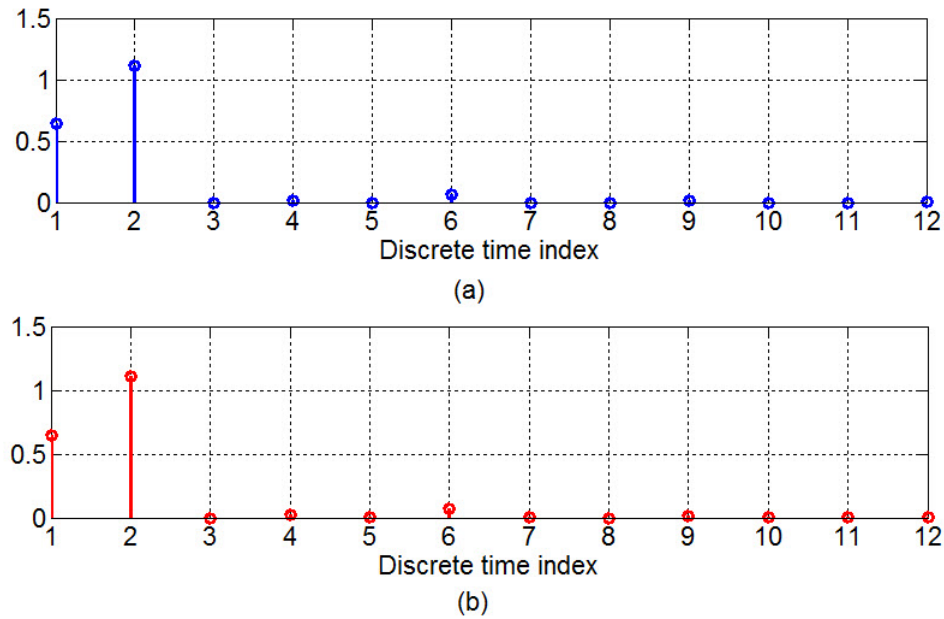


Figure 5.9: CIR for channel A of the vehicular test environment (a) known (b) unknown but estimated

the plot, it can be noticed that the estimated CIR is comparable to the known CIR.

5.2.4 Bit Loading with Estimated CIR

The estimated CIR \hat{h} is used instead of the known CIR h to operate the bit loading algorithm introduced in chapter 3. The BERs are obtained using 64 subcarriers. The results in the previous section show that the training sequence length of 1 WPM symbol is enough for WPM with 64 subcarriers to estimate the unknown CIR that can lead to an acceptable BER performance. Therefore, the estimated CIR \hat{h} is obtained using the training sequence length of 1 WPM symbol. BER plots are obtained for WPM using MMSE equalization with and without bit loading considering both known and unknown CIR. For known CIR, MMSE equalizer coefficients are obtained using (3.11) and the bit loading algorithm considers the known CIR h . However, for unknown CIR, MMSE equalizer coefficients are obtained using (3.19) and the bit loading algorithm employs the estimated CIR \hat{h} . BER plots

are obtained for channel A and channel B of three test environments from (ITU-R Rec. M.1225, 1997): (1) indoor office test environment, (2) outdoor to indoor and pedestrian test environment, and (3) vehicular test environment.

BER plots of WPM with and without bit loading considering known and unknown CIR for channel A and channel B of three test environments are shown in Fig. 5.10-5.12. In all cases, the BERs obtained for unknown CSI are close to those for known CSI while considering MMSE equalization with and without bit loading. In addition, MMSE equalization with bit loading considering unknown CIR has a better BER performance as compared to MMSE equalization without bit loading in most scenarios. However, for channel A of the indoor office test environment and the outdoor to indoor pedestrian test environment, BERs for MMSE equalization with bit loading are almost the same as those for MMSE equalization without bit loading, as shown in Fig. 5.10(a), 5.11(a). This is because when the channels are not highly dispersive, the noise power gain and signal power gain distribution across subcarriers will be relatively uniform. Therefore, the bit loading algorithm provides the bit allocation with almost the same number of bits on each subcarrier, and thus the BER performance for MMSE equalization with bit loading will be almost the same as that for MMSE equalization without bit loading. The required E_b/N_0 to achieve the BER of 10^{-3} is reduced by 2 dB for channel B of the indoor office test environment, 4 dB for channel B of the outdoor to indoor test environment, 4 dB for channel A of the vehicular test environment, and 3 dB for channel B of the vehicular test environment. Here, the BER of 10^{-3} is taken as a reference because for some test environments BERs are not below 10^{-3} .

Further, the BER performance of WPM is compared with that of OFDM. The BER plots are obtained for WPM with bit loading and OFDM with bit loading. The BER plots are obtained for both known and unknown CSI. For OFDM, one-tap equalization is used and channel estimation is performed using the LS channel estimation method in (Kumar & Grover, 2012). For unknown CSI, the length of the

training sequence is 1 MCM symbol for both WPM and OFDM. The BERs are plotted for channel A and channel B of all three test environments, as shown in Fig.

5.13-5.15.

The plots show that the BER of OFDM with unknown CSI is higher than OFDM with known CSI. This is due to inaccurate channel estimation. Note that the BERs obtained with known CSI are the minimum values and cannot be reduced further regardless of the channel estimation method used. For all the test environments, BERs for WPM using bit loading with unknown CSI are lower than those for OFDM using bit loading with known CSI. In particular, the required E_b/N_0 to achieve the BER of 10^{-3} is reduced by 3 dB for channel A of the indoor office test environment, 2 dB for channel B of the indoor office test environment, 2 dB for channel A of the outdoor to indoor pedestrian test environment, 3 dB for channel B of outdoor to indoor pedestrian test environment, 2.5 dB for channel A of the vehicular test environment, and 2 dB for channel B of the vehicular test environment.

5.3 Findings and Discussion

The performance analysis of WPM is performed with unknown CSI. At first, the analysis is performed for WPM with MMSE equalization without bit loading. The required training lengths to obtain the desired BER are investigated for different numbers of subcarriers. Numerical results demonstrate that, with a moderate overhead from the training sequence, the BER with unknown CSI is comparable to that with known CSI. Next, the analysis is extended for WPM using MMSE equalization with bit loading. Channel estimation is done using the solution from an overdetermined system of linear equations. The BER performance of WPM with bit loading using the estimated CIR while considering unknown CSI is found to be close to that for known CSI. Further, the performance of WPM is found to be better than that of OFDM.

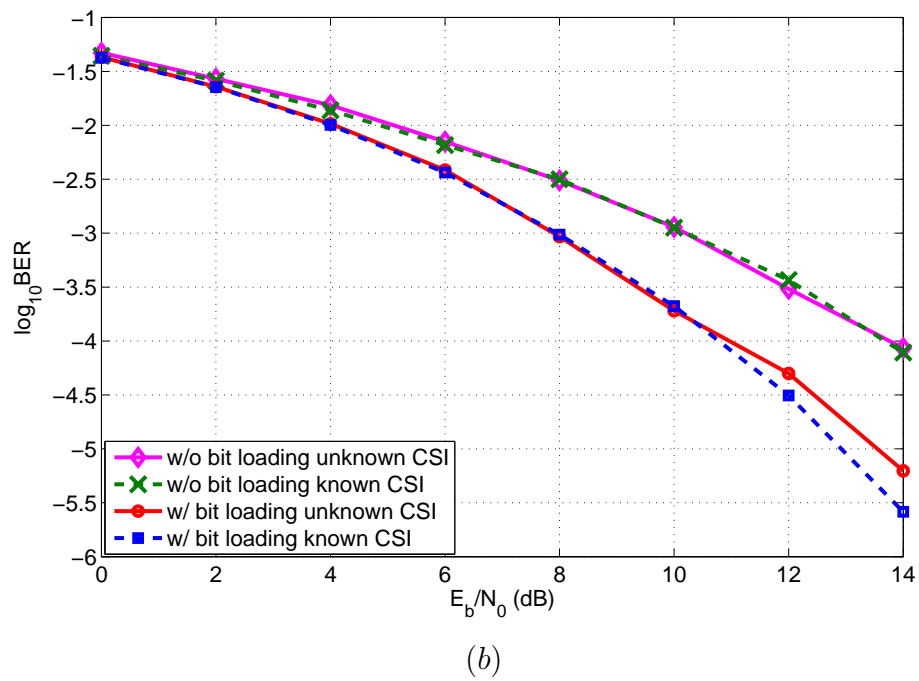
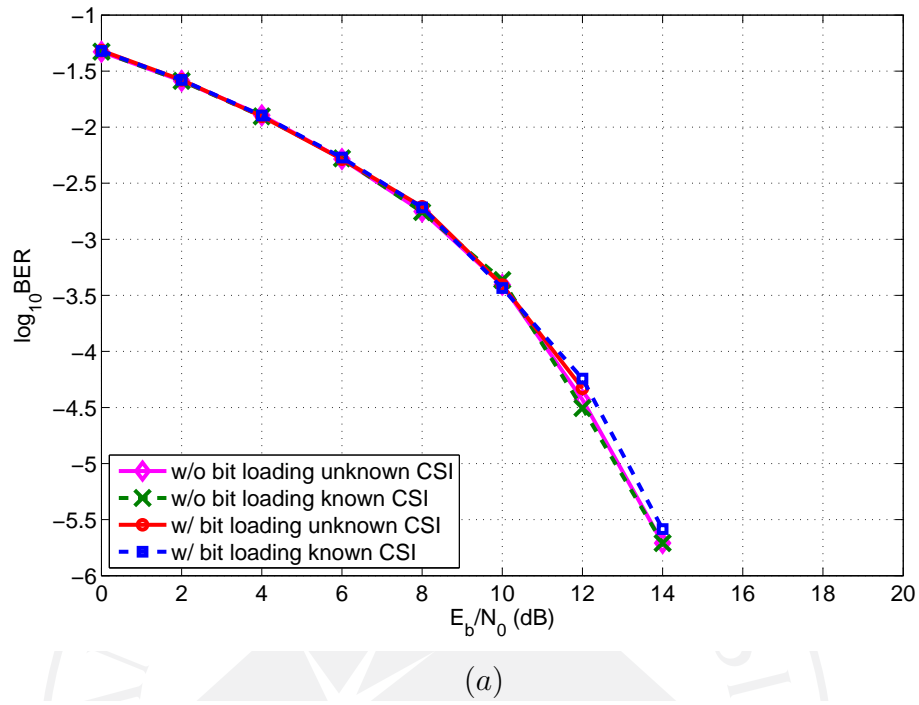


Figure 5.10: BER-versus- E_b/N_0 using MMSE equalization with and without bit loading for known and unknown CSI under the indoor office test environment (a) channel A (b) channel B

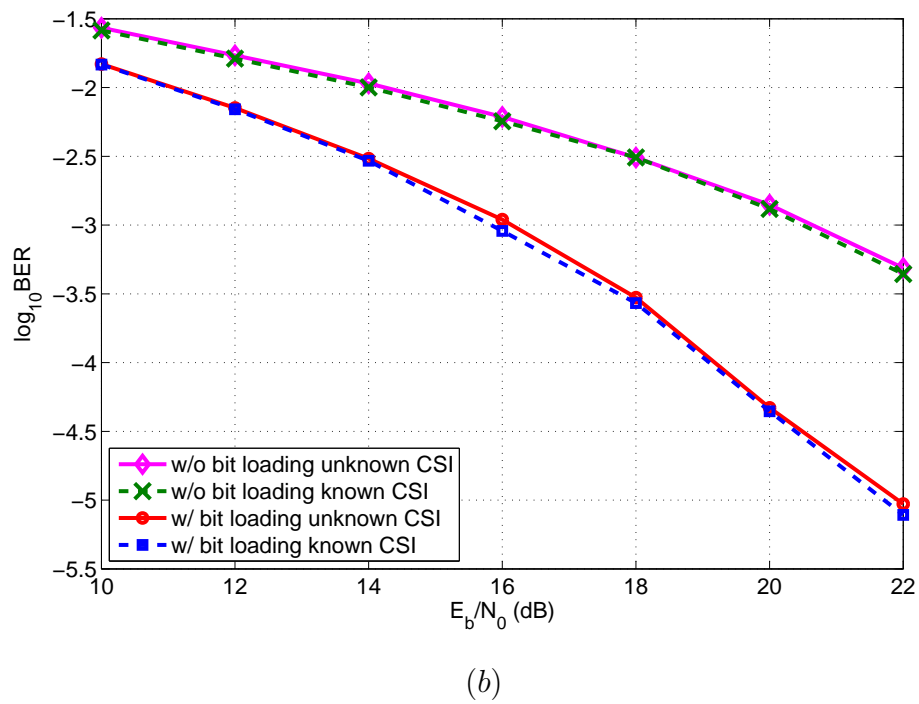
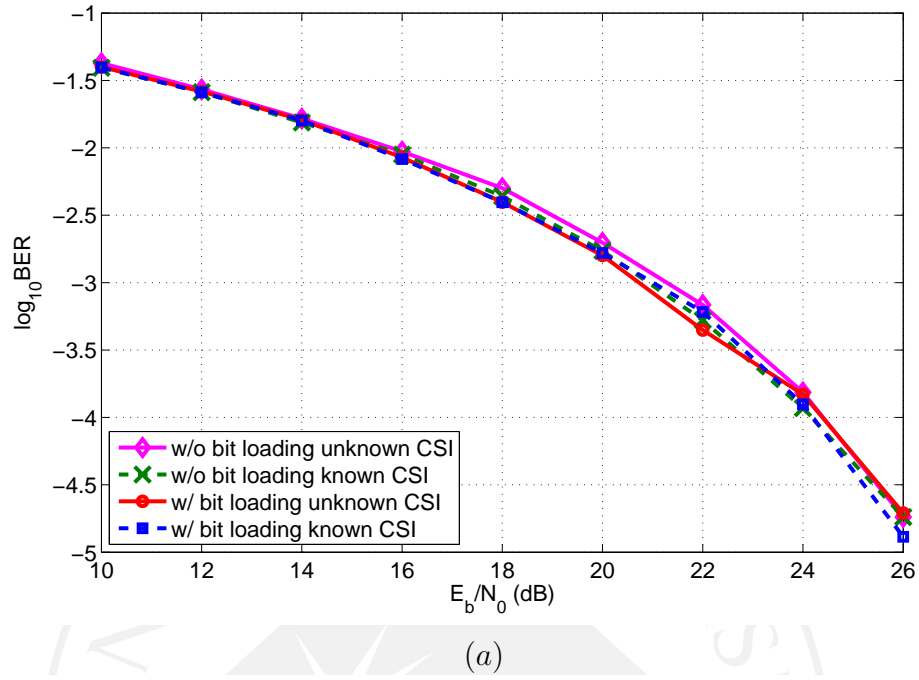


Figure 5.11: BER-versus- E_b/N_0 using MMSE equalization with and without bit loading for known and unknown CSI under the outdoor to indoor pedestrian test environment (a) channel A (b) channel B

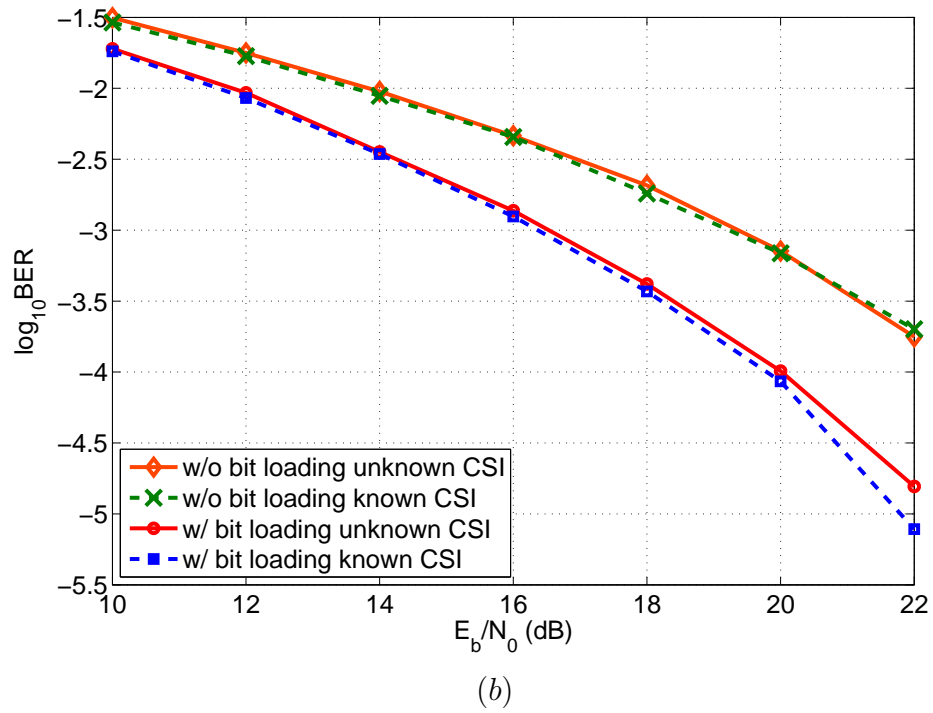
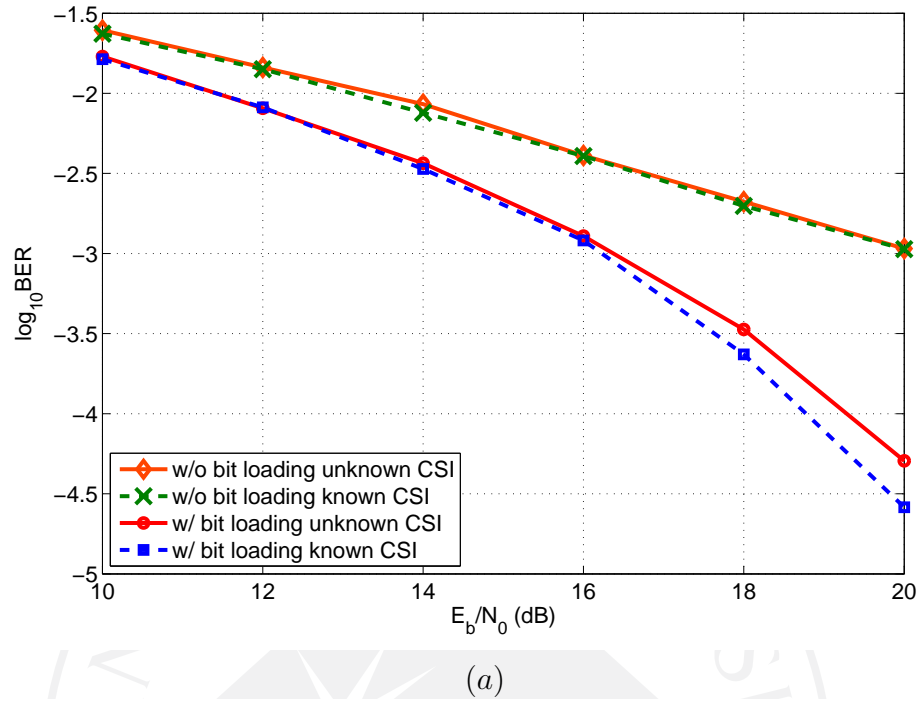
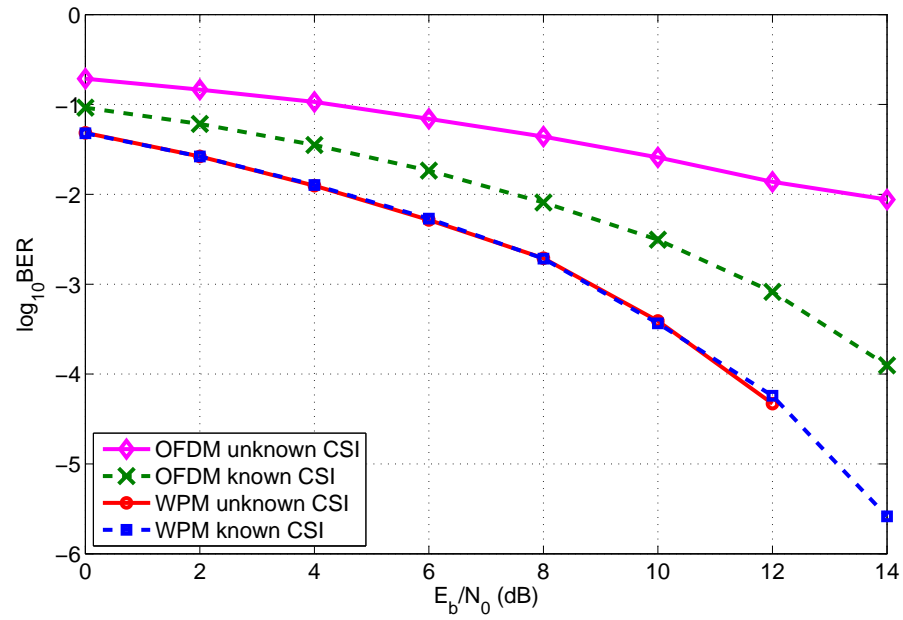
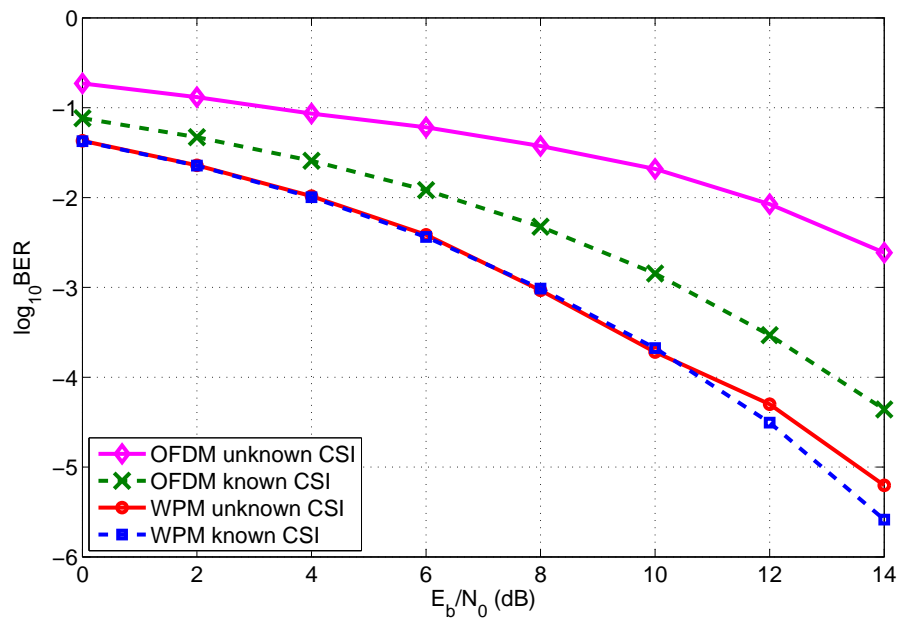


Figure 5.12: BER-versus- E_b/N_0 using MMSE equalization with and without bit loading for known and unknown CSI under the vehicular test environment (a) channel A (b) channel B



(a)



(b)

Figure 5.13: BER-versus- E_b/N_0 comparison between WPM and OFDM for the indoor office test environment (a) channel A (b) channel B

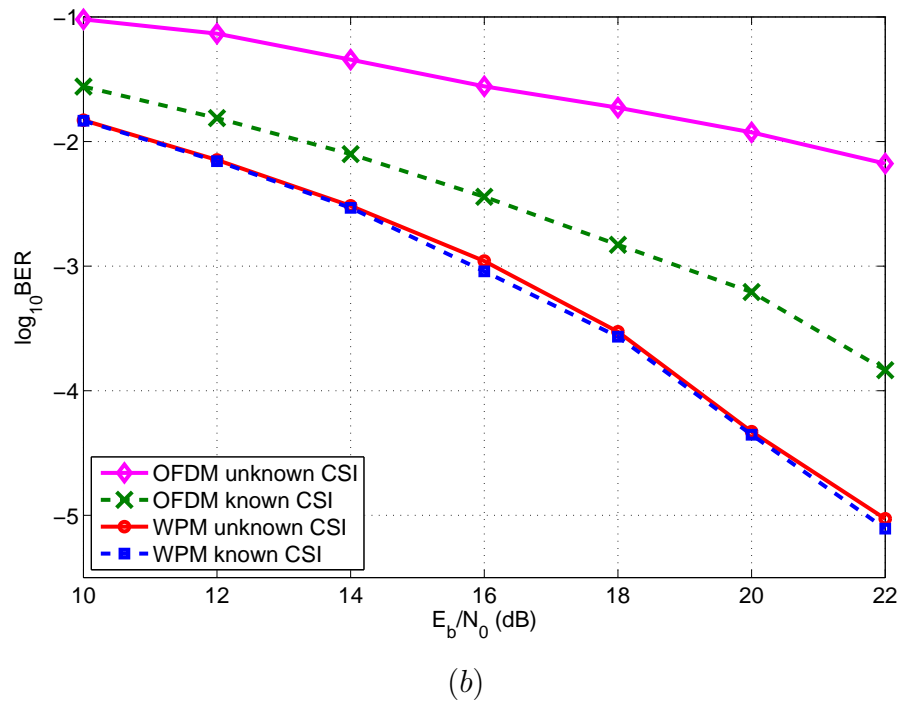
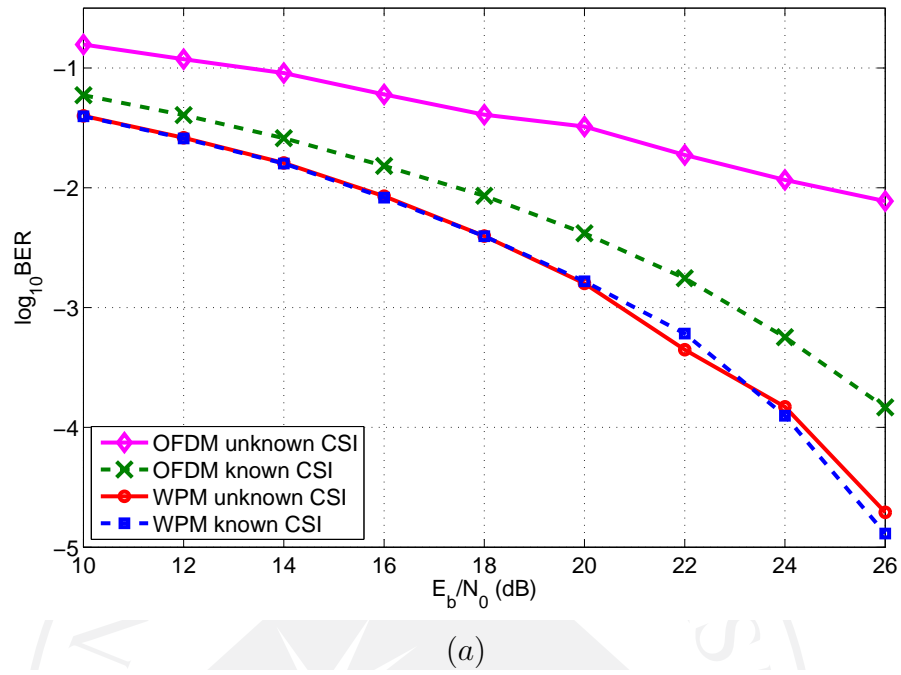
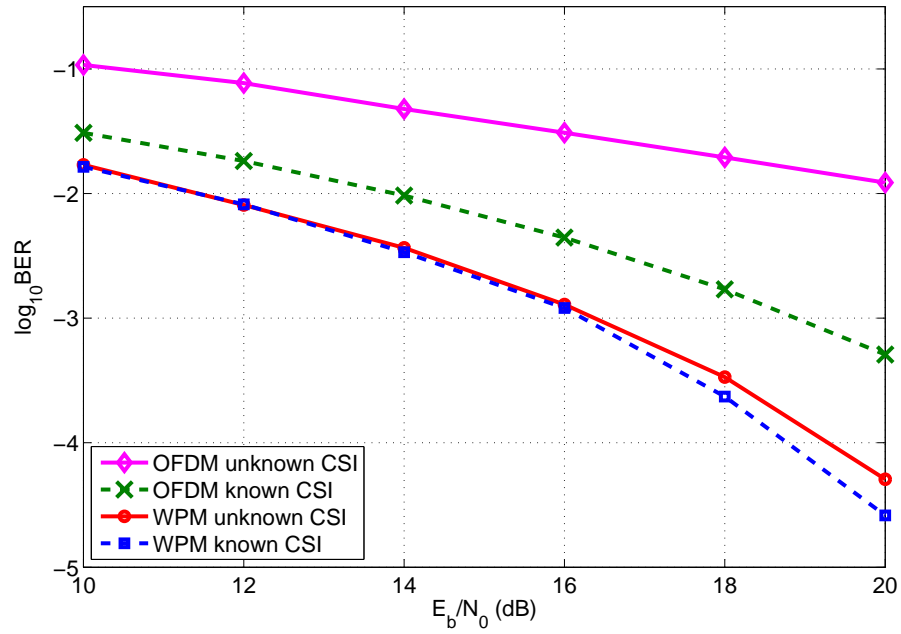
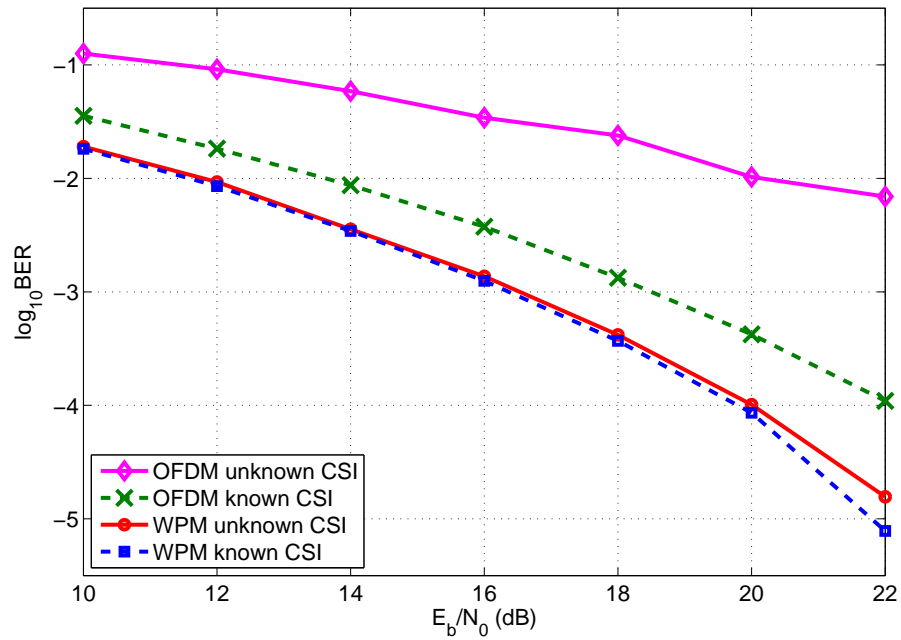


Figure 5.14: BER-versus- E_b/N_0 comparison between WPM and OFDM for the outdoor to indoor pedestrian test environment (a) channel A (b) channel B



(a)



(b)

Figure 5.15: BER-versus- E_b/N_0 comparison between WPM and OFDM for the vehicular test environment (a) channel A (b) channel B

CHAPTER 6

CONCLUSION AND SUGGESTIONS FOR FUTURE WORK

This thesis presents a bit loading algorithm for WPM employing MMSE equalization in the time domain. The proposed bit loading algorithm takes into account subcarrier signal attenuation and noise amplification induced from the imperfection of MMSE equalization. The research is performed considering known and unknown CSI. The study is performed for channel A and channel B of three test environments from ITU-R M.1225. The three test environments are indoor office test environment, outdoor to indoor pedestrian test environment, and vehicular test environment.

Analytical expressions related to the BER are derived considering known CSI and validated using simulation results obtained from program developed in MATLAB. The verified analytical expressions are used to explore the BER performance of WPM. Numerical results show that equalization with the proposed bit loading algorithm helps reduce the BER as compared with equalization without bit loading. In particular, the required E_b/N_0 to achieve the BER of 10^{-5} is reduced, with the maximum reduction of 10 dB for channel A of the vehicular test environment, and the minimum reduction of 1 dB for channel B of the vehicular test environment. In addition, the analytical expressions are used to compare the BER performances of WPM and OFDM. For WPM, MMSE equalization with bit loading is used, while for OFDM one-tap equalization with bit loading is considered. Numerical results show that, with a moderate equalizer filter length, WPM performs better than OFDM. In most of the considered scenarios, the required E_b/N_0 to achieve the BER of 10^{-5} is reduced by 1-2 dB for WPM as compared with OFDM.

The research is further extended for unknown CSI. First, an investigation is performed for WPM with MMSE equalization to find the required training sequence

lengths to achieve acceptable BER performances. The investigation is performed for different numbers of subcarriers. Numerical results show that the maximum training sequence overhead for 16, 32, and 64 subcarriers are 5%, 2%, and 1% respectively. Moreover, the results also demonstrate that WPM with MMSE equalization outperforms OFDM with one-tap equalization. Further, channel estimation is performed by solving an overdetermined system of linear equations. The estimated CIR is then used to operate the proposed bit loading algorithm for WPM with MMSE equalization. Numerical results show that, in most cases, the proposed bit loading algorithm using the estimated CIR helps reduce the BER as compared to equalization without bit loading.

Finally, the BER performance of WPM is compared with that of OFDM. Numerical results demonstrate that, for all test scenarios, WPM employing bit loading with unknown CSI has a better BER performance than OFDM employing bit loading with known CSI.

Future research could be performed to explore WPM for other applications such as spectrum sensing for cognitive radio systems. Spectrum sensing requires checking the status of each subcarrier whether it is idle or active. The idle status of a subcarrier indicates that the corresponding subcarrier is not used by a primary user. Therefore, such subcarriers with the idle status could be assigned to secondary users for efficient spectrum utilization. The subcarrier combining feature of WPM, as already illustrated to reduce the PAPR, could also be explored for checking the status of subcarriers in groups, instead of checking the status of each subcarrier separately. This subcarrier combining feature for checking the status of subcarriers in groups could be explored to reduce the computational complexity as well as the computational time. The concept could be extended for machine type communication (MTC) networks comprising of a large number of end devices such as sensor networks. In such scenarios with a large number of end devices, it is desirable to reduce the computational complexity associated with the detection of active devices.

The subcarrier combining feature of WPM could be beneficial to reduce the computational complexity by facilitating group detection of devices which are in the same subspace. Finally, this research compares WPM with OFDM. However, this research could be further extended to compare WPM with other MCM techniques such as FBMC.



BIBLIOGRAPHY

- Abdullah, K., & Hussain, M. (2009). Studies on DWT-OFDM and FFT-OFDM systems. In *proceedings of Symposium on International Conference on Communication Computer and Power (ICCCP '09)*. MUSCAT.
- Andrews, J. G., Ghosh, A., & Muhamed, R. (2007). *Fundamentals of WiMAX: Understanding Broadband Wireless Networking*. Westford, Massachusetts: Prentice-Hall.
- Bajpai, A., Lakshmanan, M. K., & Nikookar, H. (2011). Channel equalization in Wavelet Packet Modulation by minimization of peak distortion. In *proceedings of 2011 IEEE 22nd International Symposium on Personal, Indoor and Mobile Radio Communications*. Canada.
- Bouwel, C. V., Potemans, J., Schepers, S., Nauwelaers, B., & Capelle, A. V. (2000). Wavelet packet based multicarrier modulation. In *proceedings of Symposium on Communications and Vehicular Technology, (SCVT-2000)*. Belgium.
- Burrus, C. S., Gopinath, R. A., & Guo, H. (1998). *Introduction to wavelets and wavelet transform*. Houston, Texas: Prentice-Hall.
- Chang, M. C., Lay, K. T., & Chen, J. T. (2001). Dynamic water-filling for wavelet communications. In *proceedings of IEEE VTS 53rd Vehicular Technology Conference*. Greece.
- Forney, G. D., & Ungerboeck, G. (1998). Modulation and coding for linear Gaussian channels. *IEEE Transactions on Information Theory*, 44(6), 2384–2415.
- Fugal, D. L. (2009). *Conceptual wavelets in digital signal processing*. San Diego, California: Space & Signals Technical Publishing.
- Gautier, M., Arndt, M., & Lienard, J. (2007). Efficient Wavelet Packet Modulation for Wireless Communication. In *proceedings of The Third Advanced International Conference on Telecommunications (AICT 07)*. Mauritius.
- Gentle, J. E. (2007). *Matrix algebra : Theory, Computations, and Applications in*

- Statistics*. New York: Springer.
- Goldsmith, A. (2005). *Wireless communications*. Cambridge, United Kingdom: Cambridge University.
- Gracias, S., & Reddy, V. U. (1998). An equalization algorithm for wavelet packet based modulation schemes. *IEEE Transactions on Signal Processing*, 46(11), 3082–3087.
- Gupta, M. K., & Tiwari, S. (2013). Performance evaluation of conventional and wavelet based OFDM system. *International Journal of Electronics and Communication (AEU)*, 67(4), 348–354.
- Habibi, A. (1995). Introduction to wavelets. In *proceedings of MILCOM '95*. San Diego, USA.
- ITU-R Rec. M.1225. (1997). . *Guidelines for evaluation of radio transmission technologies for IMT-2000*.
- Jamin, A., & Mahonen, P. (2005). Wavelet packet modulation for wireless communications. *Wireless Communications and Mobile Computing Journal*, 5(2), 123–137.
- Johnson, C. R., Sethares, W. A., & Kelvin, A. G. (2011). *Software receiver design*. Cambridge, United Kingdom: Cambridge University.
- Khan, U., Baig, S., & J.Mughal, M. (2009). Performance comparison of Wavelet Packet Modulation and OFDM for multipath wireless channel. In *proceedings of 2009 2nd International Conference on Computer, Control and Communication*. Pakistan.
- Kumar, K., & Grover, A. (2012). Comparison of block type pilot channel estimation techniques for evaluating the performance of OFDM. *International Journal of Scientific & Eng. Research*, 3(11).
- Lindsey, A. R. (1995). *Generalized orthogonally multiplexed communication via wavelet packet bases* (Unpublished doctoral dissertation). Ohio University, United States.

- Lindsey, A. R. (1997). Wavelet packet modulation for orthogonally multiplexed communication. *IEEE Transactions on Signal Processing*, 45(5), 1336-1339.
- Misiti, M., Misiti, Y., Oppenheim, G., & Poggi, J. M. (2015). *Wavelet toolbox user lq s guide*. Natick, Massachusetts: The MathWorks, Inc.
- Mohammadi, Z., Saadane, R., Wahbi, M., & Aboutajdine, D. (2010). Recovery of ISI channels with Wavelet Packet Modulation using linear equalization and channel estimation. In *proceedings of 2010 5th International Symposium On I/V Communications and Mobile Network*. Morocco.
- Negash, B. G., & Nikookar, H. (2000). Wavelet-based multicarrier transmission over multipath wireless channels. *Electronics Letters*, 36(21), 1787–1788.
- Proakis, J. G., & Salehi, M. (2008). *Digital communications* (5th ed.). New York: McGraw-Hill.
- Ren, R., & Zhu, S. (2005). Novel adaptive subcarrier power and bit allocation using wavelet packet parallel architecture. In *proceedings of the International Conference on Algorithms and Architecture for Parallel Process (ICA3PP 2005)*. Melbourne, VIC, Australia.
- Rioul, O., & Vetterli, M. (1991). Wavelets and signal processing. *IEEE SP MAGAZINE*, 8(4), 14–38.
- Torun, B., Lakshmanan, M. K., & Nikookar, H. (2009). On the analysis of peak-to-average power ratio of Wavelet Packet Modulation. In *proceedings of 2009 European Wireless Technology Conference*. Italy.
- Torun, B., Lakshmanan, M. K., & Nikookar, H. (2010). Peak-to-Average Power Ratio reduction of Wavelet Packet Modulation by adaptive phase selection. In *proceedings of 21st Annual IEEE International Symposium on Personal, Indoor and Mobile Radio Communications*. Turkey.
- Tse, D., & Viswanath, P. (2005). *Fundamentals of Wireless Communications*. Cambridge, United Kingdom: Cambridge University.
- Wong, K. D. (2011). *Fundamental of wireless communication engineering*

technologies. Hoboken, New Jersey: John Wiley & Sons Inc.

Xian, H., Gewei, T., Ning, X. Q. X., & Shuangxi, W. (2013). A kind of PAPR reduction method based on pruning WPM and PTS technology. *Journal of Electronics(China)*, 30(3), 261–267.

Zakaria, J., & Salleh, M. F. M. (2016). PAPR reduction scheme: wavelet packet-based PTS with embedded side information data scheme. *IET Communications*, 11(1), 127–135.





APPENDIX A

MODIFIED DWT AND IDWT FUNCTIONS

Simulation programs are developed using MATLAB. MATLAB has inbuilt commands named `dwt` and `idwt` to perform DWT and IDWT operations respectively (Misiti, Misiti, Oppenheim, & Poggi, 2015). The operation of `dwt` can be explained through the block diagram shown in Fig. A.1. Here, g_n^d and h_n^d are the coefficients of the decomposition LPF and the decomposition HPF respectively.

Let us consider input signal S of length N . The input signal is fed to the LPF and the HPF. The operation of passing the input signal S through the LPF is equivalent to the convolution of the input signal S and the decomposition LPF coefficients g_n^d . The resultant signal is downsampled by a factor of 2. In downsampling, only even indexed samples are kept. The obtained output signal is known as approximation coefficients, indicated by CA. In a similar fashion, the input signal S is also fed to the HPF and downsampled by a factor of 2 to obtain detail coefficients, indicated by CD.

For the filter length of F and the input signal length of N , the convolution results in the output length of $N + F - 1$. This output is downsampled to provide CA and CD, yielding the final output length of L_c given by

$$L_c = \left\lfloor \frac{N + F - 1}{2} \right\rfloor. \quad (\text{A.1})$$

The operation of `idwt` can be explained through the block diagram as shown in Fig. A.2. Here, g_n^r and h_n^r are the coefficients of the reconstruction LPF and the reconstruction HPF respectively. First, the approximation coefficients (CA) and the detail coefficients (CD) are upsampled by a factor of 2. During the upsampling process, zeros are inserted at odd indexed elements. The upsampled approximation coefficients (CA) and detail coefficients (CD) are passed through the reconstruction

LPF g_n^r and the reconstruction HPF h_n^r , respectively. This is equivalent to the convolution of the upsampled CA and the upsampled CD with g_n^r and h_n^r respectively. The outputs from the two convolution operations are added. An appropriate length of the resultant samples are kept from the center of the result obtained from the convolution operation using the MATLAB command `wkeep`. Normally, the length of the samples that are kept, denoted by L_k , is given by

$$L_k = 2 \times L_c - F + 2 \quad (\text{A.2})$$

Substituting L_c from (A.1), the output signal length can be computed as (assuming F to be even)

$$\begin{aligned} L_{\text{output}} &= 2 \times L_c - F + 2 \\ &= 2 \times \left\lfloor \frac{N + F - 1}{2} \right\rfloor - F + 2 \\ &= 2 \times \frac{N + F - 2}{2} - F + 2 \\ &= N \end{aligned} \quad (\text{A.3})$$

Thus, the output signal length will be equal to the input signal length.

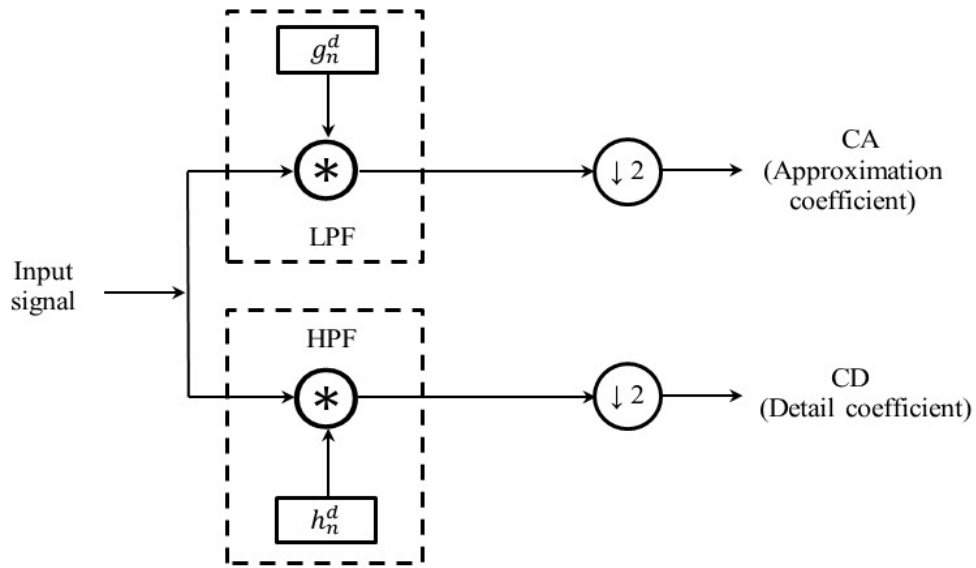


Figure A.1: Block diagram for the MATLAB dwt command

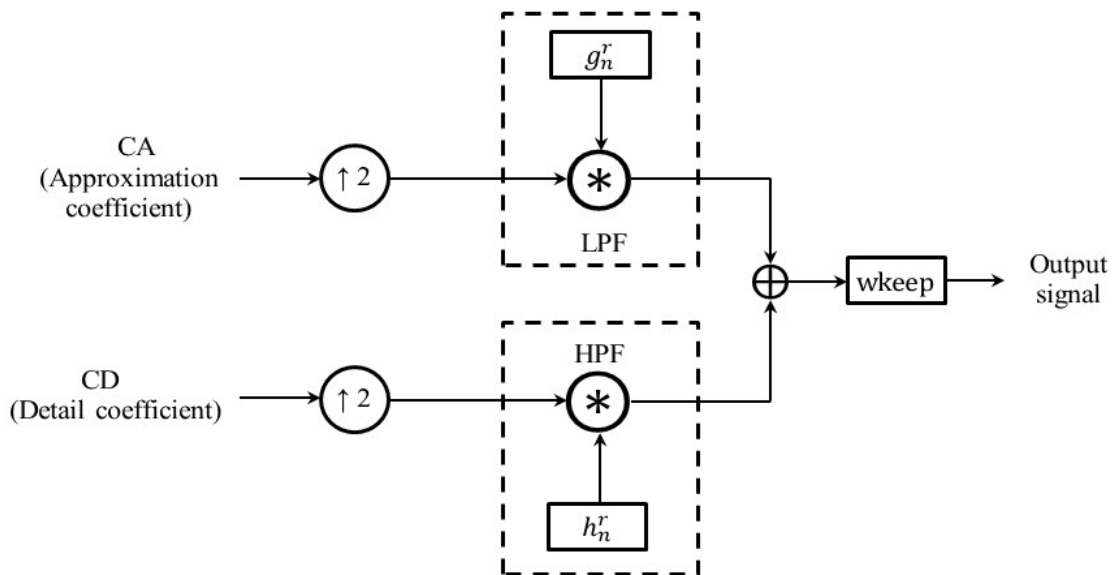


Figure A.2: Block diagram for the MATLAB idwt command

The default MATLAB dwt and idwt functions are designed for data compression; dwt is supposed to be used first, followed by idwt. However, in WPM transmissions, idwt needs to be performed first in the IDWPT block at the transmitter, while dwt is performed later in the DWPT block at the receiver. Since the MATLAB idwt command discards the data as obtained from convolution to make the output

signal length equal to the input signal length, it results in the edge effect. The edge effect results in non-zero BER values even in the absence of any noise addition for all the wavelets except for the Haar wavelet. There are some signal extension modes to minimize the edge effects, such as zero padding, symmetric padding, and periodic padding. However, the edge effect cannot be totally eliminated. Therefore, for simulation of WPM transmissions modified dwt and idwt functions are developed.

The block diagrams for the modified idwt and dwt functions are shown in Fig. A.3 and Fig. A.4, respectively. Unlike the MATLAB idwt command, in the modified idwt command, the output signals after convolutions with the LPF and HPF are kept intact without any truncation, as shown in Fig. A.3. Likewise, for the modified dwt command, downsampling of the decomposition LPF and HPF outputs is performed starting from the position index equal to the filter length F . This is because, for the convolution operation between the decomposition filter coefficients and the input signal, the complete overlap between the filter coefficients and the input signal occurs from the position index F . Moreover, for the convolution operation, the input signal is extended by zero padding, after which the filter coefficients are flipped and moved across the extended input signal.

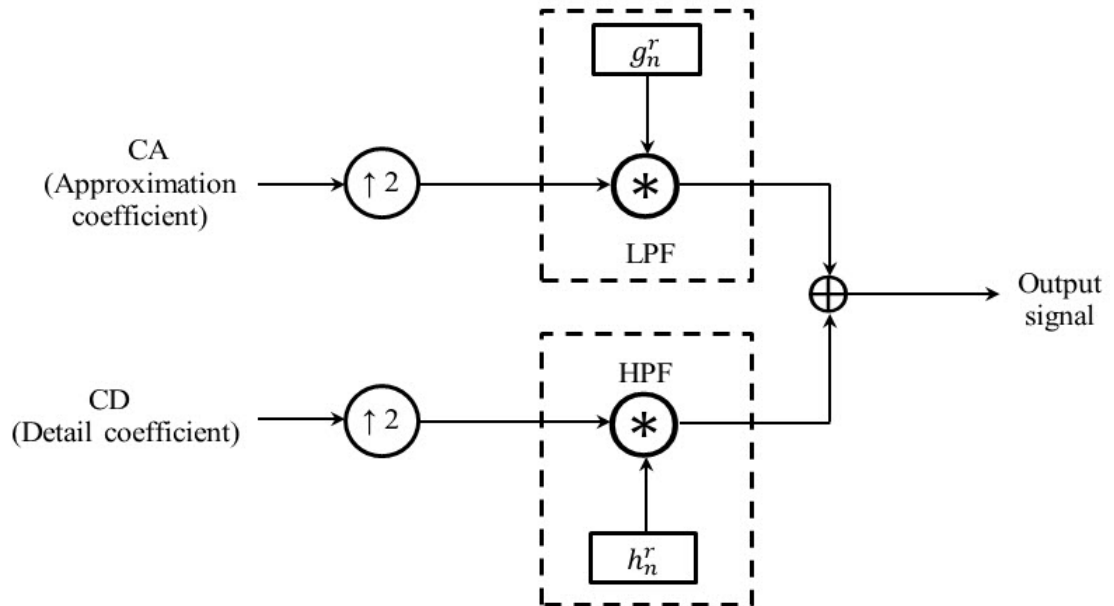


Figure A.3: Block diagram for the modified idwt command

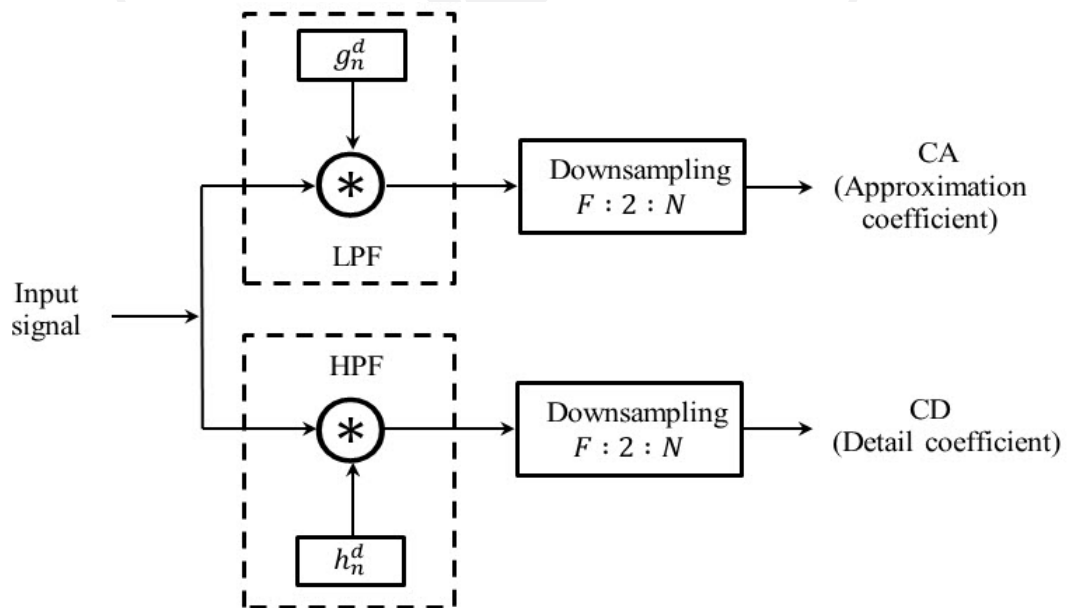


Figure A.4: Block diagram for the modified dwt command

APPENDIX B

BER ANALYSIS FOR OFDM

The BER expression for OFDM with CP can be computed in a similar fashion as for the case of WPM, as discussed in section 4.1. For simplicity, the same variables and notations are considered as introduced in chapter 4, unless an additional description is provided.

Considering that d_{\min} is constant for all signal sets, the average symbol energy, denoted by E_s , for $M_k \times M_k$ QAM is given by (Forney & Ungerboeck, 1998)

$$E_s = \frac{d_{\min}^2 (M_k^2 - 1)}{6} \quad (\text{B.1})$$

Therefore, the average energy per channel use can be written as

$$E_c = \frac{1}{N} \left(\sum_{k=0}^{N-1} \left(\frac{M_k^2 - 1}{6} \right) \right) d_{\min}^2 \quad (\text{B.2})$$

For each OFDM symbol period, the energy per OFDM symbol can be written as the product between the number of channel uses, which corresponds to the number of transmitted values, and the energy per channel use. Alternatively, it is equivalent to the product between the number of information bits transmitted and the energy per information bit. Accordingly,

$$(N + N_c) \times E_c = \left(\sum_{k=0}^{N-1} 2 \log_2 M_k \right) \times E_b \quad (\text{B.3})$$

yielding

$$E_b = \left(\frac{N + N_c}{\sum_{k=0}^{N-1} 2 \log_2 M_k} \right) \times E_c \quad (\text{B.4})$$

Substituting E_c from (B.2) in (B.4), E_b can be represented as

$$E_b = \left(\frac{N + N_c}{\sum_{k=0}^{N-1} 2 \log_2 M_k} \right) \times \frac{1}{N} \left(\sum_{k=0}^{N-1} \left(\frac{M_k^2 - 1}{6} \right) \right) d_{\min}^2 \quad (\text{B.5})$$

Thus, d_{\min} becomes

$$d_{\min} = \sqrt{\frac{N}{N + N_c} \left(\frac{\sum_{k=0}^{N-1} 2 \log_2 M_k}{\sum_{l=0}^{N-1} \left(\frac{M_l^2 - 1}{6} \right)} \right)} \times E_b \quad (\text{B.6})$$

Now, considering $M_k \times M_k$ QAM, the BER for subcarrier k can be evaluated using the union bound estimate from (Forney & Ungerboeck, 1998) as

$$\text{BER}_k \approx \frac{2(M_k - 1)}{M_k \log_2 M_k} Q \left(\frac{d'_{\min}}{\sqrt{2N_k^I}} \right) \quad (\text{B.7})$$

where, N_k^I represents the interference-plus-noise power on subcarrier k and d'_{\min} is the minimum distance at the receiver. Furthermore, considering that H_k is the FFT of CIR, N_k^I for OFDM with one-tap equalization can be expressed as $N_0/|H_k|^2$. Moreover, substituting this N_k^I along with d_{\min} from (B.6) in (B.7), the BER of subcarrier k , denoted by BER_k , can be expressed as

$$\text{BER}_k \approx \frac{2(M_k - 1)}{M_k \log_2 M_k} \times Q \left(\sqrt{\frac{N}{N + N_c} \left(\frac{\sum_{i=0}^{N-1} 2 \log_2 M_l}{\sum_{l=0}^{N-1} \left(\frac{M_l^2 - 1}{6} \right)} \right) \times \frac{|H_k|^2}{2} \times \frac{E_b}{N_0}} \right) \quad (\text{B.8})$$

Eventually, the overall BER can be computed using the weighted average of the BERs on all the subcarriers as given by

$$\text{BER} \approx \sum_{k=0}^{N-1} \frac{2 \log_2 M_k}{\sum_{l=0}^{N-1} 2 \log_2 M_l} \times \text{BER}_k \quad (\text{B.9})$$

APPENDIX C

CIR GENERATION

The CIRs used in simulation are generated based on the tapped-delay-line parameters provided in Rec. ITU-R M.1225 (ITU-R Rec. M.1225, 1997). There are three test environments

1. Indoor office test environment
2. Outdoor to indoor and pedestrian test environment
3. Vehicular test environment

Each test environment has two channels, channel A and channel B. The tapped-delay-line parameters for all test environments are listed in Table 4.1–4.3. The tapped-delay line parameters for each channel of each test environment consist of the average powers relative to the strongest tap and the corresponding time delays relative to the first tap. Denote the average power for tap n by P_n and the corresponding delay relative to the first tap by D_n . The CIR h_n is generated considering a specific data rate, denoted by R and measured in bit/sec (bps).

The average power P_n is provided in dB and the relative delay is provided in nanosecond (ns). The average power P_n needs to be converted from dB to the normal scale for the computation of h_n . The pulse period for sampling, denoted by T_{Pulse} , is computed based on the data rate R and the number of subcarriers N . The time required to transmit one MCM symbol with N subcarriers, using the data rate of R is

$$\begin{aligned}
 T_{\text{MCM}} &= \frac{\text{Total transmit bits}}{\text{Data rate}} \\
 &= \frac{b \times N}{R}
 \end{aligned} \tag{C.1}$$

Here, b indicates the average number of bits allocated to each subcarrier. Moreover, the pulse period T_{pulse} can be computed as

$$T_{\text{pulse}} = \frac{T_{\text{MCM}}}{N} \quad (\text{C.2})$$

Using the pulse period T_{pulse} , sampling instances are computed. The average power P_n is assigned to the sampling instance, that is nearest to the relative delay D_n . However, when the pulse period is longer than the delay differences between successive relative delays, then the average powers P_n for more than one tap fall within the same pulse period. In such cases, the average powers P_n that fall within the same pulse period are combined and assigned to the nearest sampling instance. The average power for more than one tap can be combined using

$$P_n = \sqrt{\sum_i P_{n,i}^2} \quad (\text{C.3})$$

To generate a Rayleigh fading channel, the CIR coefficient h_n is computed randomly based on the Rayleigh distribution. The variance σ^2 of the Rayleigh distribution is computed using the average power P_n . The k^{th} raw moment of the Rayleigh distribution is given by

$$\mu_k = \sigma^k 2^{\frac{k}{2}} \Gamma\left(1 + \frac{k}{2}\right) \quad (\text{C.4})$$

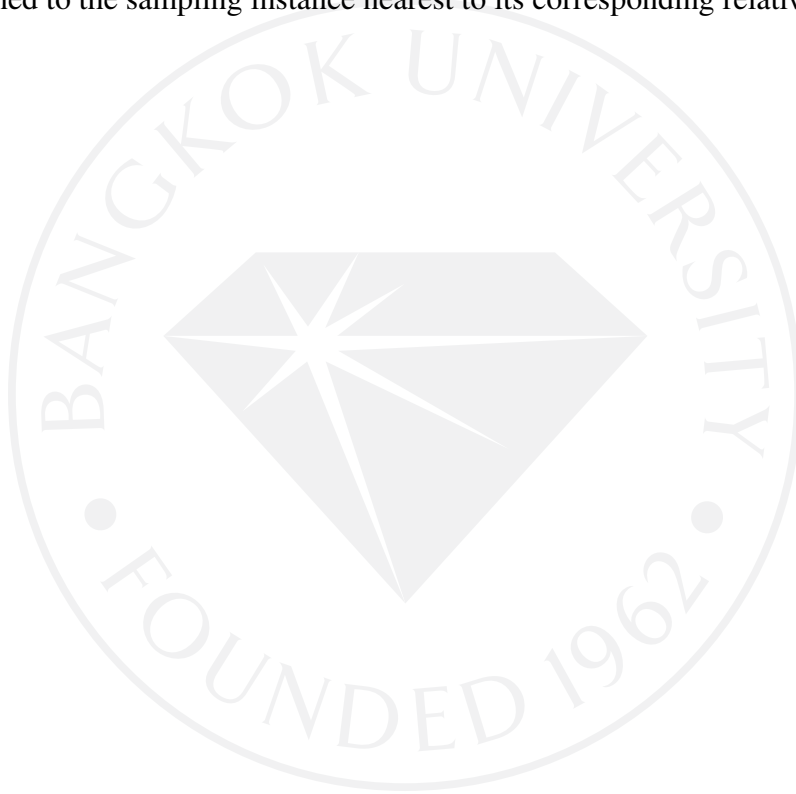
where $\Gamma(z)$ is the gamma function and $\Gamma(z) = (z - 1)!$ for an integer z . The second moment can be computed by substituting $k = 2$ in (C.4), yielding

$$\begin{aligned} \mu_2 &= \sigma^2 2^{\frac{2}{2}} \Gamma\left(1 + \frac{2}{2}\right) \\ &= 2\sigma^2 \Gamma(2) \\ &= 2\sigma^2 \end{aligned} \quad (\text{C.5})$$

The second moment μ_2 is equal to the average power P_n . Therefore, the variance σ^2 can be calculated as

$$\sigma^2 = \frac{P_n}{2} \quad (\text{C.6})$$

Finally, CIR coefficients h_n are randomly generated using the Rayleigh distribution with variance σ^2 obtained from (C.6). Each generated CIR coefficients h_n is assigned to the sampling instance nearest to its corresponding relative delay D_n .



BIODATA

Name–Last name: Sarbagya Buddhacharya

Address: Khajahana, ward no. 3, Bhairahawa,
Siddharthanagar, Rupandehi, Lumbini zone, Nepal.

Email: sarbagya.buddhacharya @ gmail.com

Contact number: +66-846361389

Educational Background: Master degree in Telecommunication Engineering,
Asian Institute of Technology, Thailand, 2010
Bachelor Degree in Electronics & Communication
Engineering, Pokhara Engineering College,
Affiliated to Pokhara University, Nepal, 2006

Bangkok University
License Agreement of Dissertation/Thesis/ Report of Senior Project

Day 10 Month 6 Year 2019

✓
Mr./ Mrs./ Ms. Sarbagya Buddhacharya now living at Baansuanthon
Soi 28 Street Rattanathibet
Sub-district Bangkasaw District Mueng
Province Nonthaburi Postal Code 11000
being a Bangkok University student, student ID 9580900026
Degree level ☐ Bachelor ☐ Master ☒ Doctorate
Program Electrical and Computer Engineering Department School of Engineering
School Graduate School hereafter referred to as "the licensor"

Bangkok University 119 Rama 4 Road, Klong-Toey, Bangkok 10110 hereafter
referred to as "the licensee"

Both parties have agreed on the following terms and conditions:


1. The licensor certifies that he/she is the author and possesses the exclusive rights of dissertation/thesis/report of senior project entitled Wavelet based multi-carrier communications with bit loading under time-domain equalization submitted in partial fulfillment of the requirement for Doctor of Engineering in Electrical and Computer Engineering of Bangkok University (hereafter referred to as "dissertation/thesis/ report of senior project").
2. The licensor grants to the licensee an indefinite and royalty free license of his/her dissertation/thesis/report of senior project to reproduce, adapt, distribute, rent out the original or copy of the manuscript.
3. In case of any dispute in the copyright of the dissertation/thesis/report of senior project between the licensor and others, or between the licensee and others, or any other inconveniences in regard to the copyright that prevent the licensee from

reproducing, adapting or distributing the manuscript, the licensor agrees to indemnify the licensee against any damage incurred.

This agreement is prepared in duplicate identical wording for two copies. Both parties have read and fully understand its contents and agree to comply with the above terms and conditions. Each party shall retain one signed copy of the agreement.



(Sarbagya Buddhacharya) Licensor



(Director, Library and Learning Center) Licensee



(Dean, School of Engineering) Witness



(Program Director) Witness